Title

THE EFFECT OF ANGULAR MOMENTUM OF THE COMPOUND NUCLEUS ON THE RATIO OF THE ISOMERS Te119 AND Te119m PRODUCED IN LOW-ENERGY BOMBARDMENTS

Author

Seegmiller, David W. Ph.D.

Publication Date

1963-08-01

UCRL-10850

University of California

Ernest O. Lawrence Radiation Laboratory

THE EFFECT OF ANGULAR MOMENTUM OF THE COMPOUND NUCLEUS OF THE RATIO OF THE ISOMERS Te^{119} AND Te^{119m} PRODUCED IN LOW-ENERGY BOMBARDMENTS

DISCLAIMER

Research and Development

UCRL-10850
UC-34 Physics
TID-4500(19th ed.)

UNIVERSITY OF CALIFORNIA

Lawrence Radiation Laboratory
Berkeley, California

Contract No. W-7405-eng-48

THE EFFECT OF ANGULAR MOMENTUM OF THE COMPOUND NUCLEUS ON THE RATIO OF THE ISOMERS Te^{119} AND Te^{119m} PRODUCED IN LOW-ENERGY BOMBARDMENTS

David W. Seegmiller

(Ph.D. Thesis)

August 1963

Printed in USA. Price $3.00. Available from the
Office of Technical Services
U. S. Department of Commerce
Washington 25, D.C.

THE EFFECT OF ANGULAR MOMENTUM OF THE COMPOUND NUCLEUS ON THE RATIO OF THE ISOMERS Te^{119} AND Te^{119m} PRODUCED IN LOW-ENERGY BOMBARDMENTS

Contents

THE EFFECT OF ANGULAR MOMENTUM OF THE COMPOUND NUCLEUS ON THE RATIO OF THE ISOMERS Te^{119} AND Te^{119m} PRODUCED IN LOW-ENERGY BOMBARDMENTS

David W. Seegmiller

Lawrence Radiation Laboratory and Department of Chemistry
University of California
Berkeley, California

August 1963

ABSTRACT

The effect of angular momentum on compound nucleus reactions was investigated by measuring the formation cross-section ratios of a pair of isomers produced through compound nuclei—xn reactions.

Five different projectiles were used to produce the compound nucleus Te^{122*}, which yielded the isomers of tellurium-119 through a 3n reaction. The projectiles ranged in size from He^3 to O^{18}.

The same isomers were also produced through 2n and 4n reactions by bombardment of the appropriate tin isotopes with He^3 and He^4.

A method involving separation of the antimony daughter was devised for determining the isomer ratios. This method was completely independent of any decay scheme.

The experimentally determined ratios (upper-state to lower-state isomer) varied from a low of about 0.75 to a high of about 25. The expected increase of ratio with energy and projectile size was verified. An apparent direct interaction of Li^7 projectiles was observed.

Excitation functions were obtained for the reactions proceeding through the Te^{122*} compound nucleus. The expected shift in peak position with projectile size was clearly demonstrated.

Compound-nucleus calculations were performed by assuming a rounded nuclear potential approximated by a parabola (Bunthorne). Good agreement was obtained between experimentally determined isomer ratios and predictions based upon the calculated average angular momentum of the compound nucleus.

Reasonable estimates of the isomer ratios were obtained by assuming that all compound nuclei with a spin greater than 8 populate the high-spin isomer, while those with a spin of 8 or less yield the low-spin isomer.

Calculations of the Vandenbosch-Huizenga type were performed for the various reactions. Different combinations of input parameters were investigated and the best results were obtained by assuming a spin cut-off parameter of $0.5\ \sigma_{rigid}$ and equal energy, dipole gamma rays of multiplicity defined by

$$\bar{N}_{\gamma} = (\sqrt{\underline{a}\ E_c})/2 ,$$

where $\underline{a} = A/8\ \text{MeV}^{-1}$ and E_c is the nuclear excitation. σ_{rigid} represents the spin-cutoff parameter calculated by assuming that the nucleus has a moment of inertia equivalent to that of a rigid sphere.

I. INTRODUCTION

This work explores the effects of angular momentum on the compound nucleus reaction mechanism. Five different projectiles, ranging in size from He^3 to O^{18}, were used to produce the compound nucleus Te^{122*}. The effects of angular momentum were studied by measurement of the formation cross-section ratios of the isomers of tellurium-119, produced by emission of three neutrons from the compound nucleus. All the reactions were studied over a wide range of projectile energies, corresponding to a broad spectrum of angular momentum.

Two other compound nuclei, leading to the same isomer pair by a 2n and a 3n reaction, were also studied. They were produced by bombardment of the appropriate tin isotopes with He^3 and He^4.

A. Compound-Nucleus Theory

One of the most successful theories for the explanation of many nuclear reactions was conceived by Niels Bohr.[1,2] This concept is commonly known as the compound-nucleus theory. The theory states that when a projectile A interacts with a target nucleus B to yield the products C and D, the reaction is in reality not a direct one, but proceeds through an intermediate state E^*,

$$A + B \longrightarrow E^* \longrightarrow C + D$$

The nucleus E^*, being made up of both the projectile and target nuclei, is known as a compound nucleus. The compound nucleus thus formed lives for a long time and de-excites independently of the mode of formation. Essential to this theory is the idea that a projectile upon entering a nucleus becomes subject to strong internal forces. The direction of motion of the projectile is drastically altered and its energy dissipated throughout the nucleus. The identity of the original projectile becomes lost. Other properties such as momentum, angular momentum, and parity must be conserved. Sooner or later, according to a statistical probability,

a nucleon (or a small group of nucleons) may find itself at the nuclear surface with enough energy to escape the strong nuclear binding forces. The theory implies that breakup of the compound nucleus is completely independent of the process by which it was formed. Thus compound nuclei E^* and E'^*, produced by two different reaction mechanisms, are indistinguishable (assuming that they are of the same Z and A, that they are at the same level of excitation, and that their angular momentum and parity are equivalent).

The validity of the theory was impressively demonstrated by Ghoshal[3] when he prepared the compound nucleus Zn^{64*} by two different paths--the first by bombardment of Ni^{60} with He^4 and the second by bombardment of Cu^{63} with protons. He found that the cross sections for the various reaction products were independent of the mode of formation.

The work presented here deals with compound nuclei produced by a number of different reactions. The nuclei are considered to be identical except for the angular momentum they possess.

B. Isomers

Normally, gamma decay of an excited nucleus from one state to another is a very rapid occurrence ($< 10^{-13}$ second). It is normally in virtual coincidence with whatever process led to the excitation, say a beta decay. Occasionally, however, the gamma process is slow enough to be measured experimentally. When this occurs the two states are said to be isomers, and the transition from one state to the other an isomeric transition. The definition is really rather arbitrary, since a compilation of nuclear data by Strominger, Hollander, and Seaborg[4] contains mean lives of isomers ranging from 4 years to 10^{-10} second.

These isomeric pairs normally owe their existence to large differences in spin and small differences in energy between the states involved. In the Mayer shell model[5] these conditions are usually met for odd A nuclei near the ends of the various shells. The large difference in spin between the states requires that the multipolarity of a γ ray

for the transition be high. Blatt and Weisskopf provide formulae for calculating the decay constants for gamma emission.[6] The isomers studied in this work are those of tellurium-119. The meta isomer has a spin of -11/2 and the ground state isomer a spin of ± 1/2. With a predicted energy separation of 300 to 320 keV between the isomer levels, and assuming an E-5 transition, the Blatt and Weisskopf formulae indicate the transition from the upper to the lower state should have a half life of approximately 80 years. In fact, the transition is not observed, and it must be concluded that it cannot successfully compete with the faster beta decay (4.7 days).

C. Angular Momentum Effects in Compound-Nucleus Reactions

Many recent investigations[7-12] have dealt with the effects of angular momentum upon both neutron and γ -ray emission from an excited nucleus.

From the classical point of view, one may consider that the entire nucleus is put into rotation upon the impact of a projectile. It is therefore assumed that the excitation energy provided by the kinetic energy of the particle and the Q of the reaction is divided between that tied up in rotation and that of thermal excitation. The energy available for particle emission is therefore the total excitation of the nucleus minus the energy associated with the rotation.[13]

It is generally valid to assume that if a compound nucleus contains an excitation energy greater than the binding energy of one of its neutrons, a neutron will be emitted. Above the emission threshold for neutrons, the probability for de-excitation by γ -ray emission is normally negligible. Mollenauer, however, has shown that the above assumptions may not be entirely correct for a nucleus containing large amounts of angular momentum.[7] This is particularly true of reactions involving heavy ions, in which the angular momentum carried in may reach very high values. Mollenauer studied several carbon ion reactions and found that the total energy appearing as γ rays was greater than the neutron binding energy.[7]

He was therefore forced to conclude that in reactions involving large amounts of angular momentum, γ -ray emission may be able to successfully compete with particle emission.

Increased γ -ray emission in systems containing high angular momentum may be explained on the following basis: since the binding energy of a neutron is normally much greater than the kinetic energy it removes, the effect of neutron emission is to considerably cool the compound nucleus but carry away very little angular momentum. With a decrease in excitation energy, the number of available high spin states in the residual nucleus should diminish rapidly. It therefore becomes difficult to populate these states by further emission of neutrons. The process is retarded to the extent that photon emission begins to compete. This is possible because the γ rays are not required to carry away as much excitation as a particle (they need not carry away a binding energy), and they may therefore lead to final states of higher energy and a consequent higher density of states.

Pik-Pichak has shown that the result of a neutron cascade, from a compound nucleus containing large amounts of angular momentum, is to leave the nucleus with insufficient internal excitation to evaporate another neutron, but with some excitation still tied up as rotational energy.[14] The net result is the shift of excitation functions toward higher energies.

If the decay of a compound nucleus leads to a pair of isomers, the effect of angular momentum is exhibited in another manner. It is normally expected, at least qualitatively, that the high spin states of the compound nucleus will decay to the high-spin isomer, while the low spin states decay to the low-spin isomer. This idea is more or less verified in thermal neutron reactions. A thermal neutron is considered to carry in no angular momentum other than its intrinsic spin. The compound nucleus may, however, be rather highly excited owing to the neutron binding energy. When the resulting compound nucleus has a spin of 1/2 and decays to isomers of spin 1/2 or 3/2 and spin 9/2 or 11/2, respectively, the ratio of formation cross sections of low-spin isomer to high-spin isomer is often of the order of 10 to 1.

Another effect that is commonly observed is the shifting of the high-spin isomer excitation function toward higher energies with respect to the low-spin isomer.[15,16] The more angular momentum carried in by the projectile, the more pronounced is the effect.

In a compound-nucleus mechanism, in order for angular momentum to be conserved, it is necessary that the projectile give to the system all the angular momentum it possesses. Since the angular momentum increases with the particle velocity, the ratio of production of a high-spin isomer to a low-spin isomer should increase with particle energy. This effect has been observed by a large number of investigators.[10,15,16,18-22] The same effect has likewise been observed quite dramatically in this investigation. On occasion the ratio is observed to decrease instead of increase. However, this is normally attributed to a direct interaction and the compound-nucleus theory is ruled out. A recent compilation of isomer ratio data shows numerous examples of each type.[23]

D. Isomers of Tellurium-119

Shortly before the commencement of this work, the total information available on the isomers of tellurium-119 was summarized in such sources as the General Electric Chart of Nuclides[24] and The Nuclear Data Sheets.[25] No information was available on the decay systematics, and even the half lives were not accurately known.

Tellurium-119 was first identified in 1943 by Lindner and Perlman.[26] The isotope was discovered during spallation studies of 200-MeV deuterons on antimony. It was first detected through the presence of its daughter Sb^{119}. Only the 4.7-day isomer of tellurium-119 was detected. This is understandable, since all counting was of β particles and the 16-h isomer of tellurium-119 shows practically no direct particulate radiation and the one prominent γ ray is only weakly converted. Goeckermann and Perlman also detected the same isomer in fission studies of bismuth.[27] Again no evidence was obtained to suggest that another isomer existed.

The 16-h isomer of tellurium-119 was first reported by Dropesky[28] and Fink.[29,30] Their work, reported in 1953, consisted of the bombardment of iodine and cesium respectively with high-energy protons. They were able to identify the two isomers and characterize them to a certain extent by means of scintillation counting. They also made the interesting observation that if, immediately following the irradiation, the tellurium was separated from the other reaction products, the yield of the 16-h isomer was very low. If, however, the reaction products were allowed to stand for several hours before the tellurium was removed, the 16-h isomer was recovered in good yield. They therefore concluded quite correctly that the 16-h tellurium was growing in from an iodine parent. Other work was also accomplished which seemed to indicate that the isomers were independently decaying to an antimony daughter. They proposed that the 4.7-d isomer was the upper state or meta isomer, and that the 16-h isomer was the ground state isomer.

About the time the investigation reported here was begun there appeared in rather close sequence four papers, all devoted to the characterization of the isomers of tellurium-119.[31-34] In general the findings of the four groups are quite harmonious. Another group (Russian) has also done work in the region, but not as extensively.[35,36] There are a few discrepancies, but they are of minor importance so far as this investigation is concerned. Kocher et al. produced the tellurium by bombarding tin with He^4,[31] Fink[32] and Gupta[33] by proton bombardments of antimony. Sorokin et al.[34] (Russian) duplicated the original work of Dropesky,[28] producing the isomers by high-energy proton bombardments of iodine. The upper-state isomer was determined unequivocally to be the 4.7-day isomer. It will henceforth in this paper be designated Te^{119m}, and the ground-state isomer Te^{119}. When refering to the two isomers in combination or when not refering to a particular isomer, the designation tellurium-119 will be used. Fink et al. measured the spins of the two isomers and determined them to be - 11/2 and + 1/2 for the meta and ground states respectively.[32] The half-life determinations were all in reasonable agreement. Te^{119m} was assigned values ranging from 4.5 to 5 days. Te^{119} was assigned a value of 15.9 ± 0.3 h by the Fink group[32] and a value of about 12 h by

the two Russian groups,[34,35] and merely listed as approximately 16 h by the other workers. This investigation has determined and uses a slightly higher value (16.7 h). Table I contains a summary of the gamma energies and their relative abundances as reported by the Fink group.[32] The results obtained by the other investigators are in reasonably good agreement with these values.

Although the above cited papers are in good agreement with respect to the various radiations and their energies, the principle purpose of each investigation, except for the last cited, was to construct a decay scheme for the isomers. Unfortunately in this respect there is consierable discrepancy. The decay schemes proposed by the four groups are shown in Figs. 1 through 4.

In most isomer ratio determinations it is essential to know with all possible exactness the decay scheme of the isomers being considered. Fortunately, in this investigation it was possible to make use of another method which is independent of the mechanism of the decay. If this were not so, there would be uncertainties in the ratios based upon the discrepancies of the decay schemes. In order to calculate absolute cross sections it is essential to known accurately the decay systematics of one of the isomers even if the cross-section ratios are known. The results given for the lower isomer are quite consistent, and reasonable calculations can probably be made from them. It is also necessary to know the conversion coefficient for the particular γ ray being counted. This has been determined by the Kocher group.[31] For the 645-keV γ ray of Te^{119} the conversion coefficient was found to be $4 \times 10^{-3} \pm 10\%$.

At the time of this writing another paper had just appeared which alters to a certain extent the conclusions of the earlier investgations.[37] The primary difference is due to the discovery of a new 720 keV gamma ray belonging to the 16 h isomer. The new results do not alter the conclusions reached in this investigation, since no recourse to decay systematics is necessary. The decay scheme proposed is shown in Fig. 5.

Table I. Summary of energies and relative intensities of γ-rays from Te^{119m} and Te^{119}.[32]

Energy (keV)	Relative gamma intensity (uncorrected for conversion)
Te^{119m} (4.7 d)	
153.7 ± 1.0	440 ± 150
165.5 ± 1.0	~ 30
270.0 ± 2.0	150 ± 50
~ 400	weak
918 ± 15	< 100
955 ± 15	~ 100
1000 ± 20	< 100
1130 ± 15	~ 50
1214 ± 10	320 ± 50
1763 ± 20	1-3
2092 ± 15	25 ± 5
Te^{119} (16 h)	
648 ± 5	97
1763 ± 20	3

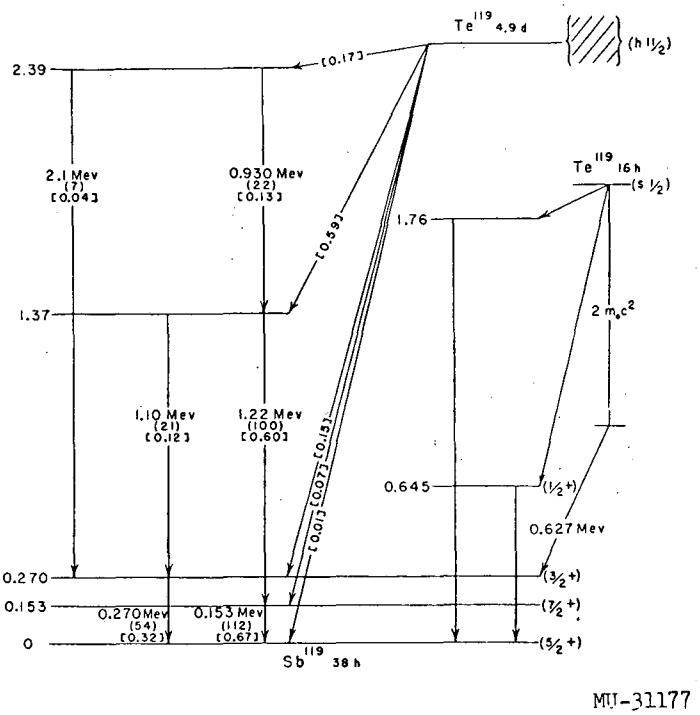

Fig. 1. Tentative decay scheme for tellurium-119 as proposed by Kocher et al. The relative intensities of the γ rays for Te^{119m} are given in parenthesis with the intensity of the 1.22-MeV γ ray taken as 100. The fraction of the disintegration is given in square brackets. (Reproduced from reference 31.)

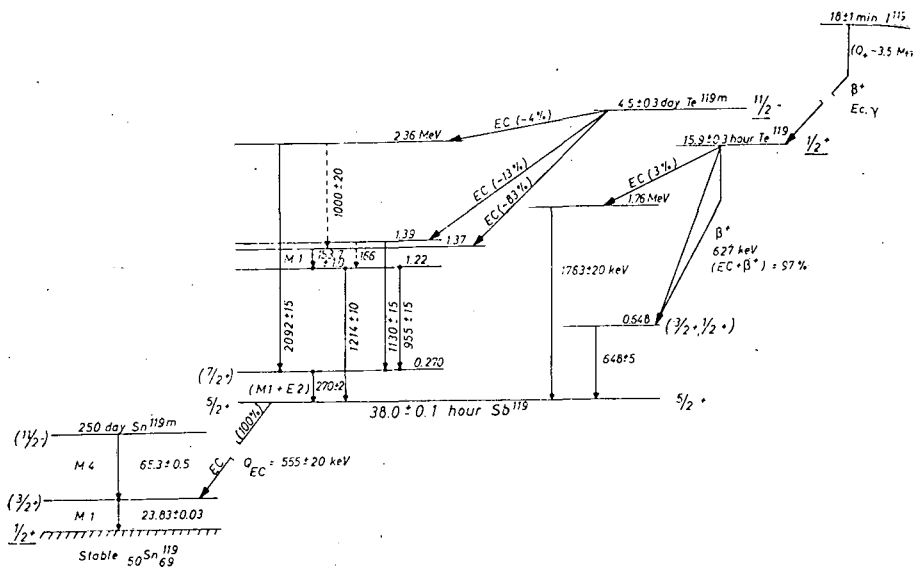

MU-31179

Fig. 2. Tentative decay scheme for tellurium-119 as proposed by Fink et al. (Reproduced from reference 32.)

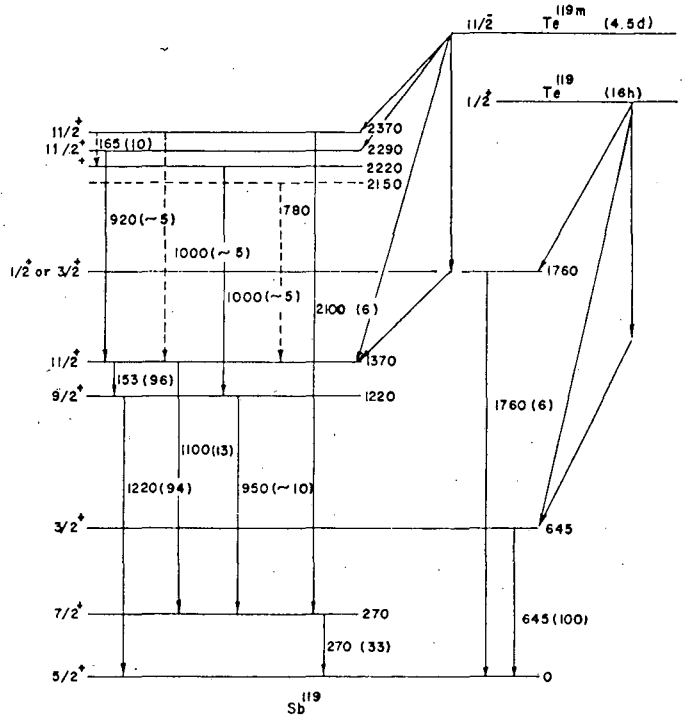

MU-31178

Fig. 3. Tentative decay scheme for tellurium-119 as proposed by Gupta et at. The numbers in parenthesis represent γ-ray intensities. (Reproduced from reference 33.)

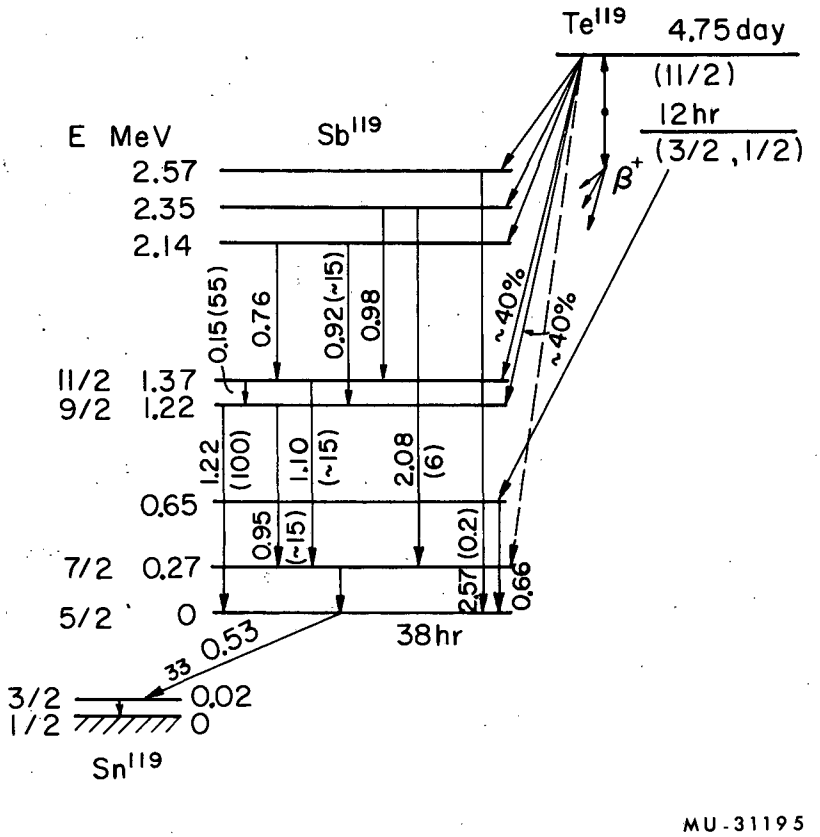

Fig. 4. Tentative decay scheme for tellurium-119 as proposed by Sorokin et al. Relative γ-ray intensities are given in parenthesis. (Reproduced from reference 34.)

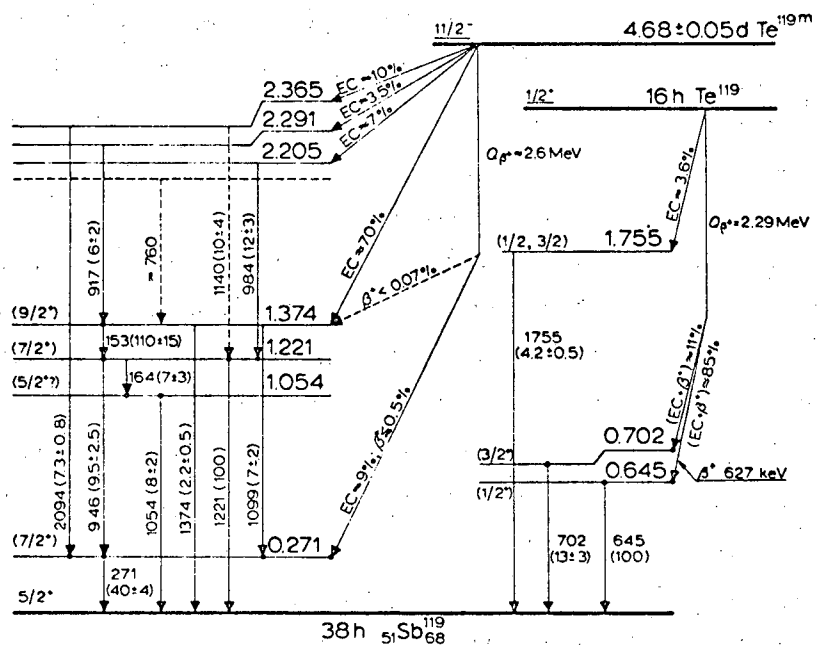

MU-31176

Fig. 5. Decay scheme for the tellurium-119 isomers as proposed by Kantele and Fink. The numbers in parenthesis indicate the relative transition intensities, corrected for conversion. Note the inclusion of a 702-keV γ ray for the 16-h isomer. (Reproduced from reference 37.)

E. This Investigation

The investigation presented here can be rather conveniently broken down into three separate experimental and two theoretical parts.

The first experimental section involves some preliminary experiments designed to characterize the isomers and to determine the feasibility of producing them by means of both light and heavy ions. Half lives were determined and several experiments performed to verify the mass assignment of the 16-h isomer. No attempt was made to determine any sort of decay scheme, since it was unnecessary for the investigation being considered.

The second experimental section involves the method by which the isomer ratio was determined. Three fortuitous circumstances allow the determination of the isomer ratios without recourse to a decay scheme. They are as follows: First, it is possible to produce each isomer in such a way that it is not contaminated with the other. Second, there is no internal transition between the two states; and third, the product resulting from the decay of the two isomers is radioactive and has a convenient half life. Based upon the foregoing circumstances, an experimental method for determining the isomer ratios was developed. This method is treated in detail in Section III.

The third experimental section involves the actual measurements of Te^{119m} - Te^{119} formation cross section ratios. In all, 70 irradiations were carried out and 75 experiments performed. Of this, a total of about 35 actually yielded isomer cross-section ratios. The other experiments all fall under the first two classifications. In numerous experiments performed by various groups a pair of isomers is produced by a number of different reactions.[10,15,17,38] So far as has been determined, however, none of these investigations has produced a given compound nucleus, leading to the isomers, in more than two ways. For example, the same compound nucleus has been produced in a number of investigations by bombardment of an isotope of mass A by protons, and by bombardment of an isotope of the same Z but of mass A-1 by deuterons. Most of the

experiments involve the preparation of various compound nuclei, all leading to the same set of isomers. In this investigation the compound nucleus Te^{122*} was produced by five different paths, namely: He^3 on Sn^{119}, He^4 on Sn^{118}, Li^7 on In^{115}, C^{12} on Pd^{110}, and O^{18} on Ru^{104}. The compound nuclei Te^{121*} and Te^{123*} have also been produced by He^3 and He^4 bombardment of the appropriate isotopes of tin. All these reactions have been carried out over a wide range of energies, and the effects of angular momentum on the formation cross-section ratio of Te^{119m} to Te^{119} are vividly seen.

The first theoretical section involves some compound-nucleus calculations performed on an IBM 650 computer. These calculations are based on a diffuse nuclear potential of expotential form, which is approximated at the top by an inverted parabolic (Bunthorne).[39,40] The program also yields transmission coefficients for penetration of the potential barrier for the various particles used in the investigation. Some qualitative predictions are made as to what one might expect to see in the isomer ratios.

The second theoretical section is more complicated and attempts to make more quantitative predictions of the isomer ratios. The calculations are performed with a program written by Robert Vandenbosh, John R. Huizenga, and W. L. Hafner at Argonne National Laboratory.[41] An IBM 7094 computer is employed. The calculation makes use of the level-density equation[42,43]

$$\rho(J) \propto \rho_0(J=0)(2J+1)\exp[-(J-1/2)^2/2\sigma^2] ,$$

where ρ is the relative level density of levels with spins J, ρ_0 is the density of levels with J = zero, and σ is a nuclear spin density parameter. The calculated cross-section ratios for isomer production are very sensitive to the parameter σ, and--to a somewhat smaller extent--on the number and multipolarity of the gammas involved in the γ-ray cascade. The parameter σ is known to increase with excitation energy, and attempts are made in this work to define its values.

II. PRELIMINARY EXPERIMENTS AND CHARACTERIZATION OF TELLURIUM-119 ISOMERS

A. Counting Techniques

The same counting techniques were employed in all parts of the work; the following discussion applies throughout.

All counting was of γ rays, and consequently a scintillation counting technique was employed. The detector was a standard 3 × 3-inch cylinder of thallium-activated sodium iodide. The crystal and a number 6363 Dumont photomultiplier tube as an integrally aligned unit were obtained from Harshaw Chemical Company.[44] The resolution of the assembly, as determined by measuring the width at half maximum of the Cs^{137} photopeak, was approximately 8.2%.

The pulse from the detector was amplified in a DD2 amplifier and fed into a multichannel analyzer. During the period of the investigation two different instruments were used. In the early experiments a PENCO model PA-4 100-channel analyzer was employed.[45] For the bulk of the work, however, a RIDL model 34-12 transistorized 400-channel analyzer was used.[46] In conjunction with the RIDL instrument, which had a typewriter printout, it was also possible to use a Moseley Autograph model 2D-2 X-Y recorder.[47] This recorder saved countless hours that would have been required to hand plot the hundreds of spectra recorded. The recorder did lack somewhat in accuracy, and in critical areas checks were always made against the typewriter printout.

The detector shield was constructed with 2-in.- thick lead walls and had inside dimensions of 24 inches in each direction. The shield was lined internally with 30-mil cadmium, 5-mil copper, and plastic sheet. One of the problems inherent in any detector shield is the production of x-rays, through the photoelectric effect, by the shield itself. The cross section for this type of reaction is often quite high, especially in materials of high Z such as lead. Spurious radiation of this type may often be reduced by lining the lead with materials of progressively smaller Z values. The particular materials are chosen for

high absorption of the fluorescent radiation from the preceding layer. This is the reason for lining the lead shield with the cadmium and copper. Heath provides plots showing the effect of just such an arrangement.[48]

The samples were counted quite close to the crystal face. Most counting was done within 1/2 inch of the aluminum can containing the phosphor. Normally such closeness to the crystal is not desirable, since it induces large Compton scattering peaks and occasionally leads to sizeable summation peaks. These effects, however, are unimportant for this investigation, and the increased counting rates obtained by being near the crystal were felt to outweigh the undesirable side effects. The most important consideration for this study was consistency. Once it had been decided to count with the samples near the detector it was necessary to use the same geometry throughout the investigation.

The crystal itself was located as near the center of the cubical shield as possible. It was supported on a plastic sample holder of such a design that samples could be inserted at varying distances from the detector. The detector and sample holder are depicted in Fig. 6.

So far as the actual counting techniques are concerned these have been elaborated upon in great detail by many authors.[48-51] Since no unusual techniques are employed in this work, no description is needed here. The reader desiring a detailed discussion of γ-ray counting techniques is referred to the above comprehensive sources.

B. High-Energy Proton Bombardments of Iodine-127

1. General Purpose

The first experiments were devoted almost entirely to a study of the 16-h isomer of tellurium-119. Much of the available information concerning this particular isomer was rather vague and inconclusive. For example, although the mass assignment was reasonably certain, the crucial experiment had not been performed in which the 16-h tellurium activity is periodically separated from its daughter, and the yields of Sb^{119} are

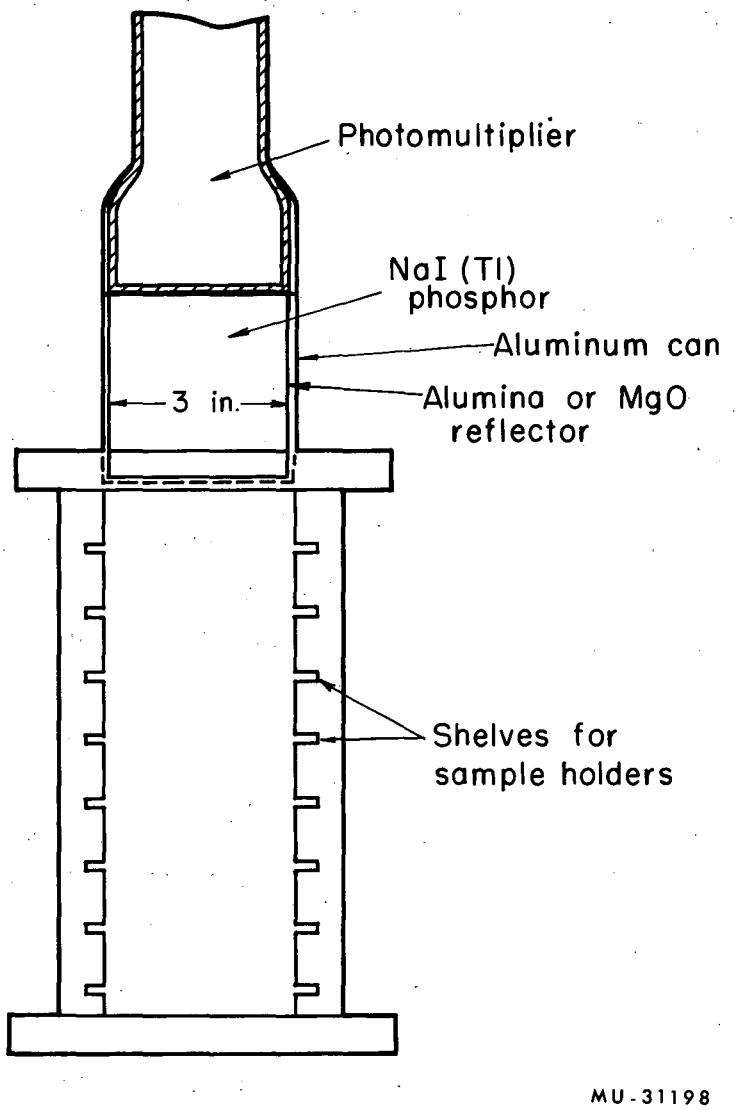

Fig. 6. Gamma-ray detector assembly.

proved to fall off with the same 16-h half life. Also the half lives for the isomer as recorded in the literature range from 12 to approximately 16 h. Dropesky[28] and Fink[29] indicated that the decay of I^{119} led directly to the 16-h ground-state isomer with no branch to the 4.7-d upper state. Since this was a necessary condition for determining the isomer ratios by the particular method used in this work, it was necessary to check this assertion. Most of the experiments were essentially a duplication of those of Dropesky.[28] Potassium iodide was bombarded in the Berkeley 184-inch synchrocyclotron with 240-MeV protons and the resulting activities were used for the investigation.

2. Target Assembly

The target assembly used in conjunction with the 184-inch synchrocyclotron is shown in Fig. 7. It consists of a copper plate with a screw tightening clamp. The foil to be irradiated is clamped to the plate so that it extends a half inch or more beyond the holder. The assembly is then inserted into the accelerator so that the foil comes into contact with the beam.

The material bombarded in these experiments was crystalline potassium iodide. The crystals were approximately 1/16 in. in diameter. A container for the crystals was made by rolling a 1.5 × 3-in. piece of aluminum foil around a piece of glass tubing to form a tube approximately 1.5 in. long and 3/16 in. in diameter. Not all the strip of aluminum was formed into the tube, but an end approximately 1 inch long was left unrolled; this served as a tab by which the target was clamped to the holder. One end of the aluminum tube was sealed off by crimping and rolling up from the bottom. The tube was then filled with 200 to 500 mg of potassium iodide and the other end sealed in a like manner. The arrangement seemed to work well, and in no case was any of the salt observed to be lost. Upon return of the target from an irradiation, the top of the tube was simply snipped off with scissors and the contents of the tube poured out.

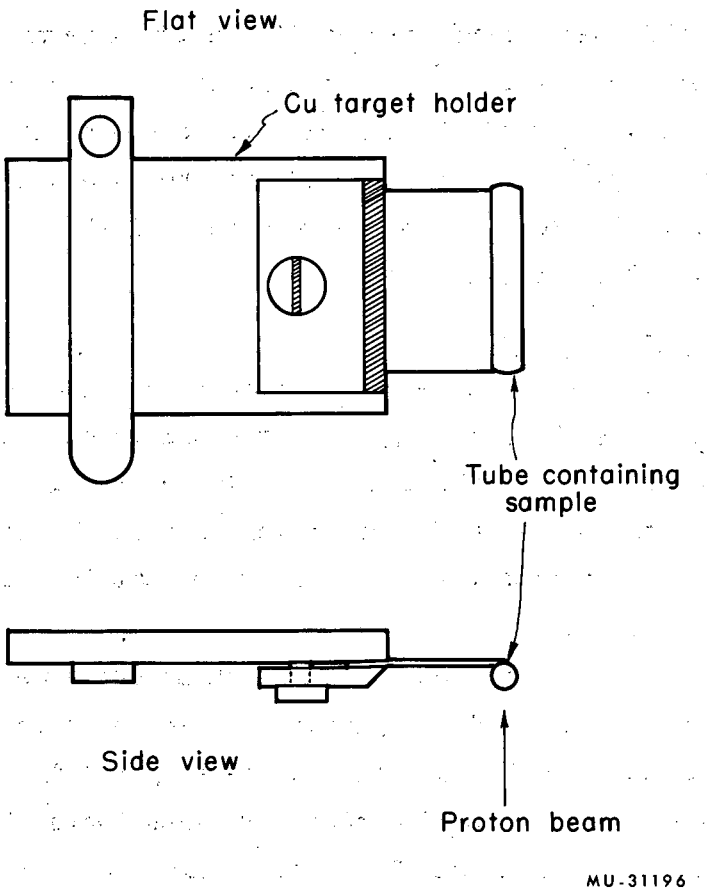

Fig. 7. Synchrocyclotron clothespin target assembly used for high-energy proton bombardments.

3. Chemical Procedures

The chemical procedures employed were essentially a combination of those used by many other investigators.[52-54] A recent review of the radiochemistry of tellurium by Leddicotte lists more than a hundred references dealing with the separation and purification of the element.[55] The flow sheet shown in Fig. 8 outlines the chemical procedure followed for most of the high-energy irradiations of potassium iodide. Certain modifications of the purification scheme were necessary for the different target materials used in the investigation. These modifications are discussed in the appropriate sections.

In these experiments, irradiations were usually for 10 to 20 minutes. Longer bombardments would be of little value, since the half life of the I^{119} that leads to the desired product is approximately 20 min. It was usually possible to obtain the target and begin the chemistry within 15 min after removal from the accelerator. The procedure used was as follows: The foil tube containing the target material was snipped from the target holder and the end of the tube cut away. The salt was dumped and washed into a separation vessel, approximately 6 in long and 1.5 in. in diameter, containing a stopcock at the bottom. The vessel was then clamped in position under a stirring motor which stirred the solution continuously. By oxidation of the iodide to iodine with $NaNO_2$ and HNO_3 the directly formed tellurium tin, antimony and other products were separated by extraction of the iodine into toluene. All but the iodine remained in the water layer, which was withdrawn by means of the stopcock at the bottom of the tube. Toluene was used in these extractions because it is less dense than water and the water layer could be easily drained out through the stopcock. The toluene layer was washed several times with water containing $NaNO_2$ and HNO_3, and the washes were discarded or added to the directly formed products previously removed. After careful purification, the iodine was allowed to decay out to yield the desired tellurium activity. The principal products were Te^{119}, Te^{118}, and Te^{117}. After approximately 1-1/2 hours the iodine was washed once more with water containing tellurium carrier and the tellurium activity that had

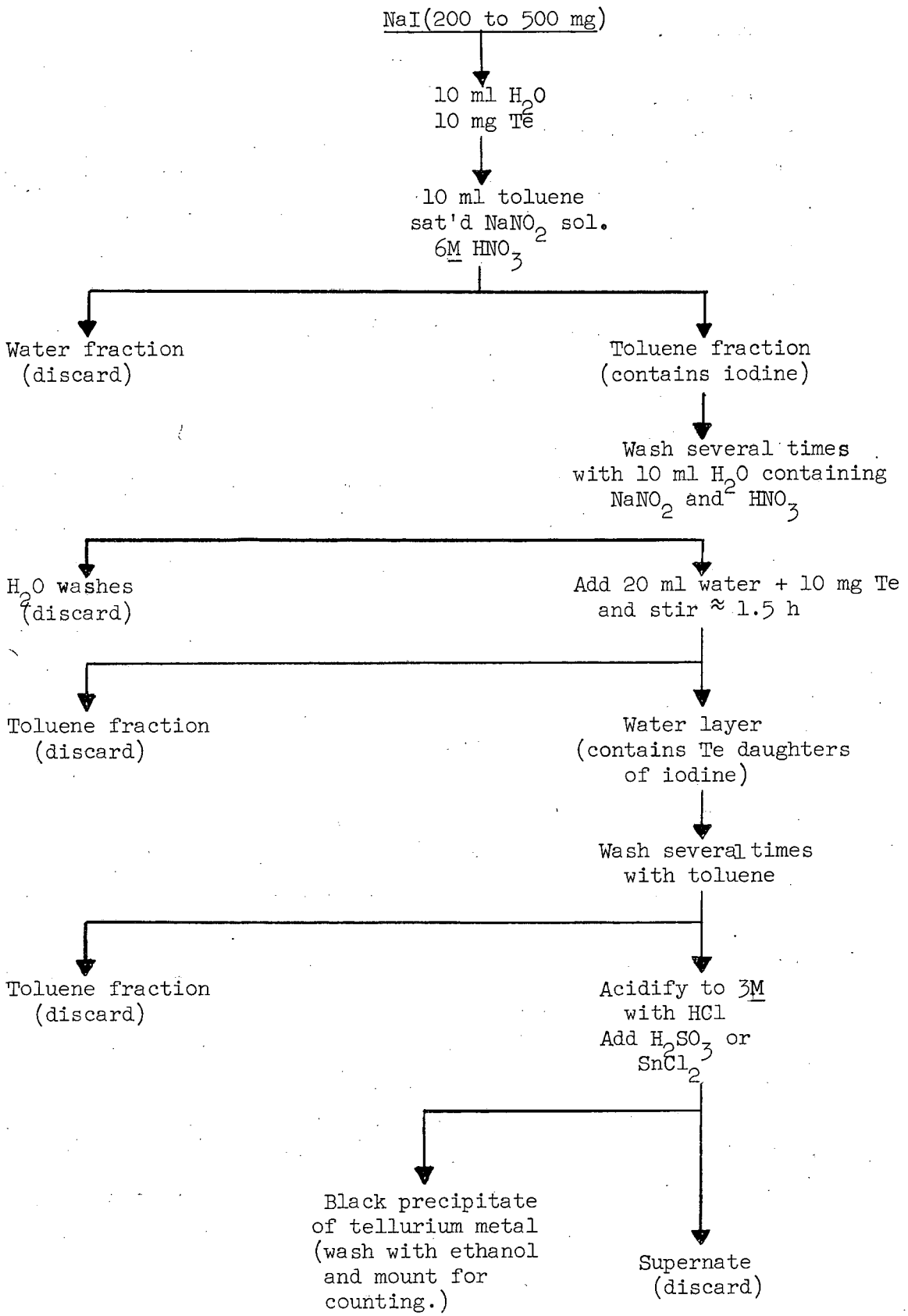

Fig. 8. Flow sheet for chemical procedures used in high-energy proton bombardments.

grown in was thereby removed. To the solution containing the tellurium activities HCl was added until the acidity was approximately 3M. Tellurium was then precipitated as the metal by addition of either $SnCl_2$ or H_2SO_3 and hydrazine dihydrochloride. The resulting finely divided metal precipitate was washed with ethanol and mounted by suction filtration on 7/8-in.-diameter filter papers. Normally the irradiations produced enough activity that six to eight samples, all with counting rates in the tens of thousands of counts per minute, could be obtained. The samples were dried at 105°C for 10 minutes and then mounted on 2.5 × 3.5-in. aluminum plates for counting. The samples were normally attached to the aluminum plates by covering with Scotch tape. Occasionally double-sided masking tape and rubber hydrochloride were used.

In many experiments, particularly those of section III, it was necessary to quantitatively remove the antimony that grew into the tellurium samples. These timed separations were accomplished according to the flow sheet shown on Fig. 9. The tellurium sample, on the filter paper, was cut from the aluminum plate and dropped into a 40-ml Pyrex centrifuge cone. To the sample was added a known amount of antimony carrier. The paper and Scotch tape were dissolved with concentrated sulfuric and nitric acids. When the dissolution was complete, the solution was boiled until only 1 to 3 ml of clear liquid remained. To the liquid was added approximately 10 mg tellurium carrier and enough HCl to make the solution about 3 M. A couple of ml of a saturated $SnCl_2$ solution was added to precipitate the tellurium. Additional tellurium carrier was added and the solution saturated with H_2S. In a 3 M HCl solution the tellurium precipitates rapidly as the sulfide but the antimony, and the tin added in the reduction, remain in solution. This precipitation was often carried out twice. The precipitation seemed to be very complete, and normally no trace of tellurium would be detected in the subsequent steps. The solution was next filtered to remove all traces of tellurium sulfide and water was added until the antimony just began to precipitate as the bright orange sulfide. It was essential to not add too much water or the large amounts of tin used in the reduction

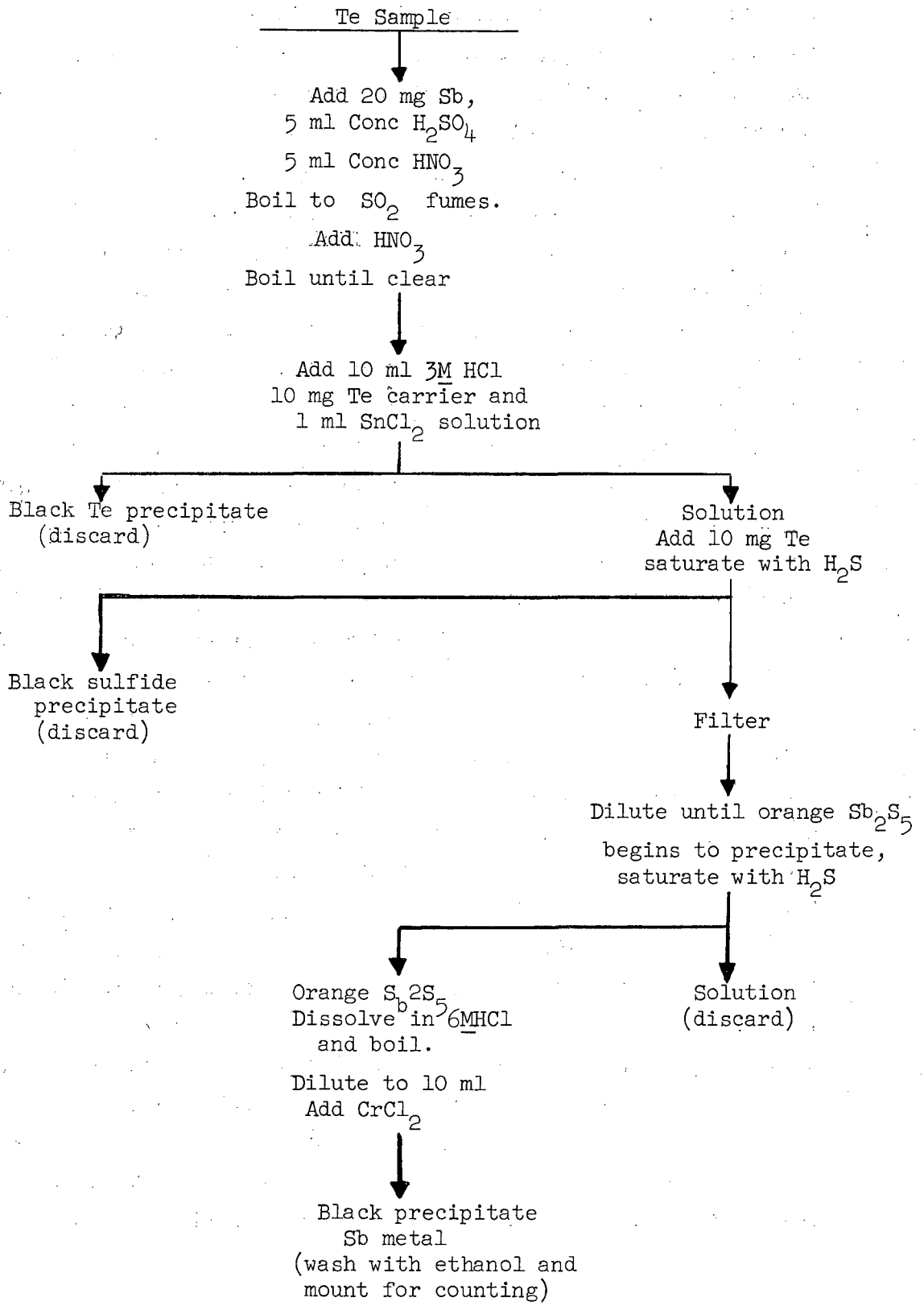

Fig. 9. Flow sheet for chemical procedure used in timed separations of Sb^{119} from tellurium-119 parents.

step also precipitated. The solution was again saturated with H_2S and the antimony sulfide removed by centrifuging. The sulfide was then dissolved in 6M HCl and boiled to expel the H_2S. The solution was diluted to about 10 ml and several ml of fresh $CrCl_2$ added. The antimony immediately was reduced to the free metal and precipitated as a black solid. It was washed with water and ethanol and mounted on a weighed filter disk. The samples were dried at 105°C and weighed to determine the yields, which were normally of the order of 40 to 60%. They were mounted in the same way as the tellurium.

It was easy to determine whether the above procedure had produced clean samples or not. The Sb^{119} has no γ rays and therefore the lack of any gamma spectrum indicated that no tellurium was present. The samples were counted by observation of a 30.5-keV x ray.

C. Mass Assignment Experiments

The work of Fink et al.[32] involved separation of the various isotopes on a mass spectrograph, and it was therefore definitely proved that the mass assignment of Te^{119} (16 h) is correct. However, at the beginning of this investigation their results had not been published and therefore several experiments were performed to confirm the mass assignment.

Pure Te^{119} was obtained by the method outlined previously. Any antimony that may have been present was removed by sulfide precipitation of the tellurium from an acid solution. Thereafter at 4-h intervals the antimony daughter that had grown in was chemically separated. The material obtained decayed with a 39-h half life and was determined to be Sb^{119}. The amount of antimony activity recovered at each timed separation fell off in such a way that the parent was estimated to have a half life of approximately 16 h. The mass assignment on this evidence was assumed to be correct.

A second separation experiment was also performed in an attempt to determine the half life of the parent of Te^{119}. Periodic tellurium separations, at 10-min intervals, were performed on the purified iodine

activity resulting from a high-energy proton bombardment of potassium iodide. The separation was very simply accomplished by means of an extraction procedure, as described previously. The iodine parent was estimated to have a half life of 15 to 20 min, in good agreement with that of I^{119} (17 min).

D. Other Reactions

1. He^4 Ion Reactions

As stated previously, one of the purposes of the early experiments was to determine the feasibility of preparing the isomers by reactions that resulted in the carrying of different amounts of angular momentum into the compound nucleus, but yielded the same amount of excitation energy. Or, in other words, could a compound nucleus that would yield the isomers of tellurium-119 be made by both heavy and light ions?

With the above purpose in mind, enriched isotopes of tin were employed in He^4 ion bombardments. It was found that the isomers could be made quite conveniently from various tin isotopes by varying the energy of the He^4 ions. The particular isotope of interest for this investigation is Sn^{118}. It was found to give good yields of both isomers with He^4 ions varying in energy from about 28 MeV up to 48 MeV, the maximum available at the 60-inch cyclotron. For actual isomer-ratio determinations it is necessary to use the separated isotope, for it is essential to obtain the correct compound nucleus. The isotopic enrichment of the material used is given in section IV, where the ratio determinations are discussed.

For the above bombardments, the targets were prepared as follows: The separated tin isotope was obtained as the oxide and it was used in the irradiations without modification. A small amount of the oxide (2 to 4 mg) was placed on a 1-in. platinum disk and one drop of a solution of Duco cement dissolved in acetone was added. Upon drying, the powder was bound tightly to the disk by a thin, almost invisible film of the cement. The disk was then covered with a thin aluminum foil and mounted

on a microblock target assembly. The target assembly has been described elsewhere[17] and is not discussed here, since it was used in a relatively few number of experiments. After irradiation, the disk containing the target material was "flamed" to burn off the cement. The tin oxide was then scraped into a 40-ml Pyrex centrifuge cone. It was necessary to perform a sodium fusion on the oxide in order to get it into solution. After the fusion had been accomplished and the tin put into solution, tellurium carrier was added and the purification carried out as discussed before.

2. Carbon-12 Ion Reactions

The compound nucleus prepared in the He^4 ion bombardments of Sn^{118} was Te^{122*}. To prepare the same compound nucleus with a C^{12} ion it is necessary to use Pd^{110} as the target material. Although with tin it was necessary to use a separated isotope, from the standpoint of determining the isomer ratios, this is not necessary for palladium. Pd^{110} is the heaviest of the naturally occurring palladium isotopes and Pd^{108} is the next heaviest. Any reaction that would yield the isomers of Te^{119} when Pd^{110} is the starting material would be expected with Pd^{108} as the starting material to yield Te^{117} or possibly Te^{118}. The lighter palladium isotopes would yield still lighter telluriums. In any case, none of the lighter tellurium activities interfere with the experiment. Te^{118} has a relatively long life (6 days), but is invariably present in all the experiments at the higher energies through a 4n reaction. Its presence, although undesirable, does not seriously interfere with the isomer ratio determination. The lighter telluriums are short-lived and decay away early.

With the above in mind, irradiations were carried out on both natural palladium which is 11.8% Pd^{110} and isotopically enriched palladium.[56] It was found that the products from the lighter palladium isotopes did not interfere with the ratio determination, but that the tellurium-119 activity obtained with natural palladium was lower than that required for good counting statistics. Therefore isotopically enriched Pd^{110} was used throughout the work. The enrichments used are tabulated in Section IV.

The mass-110 enriched palladium was obtained as the metal in granular form. It was attached to platinum disks in the same manner as the tin oxide. Irradiation was in the Berkeley heavy-ion linear accelerator. (The target assembly used at the Hilac is discussed in Section IV.) Upon completon of an irradiation, the cement was burned away, as before, and the palladium dissolved from the platinum disk with a few drops of nitric acid. The chemistry was the same as that used for the tin (except, of course, the fusion step was omitted).

Through these experiments it was found that good yields of tellurium-119 could be produced over a wide range of energies.

E. Results

The results of the first section of preliminary experiments can be summarized as follows:

(a) Through timed separation experiments it was determined that the mass assignment of the 16-h Te^{119} activity was correct.

(b) It was shown that the decay of I^{119} leads exclusively to the 16-h Te^{119} and that it is possible to thereby obtain pure Te^{119} without the presence of Te^{119m}. This is essential for the isomer ratio determination, and is discussed at length in the next section.

(c) The half life of Te^{119} was determined to be 16.7 ± 0.3 hours. It is believed that this value is quite accurate, since it was duplicated many times. Although the number is somewhat higher than reported by other groups, it should be remembered that in these experiments, but not the others, it was possible to observe the Te^{119} without interference from Te^{119m}.

(d) No evidence was seen for any internal transition from the Te^{119m} to the Te^{119}. In the directly produced materials from the proton bombardments and in both the He^4-ion and C^{12}-ion bombardments both isomers were formed in good yields. There was no indication that as the shorter-lived component died away it was replenished by the longer-lived upper state.

III. ISOMER RATIO DETERMINATION METHOD

A. Determination of the Ratio Factor F_r

1. General Discussion

Experimental errors in isomer ratio measurements often occur because of uncertainties in the decay systematics of the isomers under study. The accuracy of an isomeric yield determination depends greatly on a knowledge of the decay schemes of the isomers. Normally the reliability of the determination is no better than that of the following quantities:

(a) Fraction of the total disintegration attributable to beta emission.

(b) Fraction of the total disintegration occurring by electron capture.

(c) Percentage of the total disintegration occurring by an isomeric transition.

(d) Percentage of a particular gamma transition in the total disintegration.

(e) Internal-conversion coefficient of the chosen gamma ray (the ratio of the number of converted electrons to the number of unconverted photons).

The method set forth in this section and employed in this work relies upon none of the above factors. So far as is known, this determination is unique in this regard. The only uncertainties are those which arise commonly in experimental determinations, such as weighing errors or poor counting statistics. As indicated in the introduction, the feasibility of the approach depends upon three factors: First, it is possible to prepare each isomer in such a way that it is free from contamination by the other. When potassium iodide is bombarded with high-energy protons, a certain amount of I^{119} is produced. If the directly formed products, which contain both isomers of tellurium-119 are removed and the purified I^{119} is allowed to decay out, pure ground-state Te^{119} is obtained. The pure upper-state isomer is easily prepared by producing a mixture of the isomers by any of a number of means and allowing the shorter-lived ground-state isomer to decay away. The

second factor that allowed the determination of the ratios in this manner was that no isomeric transition occurs between the upper and lower state. The third is fulfillment of the necessary condition that both isomers decay to a radioactive daughter: both tellurium isomers yield Sb^{119}, which has a half life of 39 hours.

2. Theory and Method of Isomer Ratio Determination

Based upon the three above factors, a system was worked out such that the isomer ratios could be determined directly from the γ-ray spectra without recourse to a decay scheme. The method used is as follows: A tellurium-119 sample which contains only one of the isomers is purified of any Sb^{119} and then a chosen γ ray of the isomer is counted over a period of time. The activity of the tellurium counted is extrapolated back to the time when the original Sb^{119} was removed. The time of the tellurium purification is labeled t_o. The amount of Sb^{119} that has grown back into the sample of tellurium at any time during this decay process can be calculated from the standard equation for the growth of a daughter, which is

$$N_{Sb} = N^{o}_{Te} \frac{\lambda_{Te}}{\lambda_{Sb} - \lambda_{Te}} \left[\exp(-\lambda_{Te} t) - \exp(-\lambda_{Sb} t)\right] . \qquad (1)$$

In Eq. (1), N_{Sb} is the number of antimony atoms present after a period of growth t, N^{o}_{Te} is the number of tellurium-119 atoms present when the antimony was originally removed at time t_o and λ_{Sb} and λ_{Te} are decay constants of Sb^{119} and of the tellurium-119 isomer being observed.

After the Sb^{119} growing into the tellurium has reached its maximum activity, a Sb^{119} sample is separated. The time of the separation is labeled t_m. This sample is counted, corrected for yield, and the activity extrapolated back to the time of the separation (t_m). Since the activity is corrected for yield, the extrapolated value represents the total Sb^{119} activity present at time t_m.

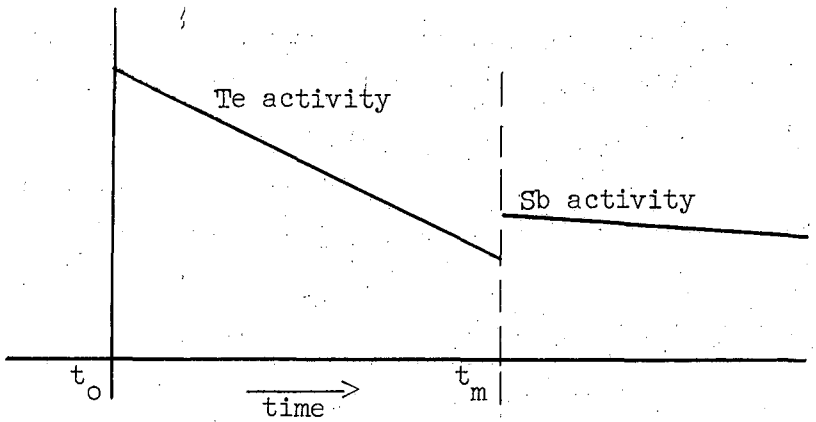

The number of atoms os Sb^{119} present at t_m is given by $N_{Sb} = (A_{Sb}/\lambda_{Sb})\ B$, where A_{Sb} is the extrapolated antimony activity, and B is a correction factor which incorporates the branching ratio, conversion coefficient, counting efficiency, etc. of the antimony. This can be rewritten in the form $N_{Sb} = A_{Sb}C$, where C is equal to B/λ_{Sb} and is completely independent of which tellurium-119 isomer is involved. Substituting the above relationship into Eq. (1), one obtains

$$N_{Sb} = A_{Sb}C = N^{o}_{Te} \frac{\lambda_{Te}}{\lambda_{Sb} - \lambda_{Te}} \left[(\exp -\lambda_{Te}t) - (\exp -\lambda_{Sb}t)\right] \qquad (2)$$

or, dividing by C,

$$A_{Sb} = N'_{Te} \frac{\lambda_{Te}}{\lambda_{Sb} - \lambda_{Te}} \left[(\exp -\lambda_{Te}t) - (\exp -\lambda_{Sb}t)\right] \qquad (3)$$

where

$$N'_{Te} = \frac{N^{o}_{Te}}{C} \quad \text{or} \quad N^{o}_{Te} = N'_{Te}C \ . \qquad (4)$$

From the counting data, A_{Sb} is known and N'_{Te} can be evaluated. N'_{Te} is related through the constant C, Eq. (4) to the true number of tellurium-119 atoms (N^{o}_{Te}) present at the beginning of the experiment.

In a similar manner the number of tellurium-119 atoms present after the original antimony purification is obtained by the extrapolation of the tellurium-119 activity to t_o. At any time, the number of tellurium-119 atoms present is related to its activity through the relation

$$A_{Te} = DN_{Te} , \qquad (5)$$

where D is a constant containing the decay constant, corrections for branching ratio, conversion coefficient, and counting efficiency of the particular isomer involved. When the time of observation is t_o, $A^{o}_{Te} = DN^{o}_{Te}$. Substitution of Eq. (4) into this equation yields

$$A^{o}_{Te} = DCN'_{Te} = EN'_{Te} \qquad (6)$$

This equation provides the relationship between the observed tellurium-119 activity at zero time and the number of tellurium-119 atoms present as calculated from the separated Sb^{119} sample. Here E is a constant which contains λ's, branching ratios, conversion coefficients, and counting efficiencies for both the Sb^{119} and the particular tellurium-119 isomer in question. Since both A^{o}_{Te} and N'_{Te} are known, the constant can be evaluated.

Exactly the same procedure is carried out for the other tellurium-119 isomer to yield the expression

$$A^{o}_{Tem} = FN'_{Tem} . \qquad (7)$$

Here F has the same meaning as E, but of course has a different value. The difference in value arises only from the different branching ratios and counting efficiencies of the second tellurium isomer. All the antimony-dependent quantities are the same, since each isomer yields the same antimony.

According to Eq. (4), N'_{Te} and N'_{Tem} are merely the numbers of atoms of each isomer divided by C, which is a strictly Sb^{119} dependent parameter. If the numbers of atoms of each isomer are equal, then according to Eq. (4) N'_{Te} must equal N'_{Tem}, and it follows by combination of Eqs. (6) and (7) that the ratio of activities must be

$$\frac{A_{Tem}}{A_{Te}} = \frac{F}{E} .$$

Therefore an isomer ratio of 1 should correspond to a counting-rate ratio of F/E. Once F and E are evaluated, the ratio of the two isomers can be easily determined at any time simply by a comparison of the counting rates of the chosen γ rays. To obtain the formation cross section one needs to compare the activities at the time of bombardment. Therefore in practice, the 16-h and 4.7-d activities are extrapolated back to the time of removal from the accelerator and the formation cross-section ratio is thereby determined.

Throughout this work the ratio $F/E = F_r$ is called the ratio factor. Evaluation of this factor is discussed in a following section.

B. Experiments

1. Procedures

The experimental procedures employed in determining the ratio factor are basically those discussed in section II. The pure Te^{119} was produced by high-energy proton bombardments of potassium iodide. The meta isomer was obtained from reactions that produced both isomers, the shorter lived ground state isomer merely being allowed to decay away before measurements were made. Often after an isomer ratio determination had been concluded, the activities of the various samples were combined and the long-lived activity used in reverifying the F_r number.

2. Choice of Gamma Rays to be Counted

The first decision required in determining the ratio factor was with respect to which γ rays should be counted. Illustrated in Fig. 10 is a γ-ray spectrum obtained from a mixture of the two isomers. The 648- and 1760-keV peaks belong to the ground-state isomer, and the balance--except for the small amount of annihilation radiation--to the upper-state isomer. Since the ground-state isomer has only two gamma peaks and the 648-keV peak is by far the more prominent, it was selected to be counted. However, for the meta isomer, three peaks at 154, 270, and 1214 keV all show up with good intensity. Originally attempts were made to obtain a ratio factor for each peak. It was soon realized, however, that two of the peaks were quite unsatisfactory. The 154- and 1214-keV peaks combine to yield a large summation peak, as shown in Fig. 10. Therefore if one of these peaks was to be used, it would be desirable to make some sort of correction for the summation. Since the amount of summation is strongly dependent upon source-to-crystal distance, any change in geometry would result in differences in the relative number of counts under the peaks and a consequent change in the ratio factor. With regard to the 1214-keV peak, it was also difficult to determine how the background should be subtracted out because of the nearby summation peak. The 154-keV peak was found to be undesirable for two reasons. First, superimposed upon the low-energy side of the peak at 127-keV is the "escape peak," which results from escape from the detector of the iodine K x-ray. This effect itself would not be too serious, but a second and more serious problem makes use of the 154-keV peak impossible. Te^{121m}, which is often formed in the irradiations, has a 201-keV γ ray. This peak is unresolvable from the 153-keV peak, and accounts at least in part for the perturbation on the high-energy side of the 153-keV peak. On the basis of the above arguments and because of consistency of results obtained in preliminary experiments, the peak chosen for use in determining F_r is that at 270 keV.

3. Background Subtraction

Although the 270-keV γ ray of the Te^{119m} spectra was the most logical peak to count for the isomer ratio determination, there was still

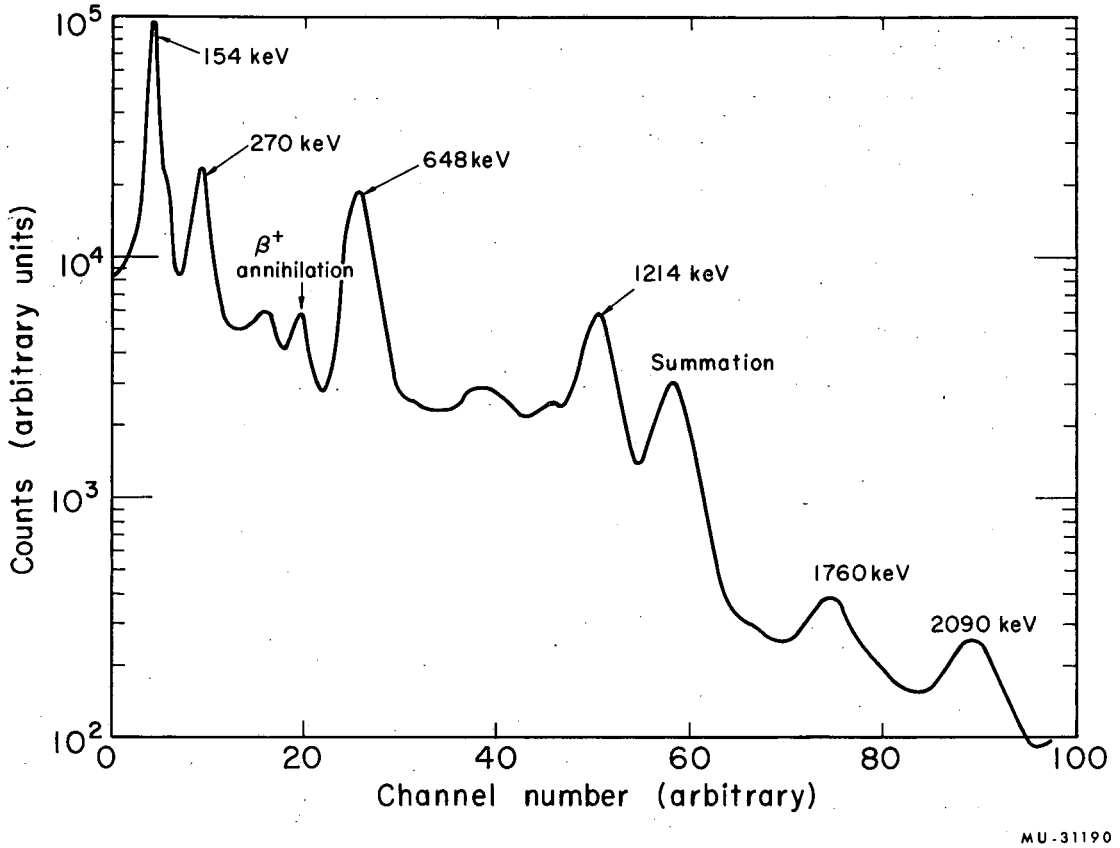

Fig. 10. Combined γ-ray spectra of Te^{119} and Te^{119m}.

a difficult problem that had to be solved. This was the variation in the shape of the spectrum caused either by large amounts of positron-annihilation radiation at 511 keV, or by large amounts of the ground-state isomer peak at 648 keV. Both these peaks tended to produce rather drastic changes in the shape of the background lying beneath the 270-keV peak, because the 270-keV peak lies in the area of their Compton-scatter radiation. Figures 11 and 12 illustrate the variation in shape caused by a change in the amount of positron-annihilation radiation. Figure 13 illustrates the additional effect of adding in the 648-keV peak due to Te^{119}. Since the background across channels 7 through 13, where the 270-keV peak falls, is normally rather smooth, the main problem involved finding out how much the background line should be moved up or down as the high-energy peak intensities varied.

To solve the problem, artifical spectra were created with various amounts of the 511- and 648-keV peaks present. An example is shown in Fig. 14, where an attempt has been made to duplicate by artifical means the true spectrum of a mixture of the tellurium isomers. The method employed in such an analysis is as follows: The tellurium activity was counted and plotted. Sources were then chosen that had peaks corresponding as nearly as possible in energy to those of the tellurium spectrum. Starting with the highest-energy gamma peaks, these sources were counted until the oscilloscope display on the analyzer indicated that a peak of approximately the same size as in the tellurium spectrum had been created. The spectrum was then plotted out, but not erased from the analyzer. The next highest energy peak was then added by the same procedure. The process was continued until the spectrum was complete. Occasionally small changes in gain were made in order to make the peaks fall in the correct channels. Figure 14 illustrates a spectrum created in this manner, and shows the shape and approximate height of the background that might be expected to fall under the 270-keV peak. Figure 15 shows the background variation that occurs as the spectrum is sequentially built up. The 270- and 154-keV peaks have also been added. Figure 16 shows in solid line the actual tellurium spectrum and in dotted line the artificial

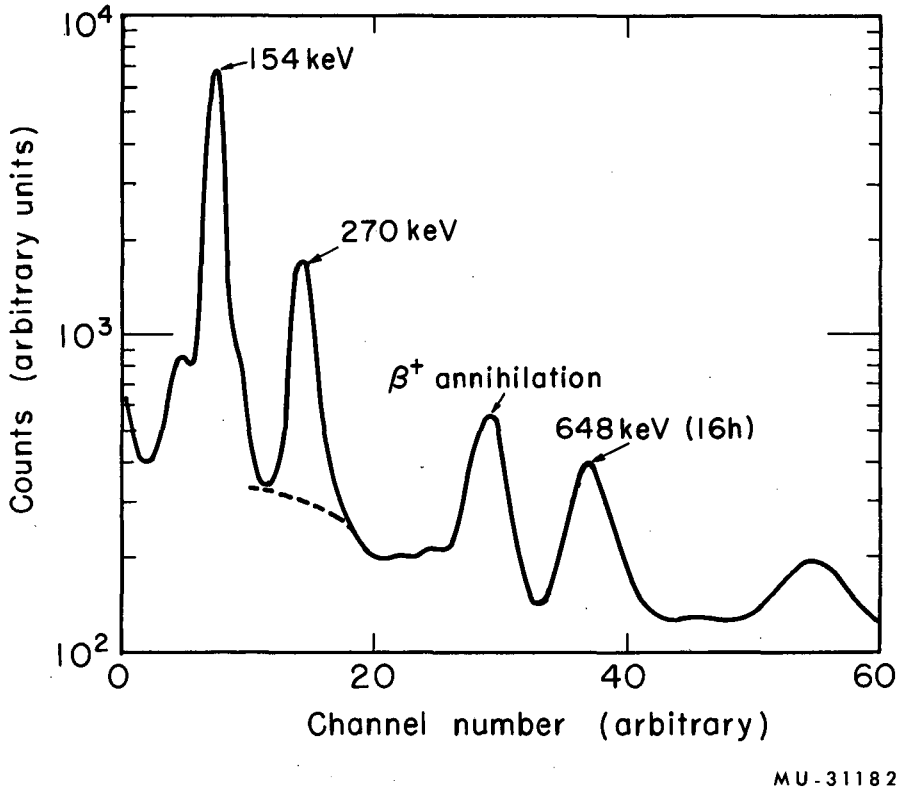

Fig. 11. Te^{119m} spectrum containing only a small amount of positron-annihilation radiation contamination.

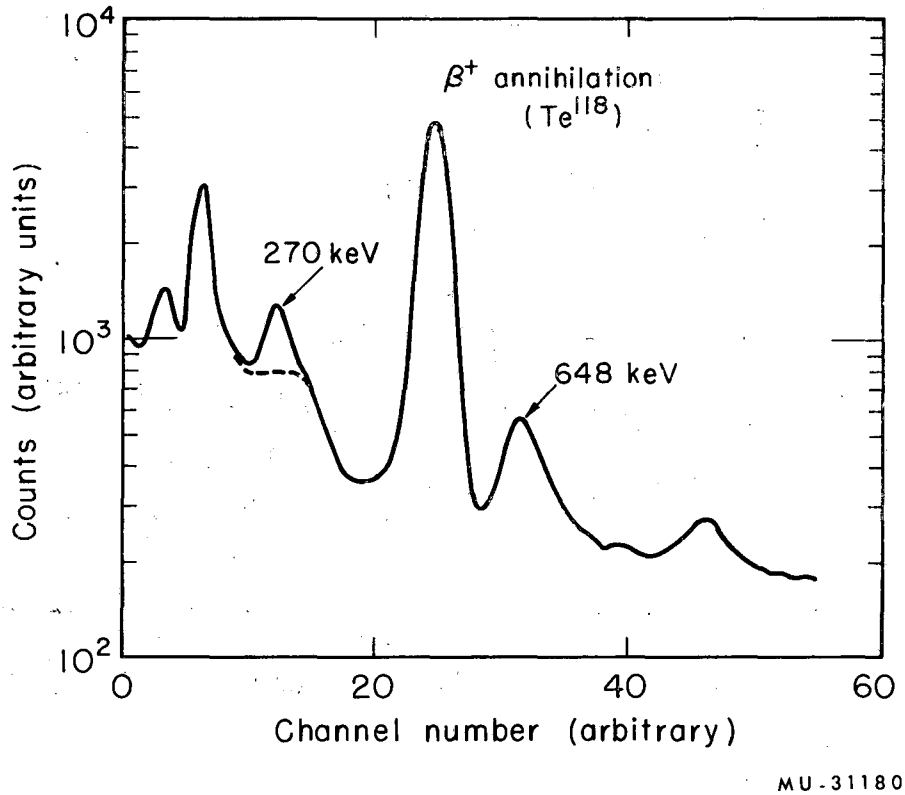

Fig. 12. Te^{119m} spectrum containing a large amount of positron-annihilation radiation contamination. Note how the background under the 270-keV Te^{119m} peak has been increased.

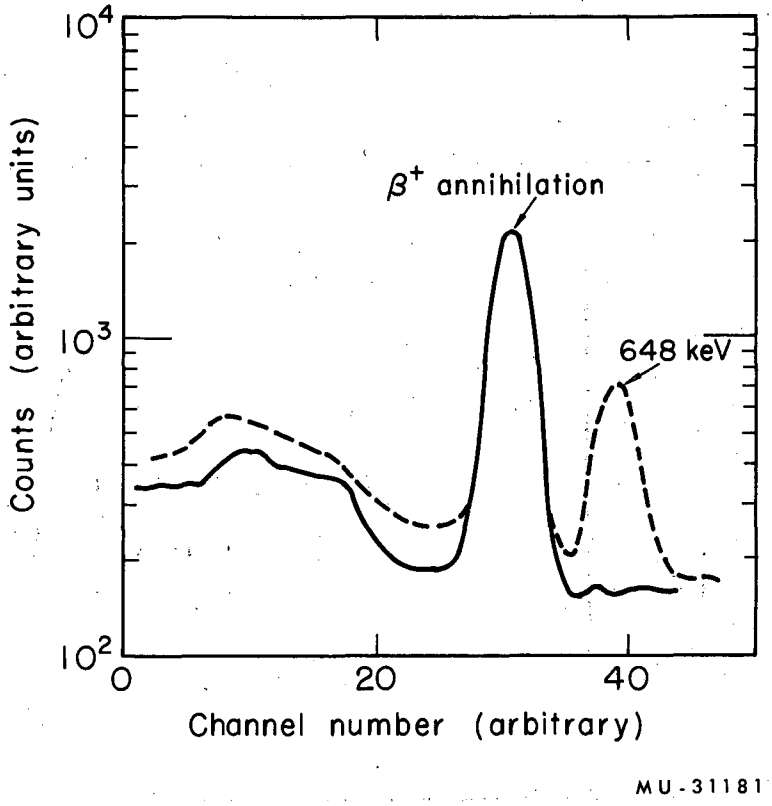

Fig. 13. Contribution of Compton scattering radiation to the background under the 270-keV peak of Te^{119m} of both positron-annihilation radiation and the 648-keV peak of Te^{119}.

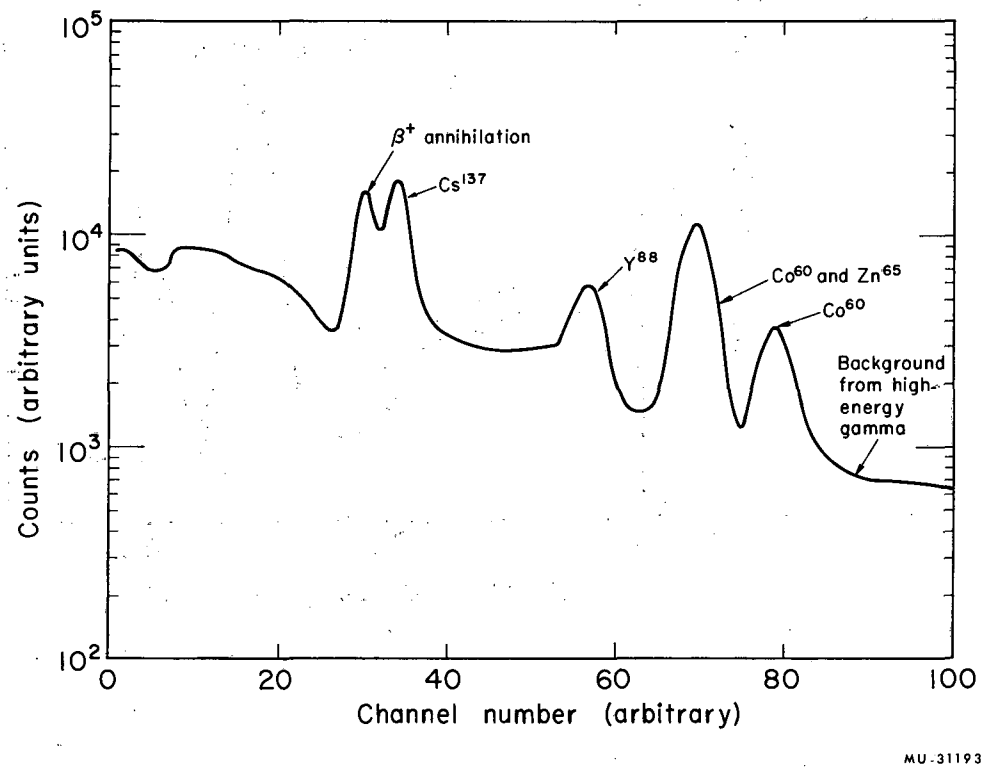

Fig. 14. Artificially created γ-ray spectrum showing the expected background shape under the 270-keV Te^{119m} γ-ray peak.

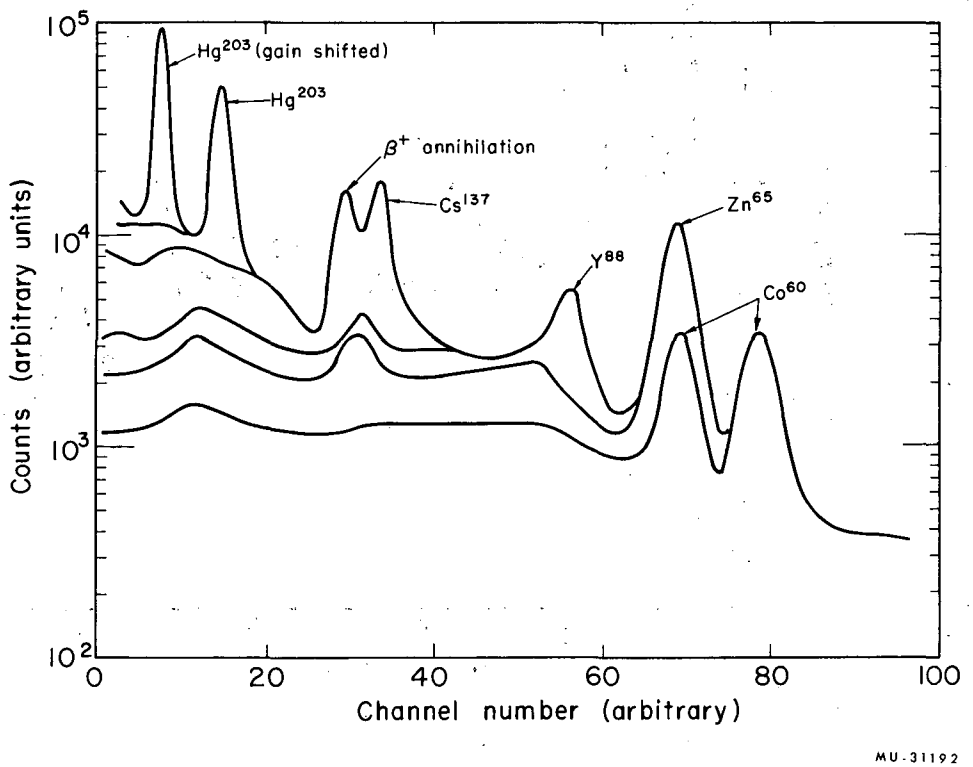

Fig. 15. Artificially created γ-ray spectrum showing the sequential buildup of background radiation under the 270-keV peak due to the various high-energy γ rays belonging to Te^{119} and Te^{119m}.

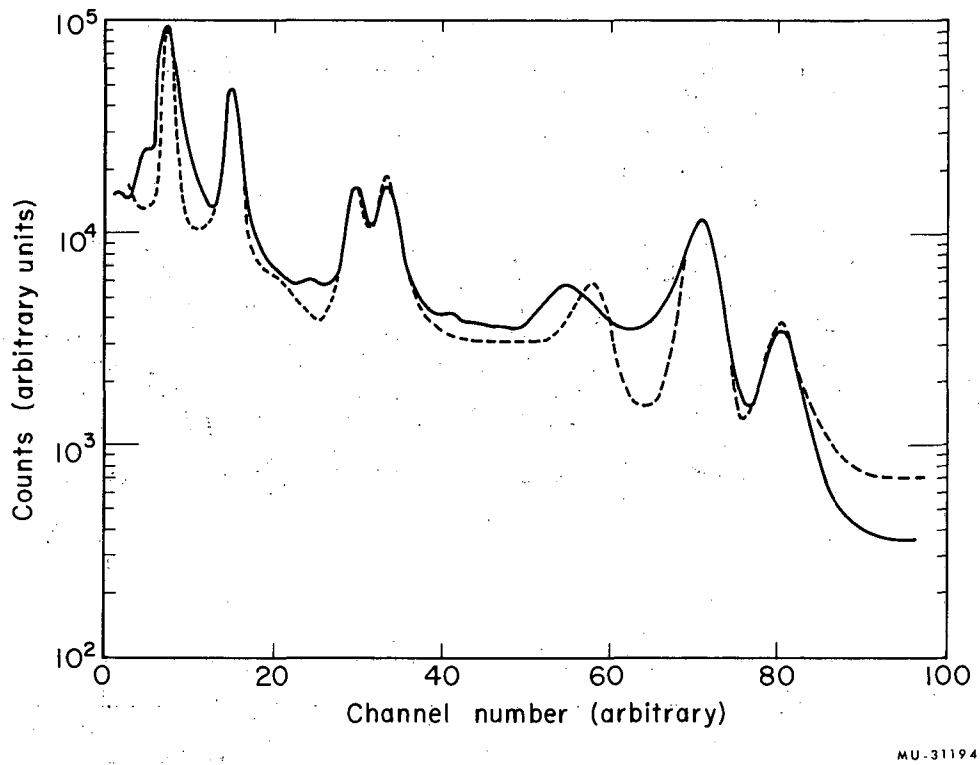

Fig. 16. Comparison of artificially created γ-ray spectrum (dashed line) and actual spectrum of Te^{119} and Te^{119m} (solid line).

spectrum created by the procedure described. By this means it was possible to obtain at least a good estimation of the background shape underlying the 270-keV peak under a variety of conditions. This method became most important when the isomer ratios were being measured at high excitation energies. At high energies the 4n reaction becomes very strong and the Te^{118} thus formed has a 3.5-min antimony daughter which is a pure positron emitter. Consequently the positron annihilation peak becomes very high. This effect is seen in Fig. 12.

The background subtraction under the 16-h 648-keV peak normally offered little problem. Most spectra were more or less of the shape shown in Fig. 10, and a nearly straight line across the bottom of the peak was a good approximation. For Te^{119} that contained no Te^{119m}, the spectrum appeared as shown in Fig. 17. The background subtraction is shown by the dotted lines. Some positron-annihilation radiation resulting from Te^{118} was always present, and this somewhat complicated the subtraction.

If the background subtraction was incorrectly accomplished it was usually observed by the scatter of points about the decay curve or by an incorrect half life. It should be mentioned that even if the background correction were not exactly right, a consistent error would not affect the isomer ratio. Since the ratio factor is determined experimentally in the same manner as the ratios, any consistent error would cancel out in division.

4. Experimental Results

On the basis of procedures described in the foregoing sections the experimental value of F_r was determined. It should be mentioned that early in the experiments the geometry of the counting arrangement was somewhat altered, the sample being moved closer to the face of the detector. Since the relative counting efficiency for two γ rays of different energy is a function of the distance from the detector, this move resulted in a somewhat different value for the constants E and F defined by Eqs. (6) and (7). The effect was rather small, and since the early geometry was used on only three isomer-ratio determinations the values are not tabulated in this work. The experimentally determined values of E and F used for the determination of isomer ratios in this investigation are listed in Tables II and III.

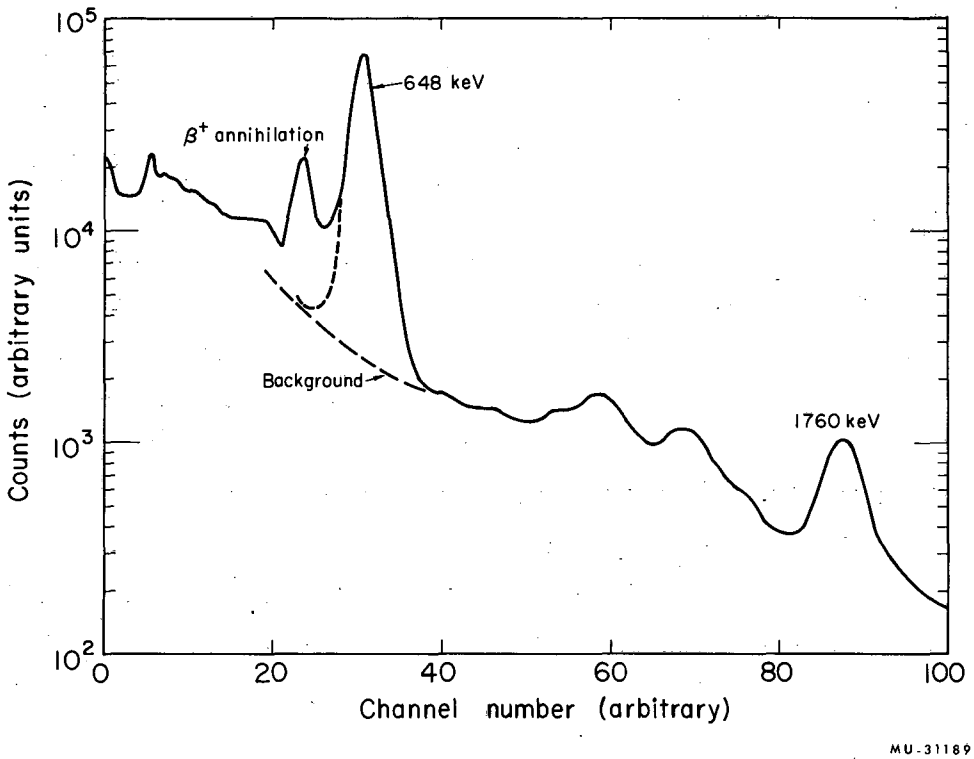

Fig. 17. Gamma-ray spectrum of ground-state tellurium-119. The positron annihilation radiation is probably due to Te^{118}. The lack of a peak at about channel 6 indicates that very little of the upper-state isomer is present (compare with Fig. 12).

Table II. Experimentally determined values for the constant E, defined $A^{o}_{Te^{119}} = E\, N'_{Te^{119}}$.

Experiment number	E	Deviation from mean
54	2.26	0.11
54	2.14	0.01
54	2.27	0.12
54	2.24	0.09
48	2.21	0.06
48	2.16	0.01
48	2.17	0.02
48	2.17	0.02
48	2.17	0.02
48	2.17	0.02
56	2.15	0.00
56	2.10	0.05
56	2.13	0.02
56	2.13	0.02
56	2.09	0.06
56	2.07	0.08
56	2.18	0.03
56	2.09	0.06
56	2.05	0.10
56	2.20	0.05
68	2.17	0.02
68	2.23	0.08
68	2.25	0.10
68	2.15	0.00
68	2.15	0.00
68	2.09	0.06

Mean = 2.15

Standard deviation = 0.059

Value of E = 2.15 ± 0.059

Table III. Experimentally determined values for the constant F, defined by $A^{o}_{Te\ 119m} = F\ N'_{Te\ 119m}$.

Experiment number	F	Deviation from mean
40	0.163	0.010
40	0.157	0.004
40	0.161	0.008
40	0.160	0.007
40	0.162	0.009
58	0.147	0.006
58	0.143	0.010
64	0.144	0.009
64	0.153	0.000
64	0.144	0.009
64	0.150	0.003
64	0.155	0.002
64	0.157	0.004
66	0.143	0.010
66	0.167	0.014
66	0.144	0.009
66	0.154	0.001
66	0.152	0.001
66	0.152	0.001

Mean = 0.153

Standard deviation = 0.0073

Value of F = 0.153 ± 0.0073

Ratio Factor F_r = F/E = (0.153 ± 0.0073)/(2.15 ± 0.059) = 0.0712 ± 0.0039

The value of E was found to be 2.15 ± 0.059 and that of F 0.153 ± 0.0073. Therefore when the number of atoms of Te^{119m} equals the number of atoms of Te^{119}, the ratio of counts under the 270-keV peak to those under the 648-keV peak should be (0.153 ± 0.003) /(2.15±0.059) = 0.0712 ± 0.0039. When the particular γ rays in question are allowed to decay away and their counting rates extrapolated back to the time of removal from the accelerator, a ratio of the 270-keV to 648-keV activities divided by 0.0712 ± 0.0039 yields the isomer ratio at the time of removal from the accelerator. An additional correction must be applied to account for the decay during bombardment in order to determine the formation cross-section ratio.

C. Correction for Decay During Bombardment

The following equation was obtained from Friedlander and Kennedy.[57]

$$N_t = (R/\lambda)(1 - e^{-\lambda t}). \qquad (8)$$

In this equation N_t is the number of atoms present at any time t during a bombardment, λ is the decay constant of the particular material being formed, and R is its rate of production. Now, the rate of decay of N_t atoms of a material at any time t is given by

$$dN/dt = N_t\lambda \text{ , or } N_t = (1/\lambda)\,(dN/dt). \qquad (9)$$

Substituting Eq. (9) into Eq. (8) yields

$$(1/\lambda)\,(dN/dt) = (R/\lambda)\,(1 - e^{-\lambda t}) \text{ or } dN/dt = R(1 - e^{-\lambda t}). \qquad (10)$$

However, if the rate of production R is constant, then R = N/t, where t is the total duration of bombardment and N is the total number of atoms produced. Since the isomer ratio is determined from the relative activities of the isomers, it is necessary to compare the disintegration

rate at the end of the bombardment with what it would have been if all the atoms produced were present together at the end of the bombardment. The disintegration rate during bombardment is given by Eq. (10). If N/t is substituted for R, the equation can be rewritten as

$$dN/dt = N(1 - e^{-\lambda t})/t , \qquad (11)$$

where N is the total number of atoms produced and t is the duration of the bombardment. If all the atoms formed were present at the end of the bombardment the disintegration rate would be $dN'/dt = \lambda N$. The correction factor is therefore the ratio of the two rates or

$$\frac{(dN'/dt)}{(dN/dt)} = \frac{N\lambda}{\frac{N}{t}(1 - e^{-\lambda t})} = \frac{\lambda t}{(1 - e^{-\lambda t})} . \qquad (12)$$

Equation (12) provides a factor that converts the measured activity at the end of the bombardment to what it would have been if all the atoms produced were present at one time. Such a factor is applied to both isomers and the true formation cross-section ratio is thereby obtained. An example of such a correction is given below:

16-hour isomer: The decay constant is 4.15×10^{-2} and the duration of bombardment is 4 h. Substitution into Eq. (12) yields a correction factor of 0.920. This means that 92% of all the Te^{119} atoms formed are present at the end of the bombardment.

4.7-day isomer: The decay constant is 6.13×10^{-3} and the duration of bombardment is 4 h. Substitution as above yields a correction factor of 0.985. Therefore 98.5% of all Te^{119m} atoms formed during the bombardment are present at its termination.

According to the above calculations, for a 4-h bombardment the ratio of the high-spin isomer to the low-spin isomer at the end of the bombardment must be multiplied by 0.920/0.985 in order to correct for the decay during the bombardment. A tabulation of correction factors showing the effect of decay during bombardment is given in Table IV.

Table IV. Correction for decay during bombardment as a function of the duration of bombardment.

Duration of bombardment (h)	Correction for ground-state isomer	Correction for meta-state isomer	Total decay factor
0.5	0.987	0.999	0.988
1.0	0.978	0.997	0.982
1.5	0.969	0.995	0.974
2.0	0.960	0.994	0.966
2.5	0.950	0.992	0.959
3.0	0.941	0.990	0.951
3.5	0.932	0.988	0.943
4.0	0.922	0.987	0.934
5.0	0.903	0.983	0.918
6.0	0.885	0.980	0.903
7.0	0.867	0.977	0.888
8.0	0.849	0.974	0.872
9.0	0.830	0.970	0.855
10.0	0.812	0.967	0.840

[a] The total decay factor is the correction for the ground-state isomer divided for the correction for the upper-state isomer. When this number is multiplied by the ratio of upper- to lower-state isomer at the end of the bombardment, the true formation cross-section ratio is obtained.

IV. ISOMER RATIO MEASUREMENTS

A. General Discussion

In this investigation three different compound nuclei, all leading to the isomers of tellurium-119, were produced. By bombardment of the appropriate tin isotopes with He^3 and He^4, the compound nuclei Te^{121*} and Te^{123*} were each produced by two different paths. He^3, He^4, Li^7, C^{12}, and O^{18} were used as the projectiles and the compound nucleus Te^{122*} was produced in five different reactions.

The accelerators used for measurements of the formation cross-section ratios were the Crocker Laboratory 60-inch cyclotron and the Berkeley heavy-ion linear accelerator (Hilac). The 60-inch cyclotron was used for most of the He^4-ion bombardments. Bombardments utilizing the other ions and a few using He^4 were conducted at the Hilac.

The target technique employed throughout the determinations was that of stacked foils. By this means ratios for the various reactions were obtained over a wide range of energies. In bombardments involving the lighter ions such as He^3, He^4, and Li^7 as many as 20 foils were employed in a single bombardment. On the other hand, in the O^{18} bombardments only five foils could be used. The backing foils upon which the target materials were electroplated were of copper, nickel, or gold. The thickness of the backing foil and that of the target material were determined by weighing on a microbalance. The balance was capable of weighing accurately to 20 micrograms, therefore any error introduced by weighing should be quite small.

Range-energy data were available for only a very few of the projectile-target combinations employed in this work. All ranges were calculated by using as a basis the data of Hubbard,[58] Northcliffe,[59] and Sternheimer.[60] The calculations of the various range-energy relationships are given in the Appendix. Also included are the range-energy plots used in these experiments.

The energy uncertainties shown in the results of this section are actually associated with the degradation of the beam caused by the target material itself. All targets except those of indium were constructed by electroplating the appropriate material on a backing foil. Indium was attached to the foil by means of an evaporation process. The foil thicknesses were chosen so that the beam degradation corresponded to conveniently spaced energy points. For the lighter projectiles the degradation of the beam energy by the target material was nearly negligible. For the heavy ions, however, the energy loss sometimes amounted to several MeV. The energy spread shown in the results is merely the energy loss encountered by the beam on passing through the target material. The separation between points represents the beam energy loss upon passing through the backing foil.

There is also a certain particle-energy uncertainty associated with the accelerator itself. The He^4 ions emerging from the Crocker Laboratory 60-inch cyclotron have a range spread in aluminum of approximately 5 mg/cm^2. This is about 2% of the total range, and amounts to about 1 MeV uncertainty at full energy (48.3 MeV).[61] The effect of passing through degrading foils is to increase the energy spread, with the result that at 20 MeV the uncertainty is somewhat greater than 1 MeV.

The beam energy of the Hilac is 10.4 ± 0.2 MeV per nucleon.[62] It therefore possesses an inherent uncertainty of approximately 2%. Also, with heavy ions the energy loss upon passing through matter is so very high that any errors in foil or degrader thickness are magnified in the beam-energy uncertainty. Since, in all reactions studied, the Hilac beam was degraded to about half its maximum energy by means of aluminum absorbers before striking the target, the energy uncertainty may be rather high. The energies are estimated to be accurate to within about 5%. Any error of this nature for a given irradiation should be a systematic one and might be hard to detect. However, comparison with other results for the same reaction would result in a scatter of data points. A certain amount of scatter is seen between experiments involving heavy ions.

The intensity, over a 2-cm^2 area, of the He^4 beam used at the 60-inch cyclotron was 0.5 to 1.0 μA. Occasionally higher-intensity beams were employed, but they often resulted in fused target foils and loss of the experiment. The beam intensity at the Hilac depended upon the ion being accelerated. In all cases except Li^7, a 3/8-in. collimator was placed in front of the target and all the beam available was used. With Li^7 the targets were constructed differently and a collimator 5/8 in. in diameter was used to scavenge all the beam possible. The following beam intensities were normally available: He^3, 0.3 to 0.5 μA; He^4, 0.5 to 1.0 μA; Li^7, 0.06 to 0.07 μA; C^{12}, 0.5 to 1.0 μA; and O^{18}, 0.1 to 0.2 μA.

Throughout the work, the normalizing parameter between the different reactions producing the same compound nucleus was the excitation energy of the compound system. It was generally assumed that, except for the angular momentum, two or more compound nuclei produced by different means but of the same excitation energy were identical. For this reason, unless otherwise stated, all tabulations and figures are plotted as a function of the excitation energy of the compound nucleus. This excitation is calculated from the laboratory-system energy of the incident particle according to

$$E^* = Q + E_L - E_R \ , \qquad (13)$$

where E^* is the excitation of the compound nucleus, E_R is the recoil energy of the system, E_L is the lab energy of the projectile, and Q is the energy provided by the reaction

$$A + B = E^* + Q \ . \qquad (14)$$

The recoil energy E_R can be calculated by means of the equation

$$E_R = E_L \, m/(m + M) \ , \qquad (15)$$

where m is the mass of the projectile and M the mass of the target. Equations (13) and (15) can then be combined to yield

$$E^* = E_L\,[M/(m + M)] + Q\ . \qquad (16)$$

The masses used in determing the value of Q for the various reactions are taken from the calculations by Seeger.[63] By means of these equations each laboratory-system bombardment energy was converted into an excitation energy of the compound nucleus. Plots showing the conversion from lab energy of the projectile to excitation energy of the compound nucleus are given in the Appendix.

It was also desirable to calculate the threshold energies for the various reactions. The general reaction may be illustrated as

$$A + B \longrightarrow Te^{119} + xn + Q'\ . \qquad (17)$$

A and B represent the various target and projectile combinations, n represents a neutron, and x a number. In this investigation x takes the values 2, 3, and 4. In the center-of-mass system Q' is the energy required or emitted by the reaction. It represents the mass deficit between products and reactants, or the energy that must be supplied by a projectile to make the reaction energetically possible.

In calculating the lab energy of a projectile necessary to provide Q' for the reaction process, one must add to Q' the recoil energy of the system and the kinetic energy of the neutrons. By this means, with zero kinetic energy assumed for the neutrons, the energy thresholds have been calculated. These values are given in Table V. Below these projectile energy thresholds it is energetically impossible for the reaction to occur.

Table V. Projectile threshold energies (laboratory system) and Coulomb barrier heights for the various reactions

Reaction	Threshold energy (MeV)	Coulomb barrier (MeV)
$He^3 + Sn^{118} \longrightarrow Te^{119} + 2n$	4.8	16.2
$He^4 + Sn^{117} \longrightarrow Te^{119} + 2n$	14.3	15.9
$He^3 + Sn^{120} \longrightarrow Te^{119} + 4n$	20.8	16.2
$He^4 + Sn^{119} \longrightarrow Te^{119} + 4n$	30.8	15.9
$He^3 + Sn^{119} \longrightarrow Te^{119} + 3n$	11.7	16.2
$He^4 + Sn^{118} \longrightarrow Te^{119} + 3n$	23.7	15.9
$Li^7 + In^{115} \longrightarrow Te^{119} + 3n$	11.8	22.4
$C^{12} + Pe^{110} \longrightarrow Te^{119} + 3n$	27.5	40.0
$O^{18} + Ru^{104} \longrightarrow Te^{119} + 3n$	29.9	47.1

Although no reaction is thermodynamically possible below the threshold energy, another factor of equal importance in this investigation is the Coulomb barrier. If a particle approaches a nucleus with a kinetic energy less than the height of the Coulomb barrier it will not be able to reach the nuclear surface. In this investigation approximately half of all the reactions have a Coulbomb barrier that is higher than the threshold energy. In these cases, any of the projectiles that have the energy necessary to penetrate the Coulomb barrier have more than enough energy to make the reaction thermodynamically possible. The Coulomb barrier in these cases forms the low-energy limit for production of the isomers.

The Coulomb barrier, in ergs, may be calculated by the quation

$$E_b = z_1 z_2 / R , \qquad (18)$$

where z_1 and z_2 are the charges of the incident particle and nucleus, in esu, and R is the distance in cm between their centers when they are in contact.[64] R is approximated according to the equation

$$R = 1.4 \times 10^{-13} (A_1^{1/3} + A_2^{1/3}) \qquad (19)$$

where A_1 and A_2 are the mass numbers of the incident particle and nucleus. The barrier heights for the reactions under consideration are listed in Table V.

The activity levels obtained in the various bombardments ranged from less than 100 counts/min for one of the O^{18} bombardments to hundreds of thousands of counts per minute for some of the He^4 bombardments. Most activities were in the range of tens of thousands to low hundreds of thousands of counts per minute. Most samples were counted for slightly longer than a week, or through approximately two half lives of the longer-lived isomer. New samples that contained the 16-h activity were counted

four or five times a day for the first two days and less often after the 16-h isomer had disappeared. When only the 4.7-d isomer remained the samples were counted once or twice a day. After counting, the sample spectra were plotted either by hand or by means of the automatic recorder described in an earlier section. After background subtraction and yield corrections the activities of the 270- and 648-keV gamma peaks were extrapolated back to the time of removal from the accelerator. The number obtained by the extrapolation represented the total activity of the peak, since all samples were corrected for yield losses in the chemistry. After correction for decay during bombardment, dividing the ratio of the 270-keV peak to the 648-keV peak by the ratio factor gave the isomer-formation cross-section ratio.

Since each sample yielded an isomer ratio, poor statistics in the counting resulted in uncertainties of the ratio. The uncertainties in the ratio were determined in the following manner. When the decay of the samples was plotted, there was normally a certain amount of scatter among the points. For the 648-keV peak the background subtraction was relatively easy to perform, and in the great majority of cases the scatter of points was negligible. Plastic templates cut to represent the slope for the correct half life on the graph paper employed often yielded a line that passed through every single point. On the other hand, the background subtraction under the 270-keV peak was more difficult, and a certain amount of point scatter about the correct half life usually occurred. When such scatter did occur two lines, each with the slope for the correct half life, were drawn bracketing the points. The intercepts of the lines were both used to calculate an isomer ratio. The ratios thereby obtained served to define the uncertainty of the determination.

On occasion, especially at high energies for which the 3n reaction cross section is small compared with that of the 4n reaction, the background subtraction under the 648-keV peak was also rather poor. This resulted in point scatter about its decay curve as well as about that of

the 270-keV peak. When this occurred, the points for each activity were bracketed with correct half-life lines. This procedure yielded two intercepts for the 270-keV peak and two for the 648-keV peak. The uncertainty of the ratio was then defined by dividing the lowest and highest 270-keV intercept respectively by the highest and lowest 648-keV peak intercept.

The uncertainty given by the above procedure always increased with projectile energy, corresponding to an increase in the size of the positron annihilation peak. At low energies, for most samples, the uncertainty was no more than about 2%, but at high energies it sometimes approached 10%.

In the plots and tabulations each of the data points represents the midpoint of the two ratios determined as described above. The deviation is the amount that must be added or subtracted to the midpoint to obtain the two graphically determined ratios.

Approximately 20 samples, chosen at random, were also analyzed by making least-squares fits of the counting data. The chosen samples had both small and large uncertainties as determined by the foregoing method. In most cases the least-squares fit was very close to the midpoint of the data obtained by the first method, but the mathematical analysis assigned much smaller errors. If, for the tabulated data obtained by the first method, one selects the midpoint as the value and the limits of the ratio as the uncertainty, the deviation thus assigned is approximately three times the standard deviation obtained by the least-squares analysis.

All graphs are plotted in terms of the graphically determined ratios and the error bars are approximately three times as long as they would be for the same counting data if a least-squares analysis were employed. The true ratio at each energy, therefore, probably lies very close to the midpoint.

All targets except those of In^{115} were prepared by electroplating the target material onto a copper, nickel, or gold backing foil. The electrolysis cell devised and used for the target preparations is shown in Fig. 18. The cell was constucted of a brass stand and a Teflon cylinder. In use, the backing foil was placed on the stand and the cylinder tightened against it to form a watertight cell by means of the wing nuts. The Teflon had enough flexibility that no gasket was necessary. The solution to be electrolyzed was placed in the cell and a platinum anode was placed in the solution and supported by means of a cork stopper. The brass stand as a whole served as an electrical connection for the foil cathode. The hole through the Teflon was 5/8 in. in diameter, and uniform plates of target material of the same size were therefore obtained. Most plating was done at a voltage of 1.5 to 3 volts. The cell proved thoroughly successful, and it was possible to use quite thin backing foils in the process. The plates thus obtained were usually in the thickness range 0.4 to 0.6 mg/cm^2.

The individual procedures used in preparing the various targets are treated in detail in Appendix C. Also given in Appendix C is the chemistry required for the purification of the tellurium obtained in bombardment of the various materials.

B. Reactions Yielding the Compound Nucleus Te^{122*}

The main emphasis of the work was directed toward the reactions which yielded the compound nucleus Te^{122*}. These reactions will therefore be discussed first. Many of the procedures employed for the various reactions, such as the target preparation and chemical purification, were more or less the same. As mentioned before, such precedures are discussed in the Appendix.

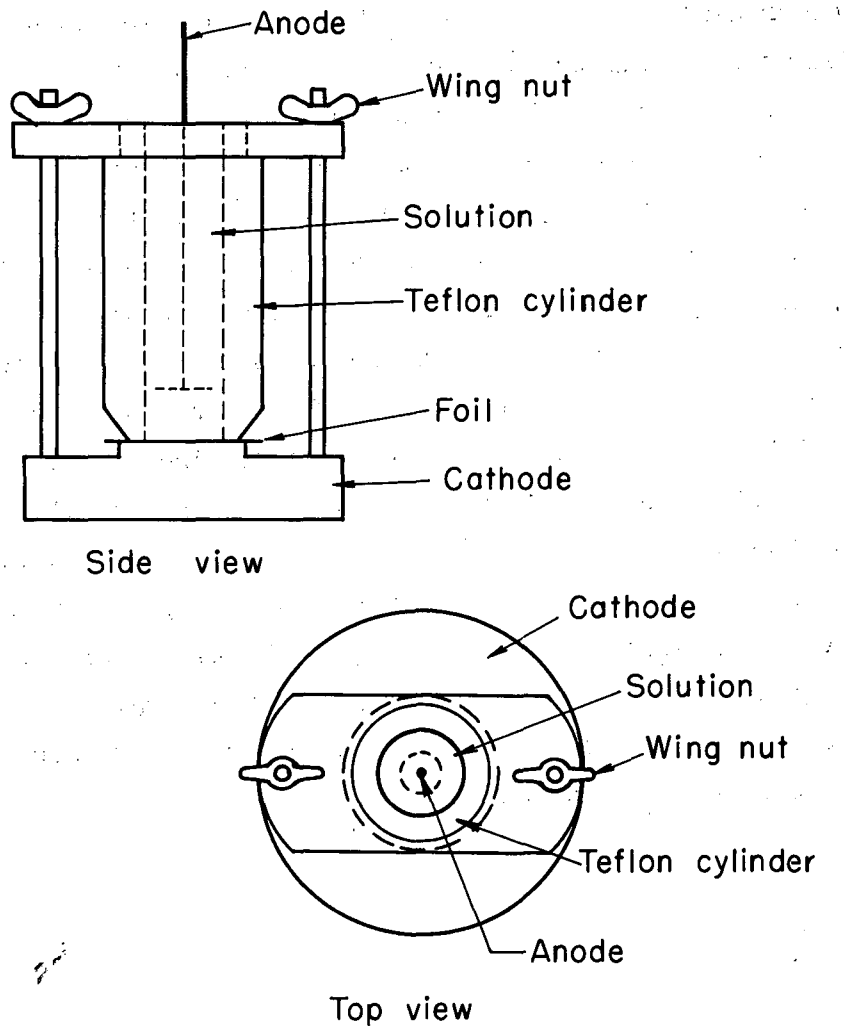

Fig. 18. Electroplating cell used for production of targets.

1. The Reaction $He^3 + Sn^{119} \longrightarrow Te^{119, 119m} + 3n$.

a. Target Assembly

All He^3 bombardments were performed at the Hilac; the target holder used is illustrated in Fig. 19. The target was assembled as follows: a foil produced by the electroplating procedure[65] consisted of a 1-in-square backing foil and a 5/8-in-diam circle of target material in the center of the square. The isotopic enrichment of the target material is given in Table VI.[66] Separators made of 20-mil aluminum and containing a 3/4-in.-diameter hole were used to keep the individual target foils apart. The targets were arranged with the plated material toward the beam, and one of the aluminum separators was placed between each foil and the next. The stack usually consisted of about 10 foils. No degraders were necessary, since the full beam energy was required. Over the front foil was placed a 1/4-mil aluminum cover foil and then a heavy aluminum collimator with a 1/2-in. hole. The accelerator itself also contained a collimator with a 3/8-in.-diameter hole. The beam was required to pass through both collimators before striking the target. The Faraday cup consisted of the target assembly itself, and the beam current could thereby be monitored. Bombardments were usually of about 4 hours' duration.

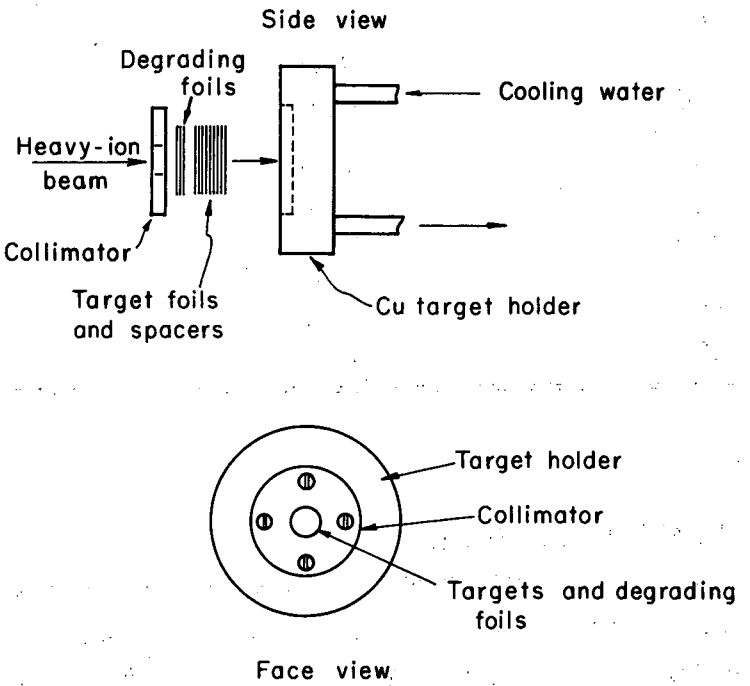

Fig. 19. Copper target assembly used for all Hilac bombardments.

Table VI. Analysis of isotopically enriched Sn^{119}.

Isotope	Atomic Percent	Precision
112	0.3	± 0.05
114	0.2	0.05
115	0.2	0.05
116	0.5	0.05
117	0.4	0.05
118	3.6	0.05
119	85.9	0.1
120	8.5	0.05
122	0.4	0.05
124	0.3	0.05

b. Experiemental Results

The end product resulting from all the above procedure is the formation cross-section ratios for the two isomers of tellurium-119. The results for the He^3 bombardments of Sn^{119} are given in Table VII. A plot of these tabulated data is given in Fig. 20.

Table VII. Formation cross-section ratios of the isomers of tellurium-119 produced in the reaction $He^3 + Sn^{119} \longrightarrow Te^{119, 119m} + 3n$.

Experiment number	Sample number	Projectile energy (MeV)	Excitation energy (MeV)	Isomer ratio (Te^{119m}/Te^{119})
44	1	31.1	46.3	1.40 ± 0.01
	2	28.6	43.8	1.05 ± 0.05
	3	25.9	41.0	0.95 ± 0.05
	4	22.7	37.9	0.90 ± 0.10
	5	19.5	34.8	0.90 ± 0.10
	6	15.6	31.0	0.55 ± 0.05
45	1	30.5 - 31.1	45.6 - 46.3	1.20 ± 0.10
	2	29.7 - 29.8	44.7 - 44.8	1.15 ± 0.15
	3	28.2 - 28.3	43.4 - 43.5	1.05 ± 0.05
	4	26.7 - 26.8	41.9 - 42.0	1.10 ± 0.10
	5	25.1 - 25.2	40.3 - 40.4	1.20 ± 0.10
	6	23.6 - 23.7	38.8 - 38.9	1.25 ± 0.05
	7	21.9 - 22.0	37.2 - 37.3	1.05 ± 0.05
	8	20.1 - 20.2	35.4 - 35.5	1.15 ± 0.05
	9	18.2 - 18.3	33.5 - 33.6	0.85 ± 0.05
	10	16.1 - 16.2	31.4 - 31.5	0.65 ± 0.05
50	1	31.0 - 31.1	46.1 - 46.2	1.40 ± 0.20
	2	29.5 - 29.6	44.6 - 44.7	1.25 ± 0.15
	3	28.0	43.2	1.20 ± 0.20
	4	26.3 - 26.4	41.5 - 41.6	0.95 ± 0.15
	5	24.3 - 24.4	39.6 - 39.7	1.40 ± 0.20
	6	22.1 - 22.2	37.4 - 37.5	1.25 ± 0.15
	7	19.8 - 19.9	34.1 - 34.2	1.20 ± 0.10
	8	17.3 - 17.4	32.7 - 32.8	1.10 ± 0.20
	9	14.4 - 14.5	29.9 - 30.0	1.05 ± 0.15
	10	11.1 - 11.2	26.8 - 26.9	0.95 ± 0.25

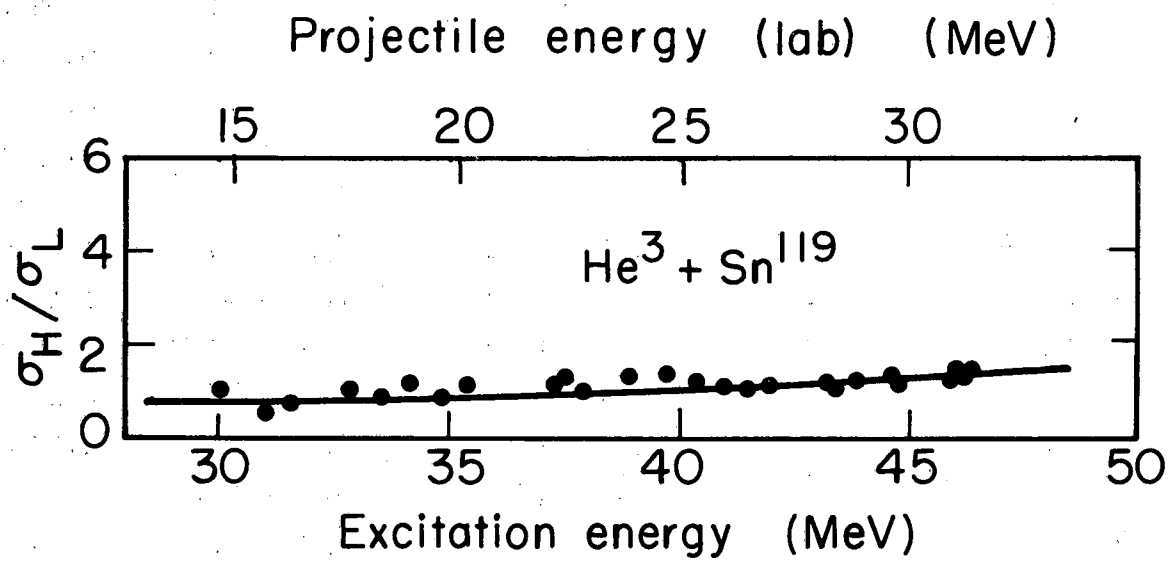

MU-31214

Fig. 20. Experimentally determined formation cross-section ratios for the isomers of tellurium-119 produced in the reaction $He^3 + Sn^{119} \longrightarrow Te^{119,\ 119m} + 3n$.

It will be noticed that the isotopically enriched Sn^{119} contained appreciable amounts of Sn^{118} and Sn^{120}. It is expected that these two isotopes will also have contributed through a 2n and a 4n reaction respectively to the tellurium-119 that was measured. However, over the energy range considered, both the 2n and 4n reaction yield almost the same isomer ratios as the 3n reaction (see Fig. 27). Therefore, the relatively small abundances of Sn^{118} and Sn^{120} probably do not alter the isomer ratio for the $He^3 + Sn^{119}$ reaction by a detectable amount.

2. The Reaction $He^4 + Sn^{118} \longrightarrow Te^{119, 119m} + 3n$

a. Target Assembly

Practically all the He^4 bombardments were carried out at the 60-inch cyclotron and consequently required a different target assembly from that used for the He^3 bombardments at the Hilac. The assembly employed is illustrated in Fig. 21. The holder consists of a water-cooled cylinder in which the target foils and spacers are held by means of a snap ring. Any collimation used is in the accelerator ahead of the target assembly, and the assembly is insulated from the machine so that it serves as a Faraday cup for monitoring the beam current. The samples were plated upon 1-in.-diameter circles instead of 1-in. squares, and the same stacking arrangement of alternate foil and spacer as discribed before was used. Bombardments were usually for 1 to 2 h. Cooling in some cases was somewhat unstisfactory, and if the beam current got above about 1 μA the targets were burned. The isotopic enrichment of the Sn^{118} used in the bombardments is given in Table VIII.[66]

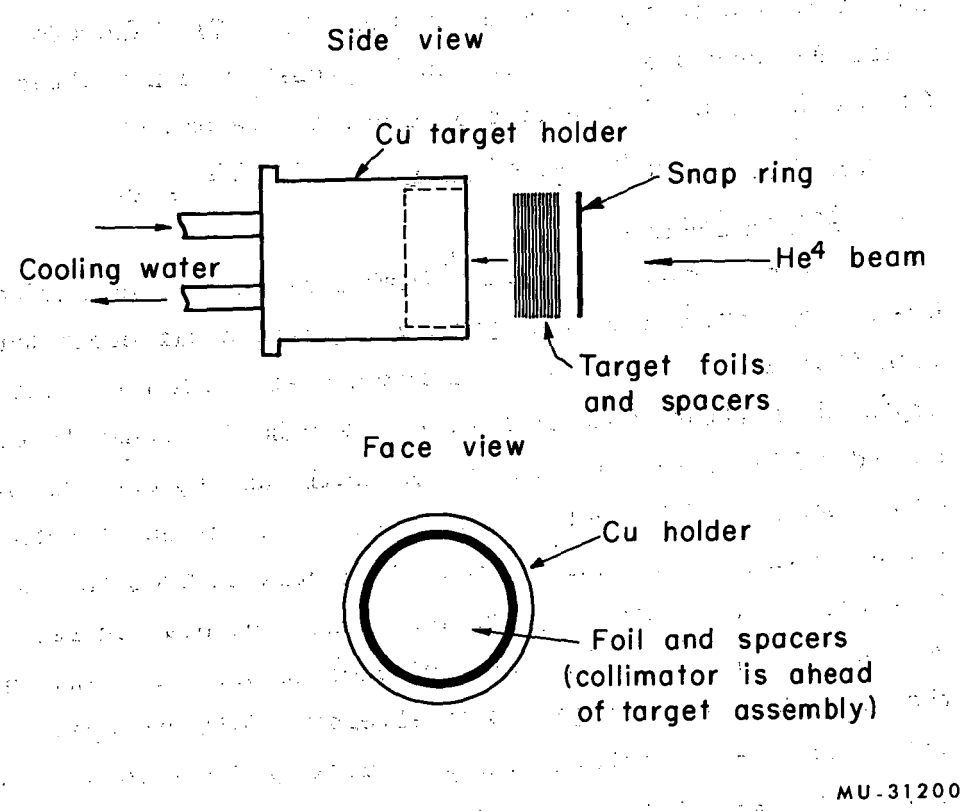

Fig. 21. Target assembly used for all He^4 bombardments at the Crocker 60-inch cyclotron.

Table VIII. Analysis of isotopically enriched Sn^{118}.

Isotope	Atomic percent	Precision
112	0.05	—
114	0.04	—
115	0.1	± 0.05
116	0.4	0.05
117	0.8	0.05
118	95.6	0.1
119	1.4	0.05
120	1.3	0.05
122	0.1	0.05
124	0.1	0.05

b. Experimental Results

The experimental results for this reaction are tabulated in Table IX and plotted in Fig. 22. The isotopic abundance of the Sn^{118} used is quite high and it is assmed that there is no contribution to the ratio from the small amounts of other isotopes present.

Table IX. Formation cross-section ratios of the isomers of tellurium-119 produced in the reaction $He^4 + Sn^{118} \longrightarrow Te^{119, 119m} + 3n$.

Experiment number	Sample number	Projectile energy (MeV)	Excitation energy (MeV)	Isomer ratio (Te^{119m}/Te^{119})
33	1	47.7	47.5	6.10 ± 0.05
	2	46.1	45.9	5.60 ± 0.05
	3	44.5	44.4	4.80 ± 0.05
	4	42.8	42.8	4.40 ± 0.05
	5	41.2	41.2	3.90 ± 0.05
	6	39.4	39.5	3.70 ± 0.05
	7	37.6	37.9	3.30 ± 0.10
	8	35.8	36.1	2.80 ± 0.05
	9	33.9	34.4	2.30 ± 0.05
	10	31.7	32.3	1.85 ± 0.05
	11	29.6	30.4	1.30 ± 0.20
34	1	48.0	47.8	5.90 ± 0.05
	2	46.1	45.9	5.50 ± 0.10
	3	44.2	44.1	4.70 ± 0.20
	4	42.1	42.1	4.30 ± 0.10
	5	40.1	40.2	3.75 ± 0.05
	6	38.0	38.2	3.25 ± 0.05
	7	35.9	36.2	2.75 ± 0.05
	8	33.4	33.7	2.15 ± 0.05
	9	30.9	31.4	1.60 ± 0.05
38	1	47.9 - 48.0	47.6 - 47.7	6.30 ± 0.20
	2	46.7 - 46.8	46.5 - 46.6	5.85 ± 0.25
	3	45.3 - 45.4	45.3 - 45.4	5.70 ± 0.20
	4	44.0 - 44.1	43.9 - 44.1	4.85 ± 0.25

Table IX. (Continued)

Experiment number	Sample number	Projectile energy (MeV)	Excitation energy (MeV)	Isomer ratio (Te^{119m}/Te^{119})
38	5	42.7 - 42.8	42.7 - 42.8	4.50 ± 0.10
	6	41.4 - 41.5	41.4 - 41.5	4.00 ± 0.20
	7	40.0 - 40.1	40.1 - 40.2	3.80 ± 0.20
	8	38.6 - 38.7	38.8 - 38.9	3.60 ± 0.10
	9	37.1 - 37.2	37.4 - 37.5	3.20 ± 0.10
	10	35.5 - 35.6	35.9 - 36.0	2.95 ± 0.05
	11	33.9 - 34.0	34.4 - 34.5	2.70 ± 0.05
	12	32.5 - 32.5	33.0 - 33.0	2.50 ± 0.05
	13	31.0 - 31.1	31.6 - 31.7	2.15 ± 0.05
	14	29.4	30.0	1.85 ± 0.05
	15	27.6 - 27.7	28.5 - 28.6	1.85 ± 0.05

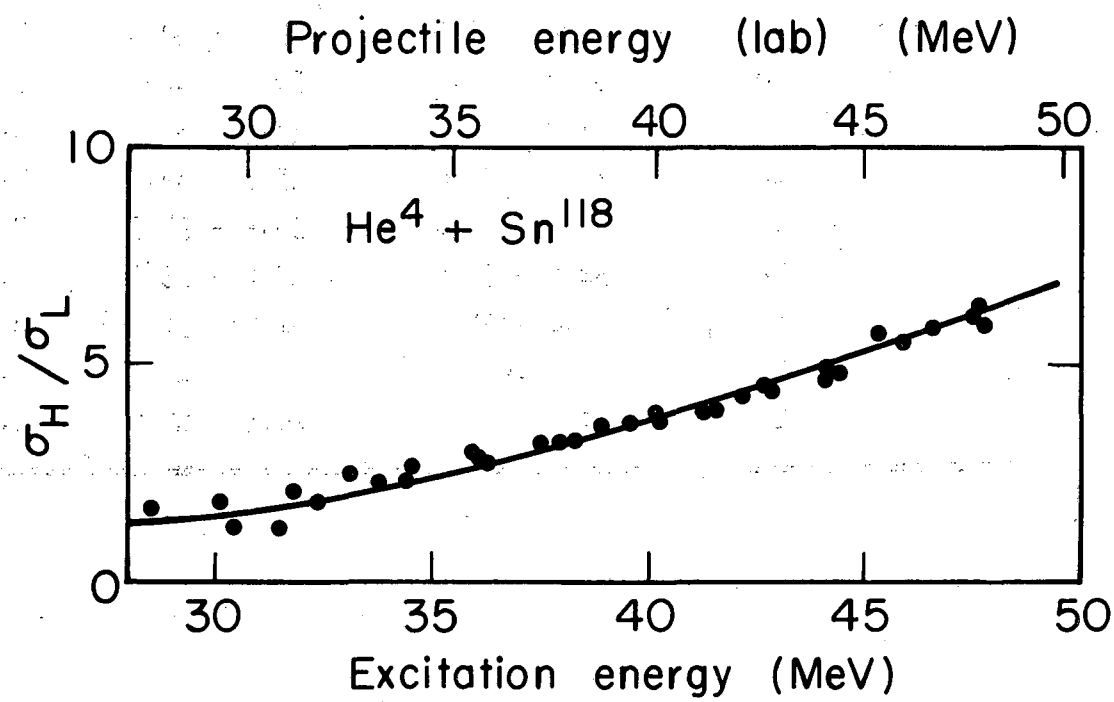

MU-31215

Fig. 22. Experimentally determined formation cross-section ratios for the isomers of tellurium-119 produced in the reaction $He^4 + Sn^{118} \longrightarrow Te^{119, 119m} + 3n$.

3. The Reaction $Li^7 + In^{115} \longrightarrow Te^{119, 119m} + 3n$

a. Target Assembly

For this reaction it was possible to use natural indium which consists of 95.8% In^{115} and 4.2% In^{113}. The target assembly was the same as that used for the He^3 reaction. It was essential to have aluminum spacers between the targets because the melting point of the indium is quite low and the stack of foils tended to fuze together. In some cases it was impossible to separate the spacer from the target because of the melted indium which acted much as a solder. In these cases, the spacer was dissolved with the rest of the target and posed no special problem.

b. Experimental Results

The results of the experiments are tabulated in Table X and plotted as a function of the excitation energy of the compound nucleus in Fig. 23.

Table X. Formation cross-section ratios of the isomers of tellurium-119 produced in the reaction $Li^7 + In^{115} \longrightarrow Te^{119, 119m} + 3n$.

Experiment number	Sample number	Projectile energy (MeV)	Excitation energy (MeV)	Isomer ratio (Te^{119m}/Te^{119})
35	3	39.4 - 39.8	52.3 - 52.7	6.95 ± 0.25
	4	36.8 - 37.2	50.8 - 51.2	6.85 ± 0.15
	5	34.0 - 34.4	48.2 - 48.6	5.40 ± 0.10
	6	31.1 - 31.4	45.5 - 45.8	4.10 ± 0.10
	7	28.0 - 28.4	42.6 - 42.9	2.85 ± 0.05
	8	24.5 - 25.0	39.3 - 39.7	1.65 ± 0.15
49	1	48.0 - 48.2	61.5 - 61.7	6.30 ± 0.30
	2	46.4 - 46.6	60.0 - 60.2	6.70 ± 0.40
	3	44.7 - 44.9	58.3 - 58.5	7.20 ± 0.40
	4	42.9 - 43.1	56.6 - 56.8	7.30 ± 0.20
	5	41.1 - 41.3	54.9 - 55.1	7.45 ± 0.15
	6	39.4 - 39.6	53.3 - 53.5	7.45 ± 0.35
	7	37.5 - 37.6	51.3 - 51.5	6.90 ± 0.20
	8	35.5 - 35.7	49.6 - 49.8	6.30 ± 0.20
	9	33.3 - 33.6	47.6 - 47.9	5.00 ± 0.30
	10	31.1 - 31.4	45.5 - 45.7	3.80 ± 0.10
	11	29.0 - 29.1	43.5 - 43.6	3.05 ± 0.05
	12	26.2 - 26.6	40.8 - 41.2	2.40 ± 0.10
	13	23.4 - 23.8	38.2 - 38.5	1.95 ± 0.05
	14	20.4 - 20.7	35.4 - 35.7	1.70 ± 0.20
69	1	53.3 - 53.6	66.5 - 66.8	6.00 ± 0.50
	2	51.7 - 51.8	64.8 - 64.9	5.65 ± 1.05
	3	49.9 - 50.2	63.1 - 63.4	6.05 ± 0.30
	4	48.1 - 48.3	61.5 - 61.7	6.20 ± 0.30
	5	46.0 - 46.4	59.6 - 60.0	6.80 ± 0.30

Table X. (Continued)

Experiment number	Sample number	Projectile energy (MeV)	Excitation energy (MeV)	Isomer ratio (Te^{119m}/Te^{119})
69	6	44.1 - 44.3	57.7 - 57.9	6.75 ± 0.45
	7	42.0 - 42.4	55.8 - 56.2	6.95 ± 0.55
	8	40.0 - 40.2	53.8 - 54.0	6.95 ± 0.45
	9	37.6 - 38.2	51.6 - 52.1	6.85 ± 0.45
	10	35.5 - 35.8	49.7 - 50.0	5.95 ± 0.30
	11	32.6 - 33.5	46.8 - 47.7	4.70 ± 0.10
	12	29.9 - 30.4	44.3 - 44.7	3.45 ± 0.05
	13	26.6 - 27.5	41.2 - 42.0	2.45 ± 0.05
	14	23.7 - 24.2	38.4 - 38.9	1.80 ± 0.10
	15	20.3 - 21.0	35.3 - 35.9	1.65 ± 0.15

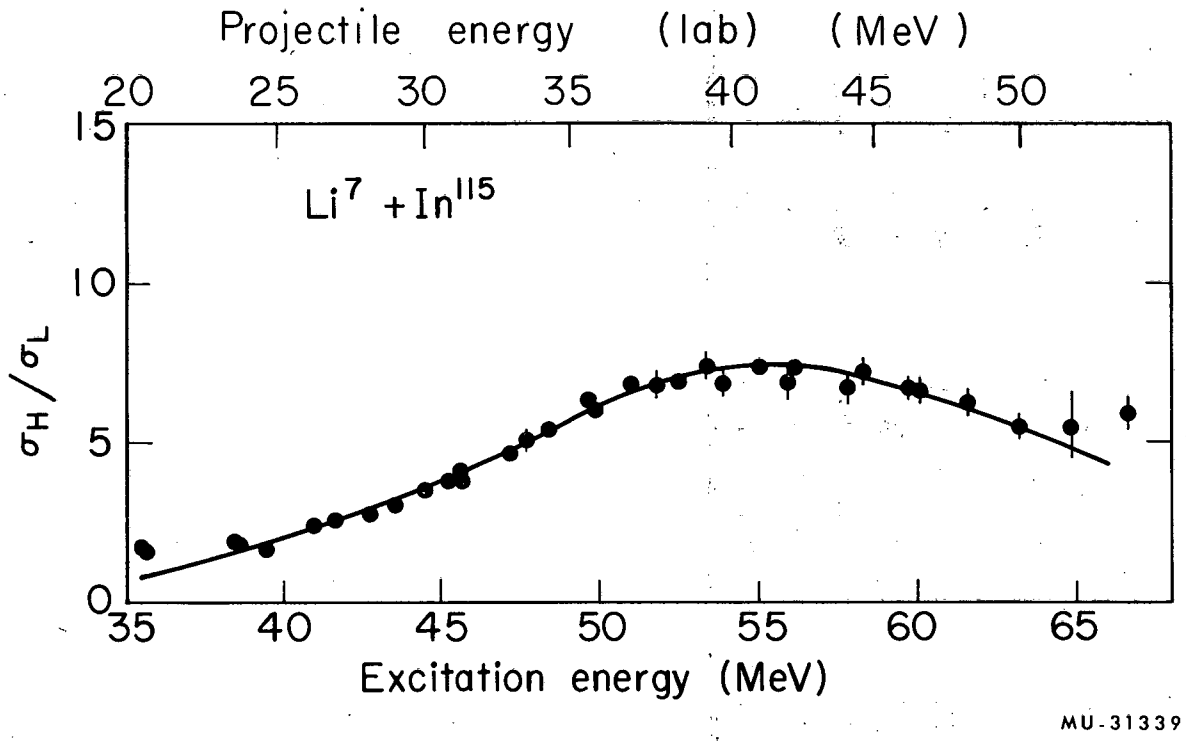

Fig. 23. Experimentally determined formation cross-section ratios for the isomers of tellurium-119 produced in the reaction $Li^7 + In^{115} \longrightarrow Te^{119, 119m} + 3n$.

It is seen that, starting at approximately 52 MeV (excitation) the ratio curve changes slope and begins to turn over. Above about 56 MeV the ratio of the upper-state to the lower-state isomer decreases with energy. The effect is anomalous with respect to all the other systems studied. Such an effect is usually attributable to some sort of direct interaction.

From a classical viewpoint, the collisions that bring into a compound nucleus the greatest amount of angular momentum are those which have a grzing trajectory. The compound nuclei resulting from nearly head-on collisions correspond to small amounts of angular momentum transfer. Therefore, if those collisions which result in large angular momentum transfers do not result in the formation of compound nuclei, the average value of the angular momentum of the compound nuclei must decrease. Such a decrease would result in a drop of the isomer ratio, as is observed in this experiment.

Kaufmann and Wolfgang have studied just such reactions, using a number of different heavy ions.[67] At energies only slightly above the Coulomb barrier the reactions of heavy nuclei appear to be either those of compound-nucleus formation or those of Rutherford scattering and Coulomb excitation. For small impact parameters the first process occurs, whereas for large impact parameters the Coulomb barrier is not penetrated and the scattering reactions take place. At energies further above the Coulomb barrier the situation is not so simple. There now appears an intermediate range of impact parameters which correspond to a grazing collision of the projectile. The particle is partially deflected by the Coulomb field, but still comes into approximately a tangential contact with the target nucleus. It may then move along the surface until its forward momentum breaks the nuclear bond formed between the nuclei. The necessary condition for such a reaction is that the centrifugal force plus the Coulomb force be greater than the nuclear binding force. Otherwise the system would amalgamate into a compound nucleus. Such grazing reactions are considered to be good mechanisms for the transfer of several nucleons.

Many recent investigations have indicated that under certain conditions the Li^7 nucleus may be considered to exist as an α and a triton cluster.[68-74] On the basis of such a model, reactions of the (Li^7, α) type may be visualized as stripping reactions in which the triton is absorbed into the target nucleus and the α particle goes on past the nucleus. Such a reaction, in which the Li^7 is shown pictorially as being composed of an α and a triton cluster, is represented in Fig. 24.

The threshold energy for the reaction $In^{115}(Li^7, \alpha)Sn^{118}$ has been calculated to be positive by about 8 MeV (assuming zero kinetic energy of the α particle). The Coulomb barrier for the reaction is 22.4 MeV, and the first indication of such a reaction in this work is at a projectile energy of 38 MeV (laboratory system.

For no breakup of the projectile there is an increase of angular momentum with energy for the compound-nucleus process. The increased prevalence of the grazing processes, with a charged projectile passing by, may more than offset this increase and instead cause a decrease of angular momentum with energy. On the basis of this argument, it is proposed that the decrease in isomer ratio with energy is attributable to a direct interaction in which a triton becomes amalgamated with the target nucleus and an α particle proceeds on by. Such an effect may also have been seen by Richard Kiefer in a similar investigation.[75]

4. The Reaction $C^{12} + Pd^{110} \longrightarrow Te^{119, 119m} + 3n$

a. Target Assembly

As discussed earlier, it was necessary in this investigation to use isotopically enriched Pd^{110} even though the lighter isotopes of palladium do not produce interfering activities. The isotopic analysis of the palladium used is listed in Table XI[66]

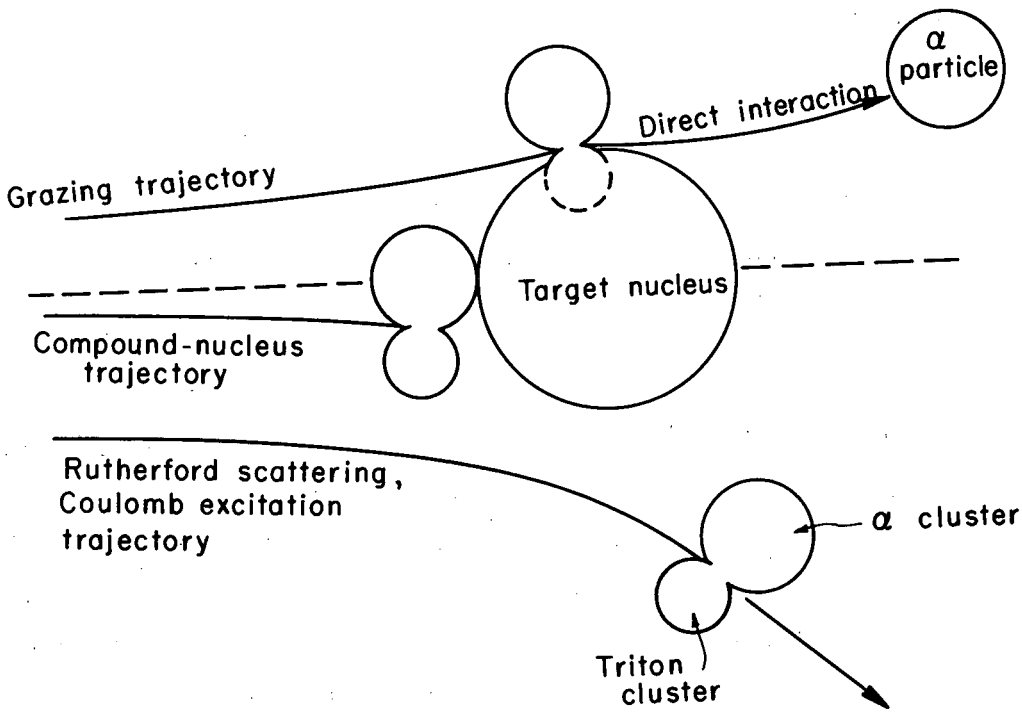

Fig. 24. Illustration of the direct-interaction mechanism proposed as an explanation of the decrease in isomer ratio with energy for the Li^7 + In^{115} reaction.

Table XI. Analysis of isotopically enriched Pd^{110}

Isotope	Atomic percent	Precision
102	0.3	± 0.05
104	1.6	0.1
105	1.8	0.1
106	2.2	0.1
108	14.6	0.1
110	79.5	0.2

b. Experimental Results

The isomer ratios are tabulated in Table XII and shown graphically in Fig. 25. Since it was difficult to obtain more than about five points from each bombardment, a relatively large number of irradiations were conducted. This introduced a certain amount of energy inconsistency and the scatter of points is noticeably greater than that for the lighter projectiles. Also, because of the high Coulomb barrier the bombardments were at higher energies where the background subtraction becomes more indefinite. This effect is manifested as an increase in the ratio uncertainty with increasing energy.

Table XII. Formation cross-section ratios of the isomers of tellurium-119 produced in the reaction $C^{12} + Pd^{110} \longrightarrow Te^{119, 119m} + 3n$

Experiment number	Sample number	Projectile energy (MeV)	Excitation energy (MeV)	Isomer ratio (Te^{119m}/Te^{119})
36	1	44.5 - 45.0	39.7 - 40.1	2.80 ± 0.10
	2	48.2 - 49.7	42.7 - 44.0	4.55 ± 0.15
37	1	58.0 - 58.5	54.4 - 54.8	9.90 ± 0.40
	2	52.0 - 52.8	49.0 - 49.8	7.25 ± 0.25
	3	45.7 - 46.5	43.5 - 44.2	4.65 ± 0.35
	4	39.0 - 40.0	37.5 - 38.5	2.05 ± 0.15
	5	61.7 - 62.5	57.8 - 58.5	11.00 ± 0.60
	6	56.2 - 57.0	52.7 - 53.5	8.30 ± 0.30
	7	50.3 - 51.0	47.6 - 48.2	6.30 ± 0.10
	8	44.0 - 44.8	42.0 - 42.7	3.30 ± 0.10
43	1	61.5 - 62.0	57.6 - 58.0	10.75 ± 0.55
	2	59.0 - 59.5	55.3 - 55.8	9.65 ± 0.45
	3	56.5 - 57.0	53.0 - 53.6	7.85 ± 0.35
	4	54.0 - 54.5	50.8 - 51.3	7.55 ± 0.65
	5	51.0 - 51.5	48.2 - 48.6	6.15 ± 0.55
	6	42.0 - 42.5	40.2 - 40.7	2.55 ± 0.25
52	1	57.3 - 57.5	53.8 - 53.6	9.05 ± 0.45
	2	52.0 - 52.2	49.0 - 49.2	6.75 ± 0.95
	3	46.6 - 46.8	44.2 - 49.2	5.05 ± 0.35
63	1	62.7 - 64.0	58.7 - 59.8	12.25 ± 0.65
	2	57.2 - 59.6	53.6 - 55.3	8.75 ± 0.25
	3	49.0 - 49.3	46.4 - 46.7	4.90 ± 0.10
	4	45.2 - 45.5	43.0 - 43.3	3.45 ± 0.25
	5	40.7 - 41.5	39.1 - 39.8	2.10 ± 0.10

Table XII. (Continued)

Experiment number	Sample number	Projectile energy (MeV)	Excitation energy (MeV)	Isomer ratio (Te^{119m}/Te^{119})
70	1	66.6 - 67.8	62.2 - 63.3	15.1 ± 1.20
	2	63.3 - 64.7	59.2 - 60.4	13.10 ± 1.00
	3	60.8 - 61.4	56.8 - 57.4	10.80 ± 0.60
	4	57.5 - 58.5	54.0 - 54.9	9.40 ± 0.50
	5	53.5 - 54.5	50.4 - 51.4	7.30 ± 0.40
	6	48.5 - 48.8	46.0 - 46.3	4.30 ± 0.50
	7	43.7 - 44.5	41.6 - 42.8	2.10 ± 0.10
	8	38.5 - 39.4	37.1 - 38.0	1.60 ± 0.20

5. The Reaction $O^{18} + Ru^{104} \longrightarrow Te^{119, 119m} + 3n$

a. Target Assembly

Isotopically enriched Ru^{104} was used as the target material.[66] The isotopic analysis is given in Table XIII. The target assembly was the same as that used for the other Hilac bombardments.

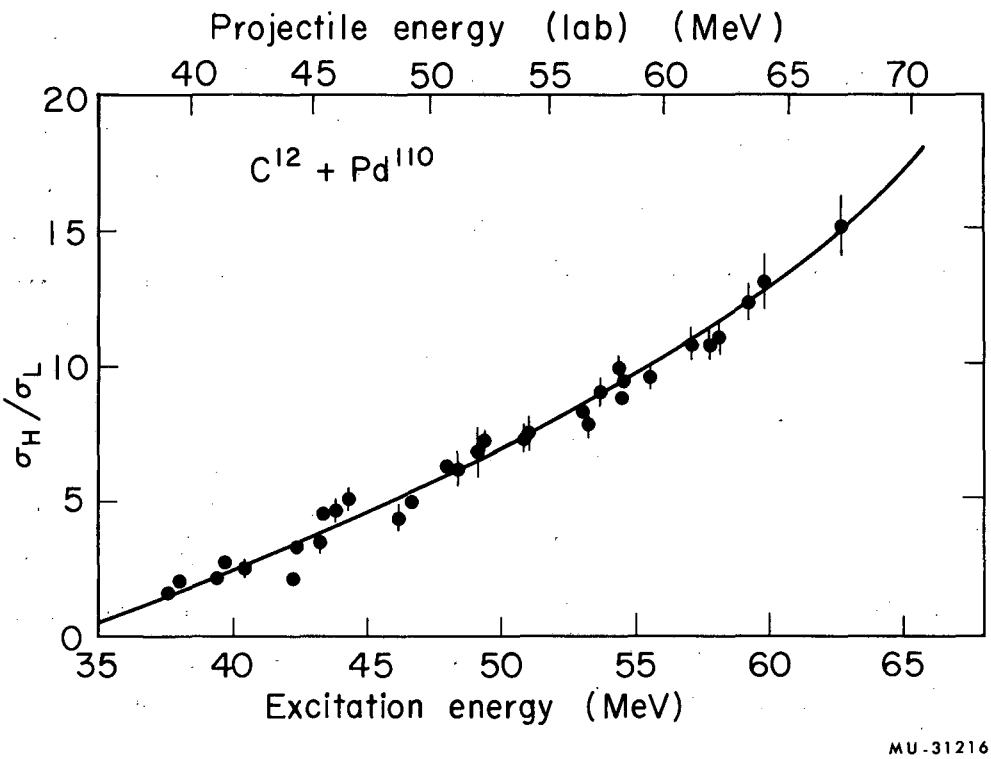

Fig. 25. Experimentally determined formation cross-section ratios for the isomers of tellurium-119 produced in the reaction $C^{12} + Pd^{110} \longrightarrow Te^{119,\ 119m} + 3n$.

Table XIII. Analysis of isotopically enriched Ru^{104}.

Isotope	Atomic percent	Precision
96	< 0.03	—
98	< 0.02	—
99	0.08	—
100	0.12	—
101	0.27	—
102	1.32	± 0.05
104	98.16	0.05

b. Experimental Results

The experimental results are tabulated in Table XIV and illustrated in Fig. 26. The uncertainties in the energy and ratio mentioned for the carbon reaction are even more magnified for the O^{18} data. Only two experiments were performed because of the cost and nonavailability of O^{18}. The agreement between the two experiments is, however, surprinsingly good considering the difficulties encountered in working with the ruthenium.

Table XIV. Formation cross-section ratios of the isomers of tellurium-119 produced in the reaction $O^{18} + Ru^{104} \longrightarrow Te^{119, 119m} + 3n$.

Experiment number	Sample number	Projectile energy (MeV)	Excitation energy (MeV)	Isomer ratio (Te^{119m}/Te^{119})
60	1	78.2 - 79.5	68.0 - 69.1	25.50 ± 1.80
	2	72.7 - 74.0	63.2 - 64.4	18.80 ± 1.20
	3	68.0 - 69.0	59.3 - 60.1	14.25 ± 0.75
	4	62.6 - 63.5	54.8 - 55.5	10.25 ± 0.55
	5	56.5 - 58.3	49.6 - 51.1	6.40 ± 0.30
65	1	73.5 - 75.7	64.0 - 65.7	19.75 ± 1.35
	2	68.7 - 69.5	59.8 - 60.6	14.8 ± 0.70
	3	63.0 - 64.5	55.1 - 56.4	9.45 ± 0.35
	4	57.5 - 59.0	50.4 - 51.7	7.30 ± 0.30

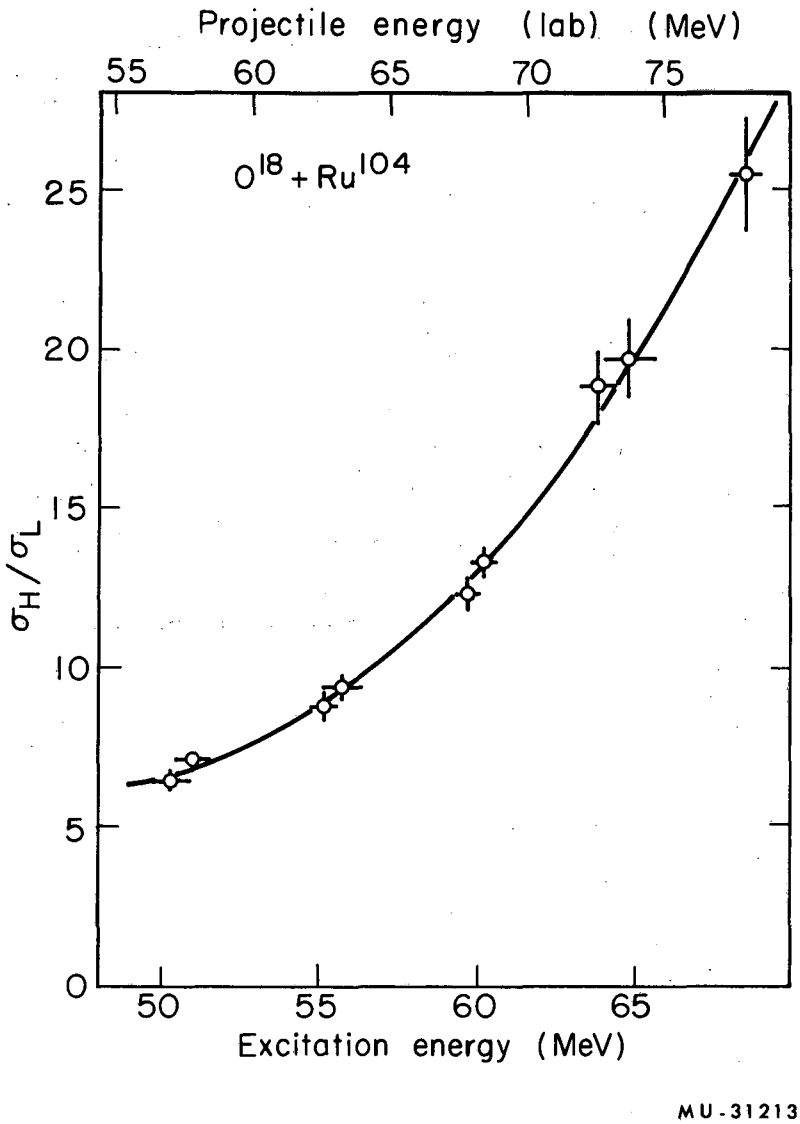

Fig. 26. Experimentally determined formation cross-section ratios for the isomers of tellurium-119 produced in the reaction $O^{18} + Ru^{104} \longrightarrow Te^{119, 119m} + 3n$.

C. Reactions Yielding the Compound Nuclei Te^{121*} and Te^{123*}

1. General Discussion

The compound nucleus Te^{121*} was prepared by bombardment of Sn^{118} and Sn^{119} with He^3 and He^4 ions respectively. Te^{123*} was prepared analogously by bombardment of Sn^{120} and Sn^{119} with He^3 and He^4. The isotopic enrichments of the Sn^{118} and Sn^{119} have already been given in earlier sections. The enrichment of the other two isotopes is given in Tables XV and XVI.

The target assemblies were the same as those previously described for other He^3 and He^4 bombardments.

Table XV. Analysis of isotopically enriched Sn^{117}.

Isotope	Atomic percent	Precision
112	0.3	± 0.05
114	0.2	0.05
115	0.2	0.05
116	2.8	0.05
117	85.4	0.2
118	7.8	0.1
119	1.0	0.05
120	1.6	0.05
122	0.3	0.05
124	0.3	0.05

Table XVI. Analysis of istopically enriched Sn^{120}.

Isotope	Atomic percent	Precision
112	0.004	± 0.002
114	0.009	0.004
115	0.024	0.015
116	0.088	0.014
117	0.073	0.002
118	0.562	0.029
119	0.775	0.027
120	98.14	0.07
122	0.240	0.003
124	0.074	0.017

2. Experimental Results

The experimental results are tabulated in Tables XVII through XX. The results are plotted together in Fig. 27. Although these reactions are probably not as fruitful in showing angular momentum effects as the foregoing ones, since no heavy particles are involved, they help to show the effects of the neutron evaporation on the isomer ratio. When they are included, the work deals with the production of the tellurium-119 isomers from a compound nucleus by 2n, 3n, and 4n reactions.

Table XVII. Formation cross-section ratios of the isomers of tellurium-119 produced in the reaction $He^3 + Sn^{118} \longrightarrow Te^{119, 119m} + 2n$.

Experiment number	Sample number	Projectile energy (MeV)	Excitation energy (MeV)	Isomer ratio (Te^{119m}/Te^{119})
59	1	23.9 - 24.0	36.2 - 36.3	1.85 ± 0.05
	2	22.1 - 22.2	34.6 - 34.7	1.75 ± 0.15
	3	20.4 - 20.5	33.0 - 33.1	1.60 ± 0.05
	4	18.7 - 18.8	31.2 - 31.3	1.50 ± 0.10
	5	16.7 - 16.9	29.2 - 29.3	1.40 ± 0.10
	6	14.6 - 14.7	27.2 - 27.3	1.00 ± 0.05

Table XVIII. Formation cross-section ratios of the isomers of tellurium-119 produced in the reaction $He^4 + Sn^{117} \longrightarrow Te^{119, 119m} + 2n$.

Experiment number	Sample number	Projectile energy (MeV)	Excitation energy (MeV)	Isomer ratio (Te^{119m}/Te^{119})
61	1	38.1 - 38.7	38.6 - 38.7	5.15 ± 0.25
	2	36.8 - 36.9	37.4 - 37.5	5.10 ± 0.40
	3	35.3 - 35.4	35.9 - 36.0	4.85 ± 0.15
	4	33.8 - 33.9	34.5 - 34.6	4.20 ± 0.30
	5	32.2 - 32.3	32.8 - 32.9	3.60 ± 0.10
	6	30.7 - 30.8	31.5 - 31.6	3.05 ± 0.05
71	1	38.3 - 38.4	38.9 - 39.0	5.50 ± 0.20
	2	36.9 - 37.0	37.4 - 37.5	4.95 ± 0.15
	3	35.4 - 35.5	35.8 - 35.9	4.65 ± 0.35
	4	33.9 - 34.0	34.5 - 34.6	4.20 ± 0.10
	5	32.3 - 32.4	33.0 - 33.1	3.60 ± 0.10
	6	30.7 - 30.8	31.4 - 31.5	3.25 ± 0.15
	7	29.1 - 29.2	29.9 - 30.0	2.70 ± 0.10
	8	27.3 - 27.4	28.2 - 28.3	2.20 ± 0.10

Table XIX. Formation cross-section ratios of the isomers of tellurium-119 produced in the reaction $He^3 + Sn^{120} \longrightarrow Te^{119, 119m} + 4n$.

Experiment number	Sample number	Projectile energy (MeV)	Excitation energy (MeV)	Isomer ratio (Te^{119m}/Te^{119})
55	1	31.1	44.7	1.75 ± 0.05
	2	29.7	43.2	1.65 ± 0.05
	3	28.3 - 28.4	41.9 - 42.0	1.45 ± 0.05
	4	26.8	40.5	1.45 ± 0.05
	5	25.3	39.0	1.20 ± 0.10
	6	23.6	37.5	1.30 ± 0.10
59	1	31.1	44.7	1.80 ± 0.10
	2	29.6	43.2	1.60 ± 0.05
	3	28.2	41.8	1.55 ± 0.05
	4	25.6	39.3	1.45 ± 0.05
74	1	31.1	44.7	1.75 ± 0.05
	2	29.7	43.2	1.65 ± 0.05
	3	28.4	41.9	1.45 ± 0.05
	4	27.1	40.7	1.30 ± 0.01
	5	25.7	39.5	1.20 ± 0.01
	6	24.2	38.0	0.85 ± 0.15

Table XX. Formation cross-section ratios of the isomers of tellurium-119 produced in the reaction $He^4 + Sn^{119} \longrightarrow Te^{119, 119m} + 4n$.

Experiment number	Sample number	Projectile energy (MeV)	Excitation energy (MeV)	Isomer ratio (Te^{119m}/Te^{119})
61	1	47.9 - 48.0	48.8 - 48.9	3.75 ± 0.05
	2	46.6 - 46.7	47.5 - 47.6	3.60 ± 0.10
	3	45.3 - 45.4	46.3 - 46.4	3.20 ± 0.10
	4	43.9 - 44.0	44.8 - 44.9	3.05 ± 0.05
	5	42.5 - 42.6	43.5 - 43.6	2.80 ± 0.05
	6	41.0 - 41.1	42.0 - 42.1	2.40 ± 0.10
	7	39.6 - 39.7	40.7 - 40.8	2.15 ± 0.15
62	1	47.9 - 48.0	48.7 - 48.8	3.70 ± 0.10
	2	46.4 - 46.5	47.3 - 47.4	3.55 ± 0.15
	3	45.0 - 45.1	46.0 - 46.1	3.25 ± 0.05
	4	43.6 - 43.7	44.7 - 44.8	3.15 ± 0.05
	5	42.2 - 42.3	43.3 - 43.4	2.75 ± 0.05
	6	40.7 - 40.8	41.7 - 41.8	2.60 ± 0.20
	7	39.3 - 39.4	40.0 - 40.5	2.25 ± 0.15
	8	37.8 - 37.9	39.0 - 39.1	2.35 ± 0.15
	9	36.2 - 36.3	37.5 - 37.6	2.40 ± 0.10
	10	34.7 - 34.8	36.0 - 36.1	2.40 ± 0.20
73	1	41.6	42.7	2.75 ± 0.05
	2	40.3	41.4	2.45 ± 0.05
	3	39.1	40.1	2.20 ± 0.05
	4	36.8	38.0	1.80 ± 0.10

Table XX. (Continued)

Experiment number	Sample number	Projectile energy (MeV)	Excitation energy (MeV)	Isomer ratio (Te^{119m}/Te^{119})
73	5	35.5	36.8	1.60 ± 0.10
	6	34.2	35.5	1.40 ± 0.10
	7	32.8	34.2	1.25 ± 0.05
	8	31.5	33.0	1.05 ± 0.05
	9	30.0	31.6	0.95 ± 0.05

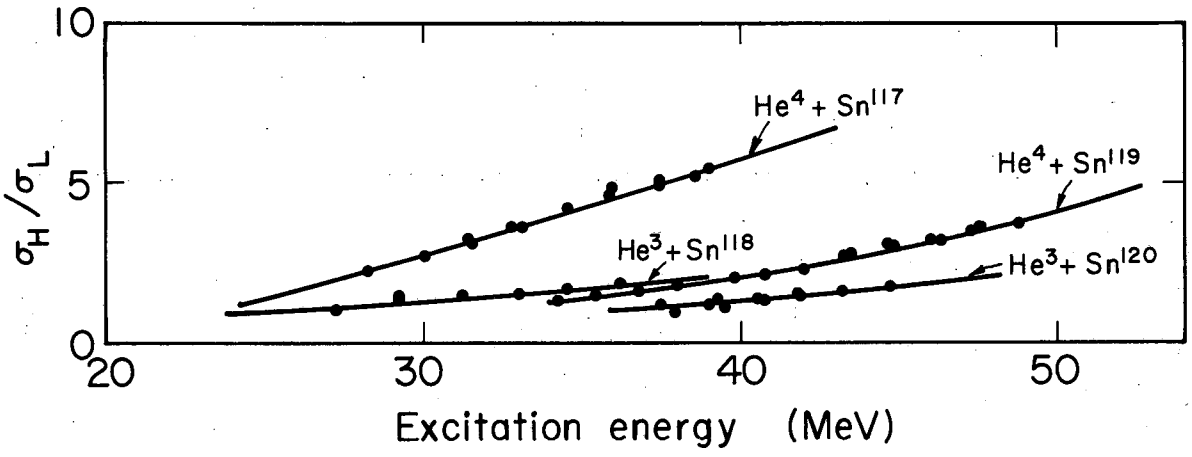

Fig. 27. Experimentally determined formation cross-section ratios as a function of the excitation energy of the compound nucleus for the reactions

$$He^3 + Sn^{118} \longrightarrow Te^{119,\ 119m} + 2n ,$$

$$He^4 + Sn^{117} \longrightarrow Te^{119,\ 119m} + 2n ,$$

$$He^3 + Sn^{120} \longrightarrow Te^{119,\ 119m} + 4n ,$$

$$He^4 + Sn^{119} \longrightarrow Te^{119,\ 119m} + 4n .$$

D. Excitation Functions

Excitation functions were determined for the reactions proceeding through the Te^{122*} compound nucleus. The cross sections were measured by analyzing the counting data for the ground-state isomer. For this isomer the 648-keV peak accounts for about 95% of the total gamma emission and is very weakly converted. Positron emission is also very minor. The upper-state isomer cross sections were calculated by merely multiplying the ground-state isomer cross section by the appropriate isomer ratio. The determination of the absolute counting efficiency of the counter assembly is described in the Appendix.

The excitation functions are shown in Fig. 28. The data obtained for the Li^7 and C^{12} reactions were consistent and the peak placements and heights are considered to be quite reliable. Only one irradiation yielded data for the O^{18} reaction and therefore no independent check could be made. For the He^3 and He^4 bombardments the beam integrations were apparently rather erratic, and although the peak positions for different irradiations was constant, the height was quite variable. Therefore, one should not place too much confidence in the absolute cross sections for these reactions. The cross sections chosen for each reaction were those which seemed most consistent among the various bombardments and with regard to the other reactions.

The influence of the Coulomb barrier is evident for the O^{18} reaction. The initial increase of cross section with energy is undoubtedly related to this effect. The direct interaction apparently occurring in the Li^7 reaction is not important below about 56 MeV, and is not evident in the excitation function.

There is a displacement of the peak toward higher energies with the heavier particles. The expected shift of the high-spin isomer peak with respect to the low-spin isomer peak is also discernible, and appears to amount to about 2 MeV.

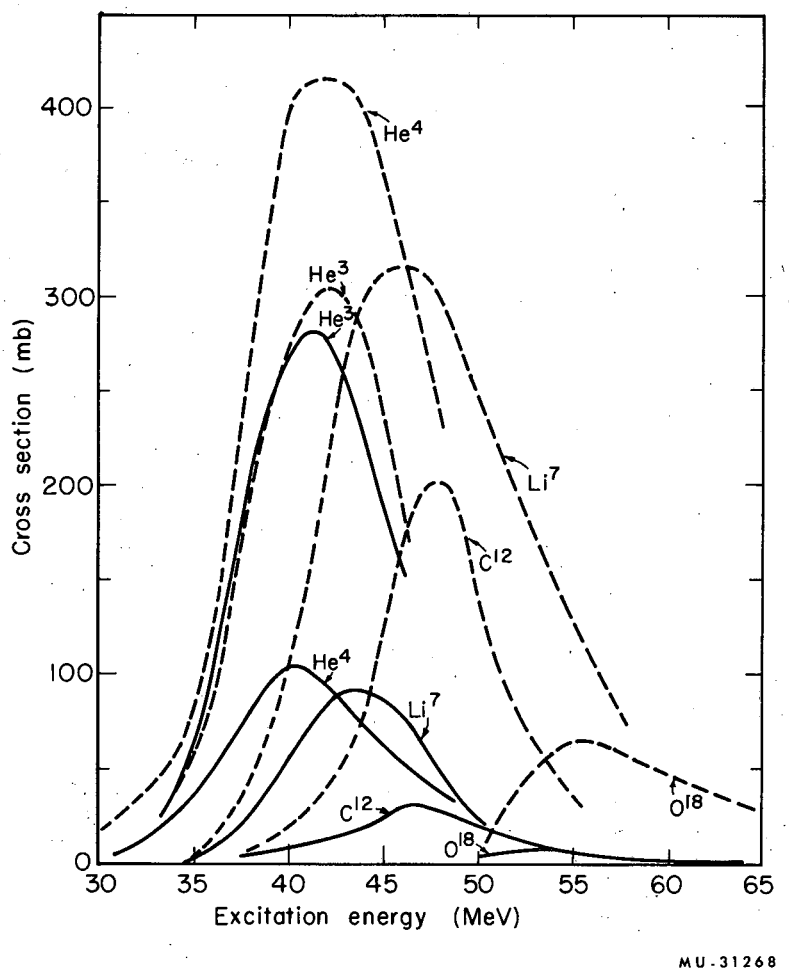

Fig. 28. Excitation functions for the reactions proceeding through the compound nucleus Te^{122*}. Solid curves represent the ground-state isomer and dashed curves the upper-state isomer.

V. COMPOUND-NUCLEUS CALCULATIONS AND QUALITATIVE PREDICTIONS OF ISOMER RATIOS

This section involves some rather qualitative comparisons between the experimental results and what would be expected on the basis of the angular momentum distribution of the compound nucleus. The effects of neutron emission and the γ-ray cascade are not considered. Also neglected are the intrinsic spins of the target and projectile. In order for the isomers studied to be formed, it is necessary that a compound nucleus be created. Therefore, in explaining the results it is assumed that the total reaction cross section is essentially that of compound-nucleus formation and that direct reactions are unimportant. Recent work by Alexander and Simonoff indicates that in the energy region considered this is probably a good assumption.[9] As discussed in a preceding section, at higher energies an exception must be made for the Li^7 reaction, in which a direct interaction apparently accounts for a large percentage of the total reaction cross section.

A. Calculations

The calculations were performed on an IBM 650 computer with a program written by Darrah Thomas.[39,40] The calculation assumes a diffuse-well model with a radius parameter of 1.2 fermis and a potential function of the form

$$V(R) = V_c + V_\ell + V_n \,, \tag{20}$$

where V_c represents the Coulomb potential

$$V_c = Z_1 Z_2 e^2 / R \,, \tag{21}$$

and V_ℓ is the centrifugal potential

$$V_\ell = [h^2\, \ell(\ell + 1)]/(2\mu R^2) \quad . \tag{22}$$

Here Vn is a nuclear potential of the form proposed by Igo for an α particle,[76]

$$V_n = V_o \exp[(R_o - R)/c] \quad . \tag{23}$$

For calculation of transmission coefficients the potential function eq. (20) is approximated at the barrier, by a parabola with height and second derivative matching at the maximum. The transmission coefficients are than calculated by the method of Hill and Wheeler,[77] who showed that for a parabolic potential they are of the form

$$T = 1/[1 + \exp 2\pi\, (B-E)/\hbar\omega] \quad . \tag{23}$$

In Eq. (23) B is the height of the barrier, E is the energy of the system, and ω is the vibrational frequency of the harmonic oscillator with the reduced mass of the system μ, and a potential energy function given by the negative of the potential energy function describing the barrier V(R).

The parameters that must be provided for the calculation are Z_1, Z_2, μ, ℓ, V_o, R_o, and c. Using these parameters, the program finds the value of R for which V(R) is a maximum. It then prints out V_{max}, R, ℓ, and $\hbar\omega$ for all values of ℓ such that $|V_n| < 10$ MeV. For these values of ℓ and for selected values of the projectile energy it calculates and prints out ℓ, T_ℓ, and the formation cross section for each value of ℓ,

$$\sigma_\ell = \pi\lambda\!\!\!^{-2}\, (2\ell + 1)\, T_\ell \quad . \tag{24}$$

The program also provides the cross section summed over all values of ℓ

$$\sigma_t = \pi\lambda\!\!\!^{-2} \sum_{\ell=0}^{\infty} (2\ell + 1)T_\ell \qquad (25)$$

and the average value of ℓ,

$$\langle \ell \rangle = \sum_{\ell=0}^{\infty} \ell\sigma_\ell \Big/ \sum_{\ell=0}^{\infty} \sigma_\ell \, . \qquad (26)$$

Since Eq. (25) is the total cross section, it represents the cross section for compound-nucleus formation.

B. Comparison of Calculations and Experimental Results

The calculations described above were performed for all target and projectile combinations over a wide range of energies at 2-MeV intervals. The energy range considered for each reaction was from the threshold energy or Coulomb barrier (whichever was higher), up to about 10 MeV above the highest energy experimentally studied.

When the calculated average angular momentum ($\langle \ell \rangle$) for each reaction is plotted against the excitation energy of the compound system, Fig. 29 is obtained. Points at which the curves for the various reactions cross correspond to a pair of compound nuclei produced by different reactions, but of the same average angular momentum and excitation energy. For example, at an excitation energy of about 50 MeV, compound nuclei resulting from He^4 bombardment of Sn^{118} have the same average angular momentum as those resulting from C^{12} bombardment of Pd^{110}. Since the compound nuclei produced by the two different reactions are identical with respect to angular momentum and excitation energy, the relative yields of the two tellurium-119 isomers, resulting from the emission

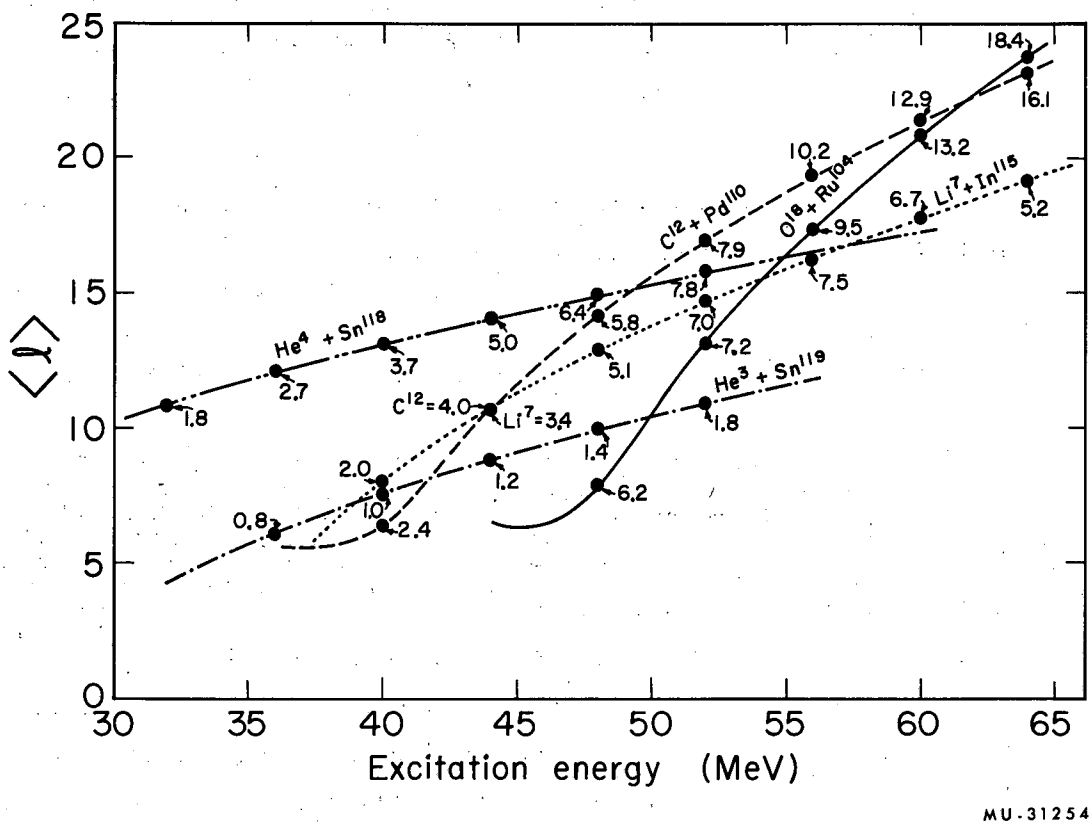

Fig. 29. Plot of calculated average angular momentum $\langle \ell \rangle$ for each reaction as a function of the excitation energy of the compound nucleus. Points at which the curves cross correspond to the compound nuclei produced by different reactions, but identical in energy and spin. The points show experimentally determined ratios corresponding to various combinations of $\langle \ell \rangle$ and excitation energy.

by the compound system of three neutrons, should also be the same. In other words, at an excitation energy of 50 MeV the He^4 reaction should produce the same tellurium-119 isomer ratio as the C^{12} reaction The plot also shows experimentally determined ratios for the different reactions at various E_x and $\langle \ell \rangle$ combinations.

Figure 30 is a plot of the experimentally determined isomer ratios as a function of the excitation energy of the compound nucleus. It is observed that the He^4 and C^{12} isomer ratio curves do cross precisely where the calculation predicts. If the assumptions made are valid, for each intersection occurring on the plot of $\langle \ell \rangle$ versus excitation energy there should be a corresponding intersection for the same pair of reactions, at a similar excitation energy, on the plot of isomer ratio versus excitation energy.

Figure 29 shows a total of nine intersections of the various reaction curves. It is notable that most of the experimentally determined isomer ratio curves (Fig. 30) cross very nearly at the excitation energy predicted by the compound-nucleus calculation. The various points of intersection of the two plots are tabulated for comparison in Table XXI. The two predicted intersections that do not occur involve reactions taking place in the vicinity of the Coulomb barrier, and in this region the calculation evidently understimates the average angular momentum of the system.

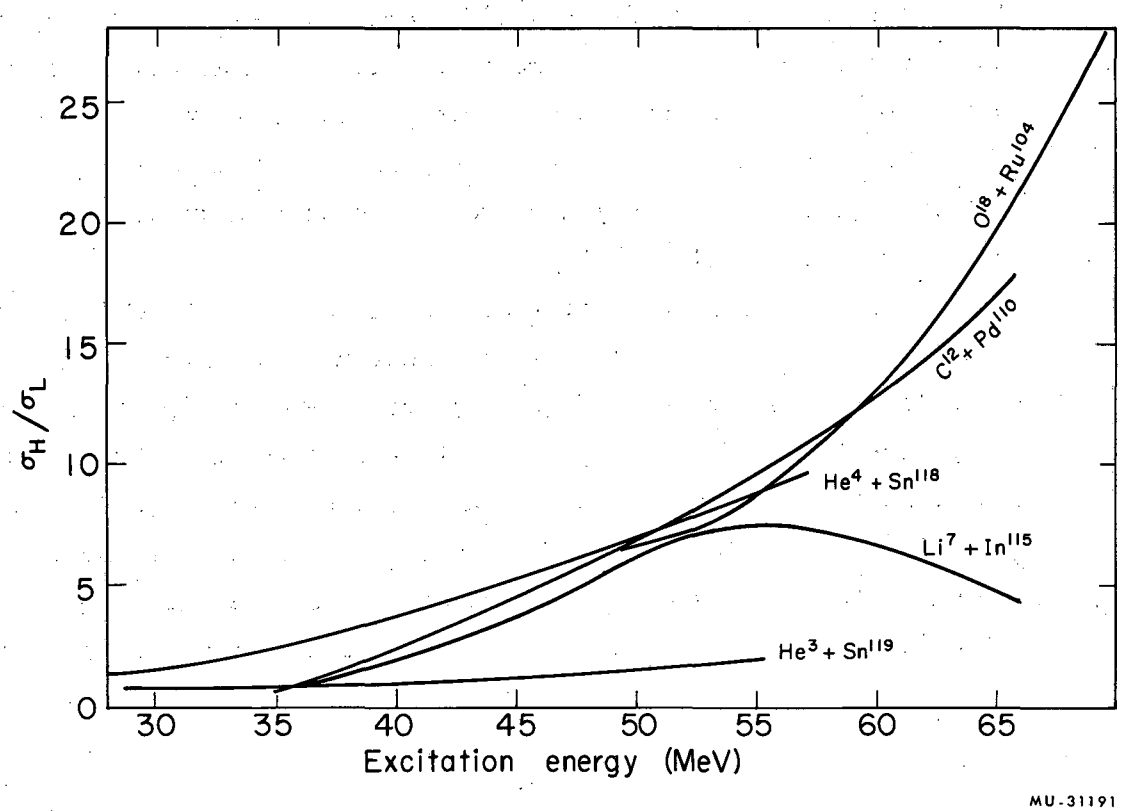

Fig. 30. Experimentally determined isomer ratios for the various reactions proceeding through the compound nucleus Te^{122*} as a function of the excitation energy of the compound nucleus. The curves are extrapolated for a short distance past the experimentally determined values.

Table XXI. Comparison of the calculated and experimentally determined points of intersection for the various reaction pairs.[a] Energies listed are excitation energies of the compound nucleus.

Reaction pair	Calculated intersection (MeV)	Experimental intersection (MeV)
$He^3 + Sn^{119}$ $Li^7 + In^{115}$	39	36
$He^3 + Sn^{119}$ $C^{12} + Pd^{110}$	40	36
$He^3 + Sn^{119}$ $O^{18} + Ru^{104}$	50	none
$Li^7 + In^{115}$ $C^{12} + Pd^{110}$	44	none
$Li^7 + In^{115}$ $O^{18} + Ru^{104}$	54	53
$Li^7 + In^{115}$ $He^4 + Sn^{118}$	57	56
$He^4 + Sn^{118}$ $C^{12} + Pd^{110}$	50	50
$He^4 + Sn^{118}$ $O^{18} + Ru^{104}$	55	55

Table XXI. (Continued)

Reaction	Calculated intersection (MeV)	Experimental intersection (MeV)
$C^{12} + Pd^{110}$ $O^{18} + Ru^{104}$	62	59

[a]The He^3 data were extrapolated in a reasonable manner to the energies where the intersections occurred. The Li^7 data were extrapolated from about 52 MeV on the assumption that no direct interaction took place.

The above discussion indicates that at certain energies different reactions can be predicted to yield the same isomer ratios. By a similar analysis, the relative isomer ratios produced by different reactions at a given level of excitation can also be predicted. Figure 31 shows the distributions of angular momentum in the compound systems produced by three different reactions, all yielding about the same excitation energy. It is obvious that the compound nucleus produced by the C^{12} reaction has more angular momentum and therefore should yield a higher Te^{119m}/Te^{119} ratio than the Li^{7} reaction. The Li^{7} reaction should likewise yield a higher ratio than the He^{3} reactions. Observation of Fig. 30 verifies that these predictions are correct. A similar plot at an excitation energy of 50 MeV, where a great deal of overlap occurs, is shown in Fig. 32. It can be seen that although the cross section for compound-nucleus production for the C^{12} reaction is lower than for the He^{4} reaction, the distributions in ℓ peak at about the same point and consequently the isomer ratio should be about the same. This is likewise experimentally verified. The calculation predicts that the isomer ratio from the O^{18} reaction should be about equal or less than that of the He^{3} reaction. In reality, the O^{18} reaction gives a much higher ratio than the calculation predicts. As stated before, the calculation seems to underestimate the amount of angular momentum put into the compound system when the reaction occurs close to the Coulomb barrier. Recent work on angular distributions of fission fragments by Viola, Thomas, and Seaborg leads to the same conclusion.[78]

The foregoing discussion seems to bear out the previously stated assumption that when decaying to a pair of isomers, those compound nuclei having high angular momentum prefer to populate the high-spin isomer and those having low angular momentum the low-spin isomer. Hence, an increase in the average angular momentum of the compound nucleus leads to an increase in the isomer ratio. Figure 33 is a plot of the experimentally determined isomer ratios as a function of the calculated average angular

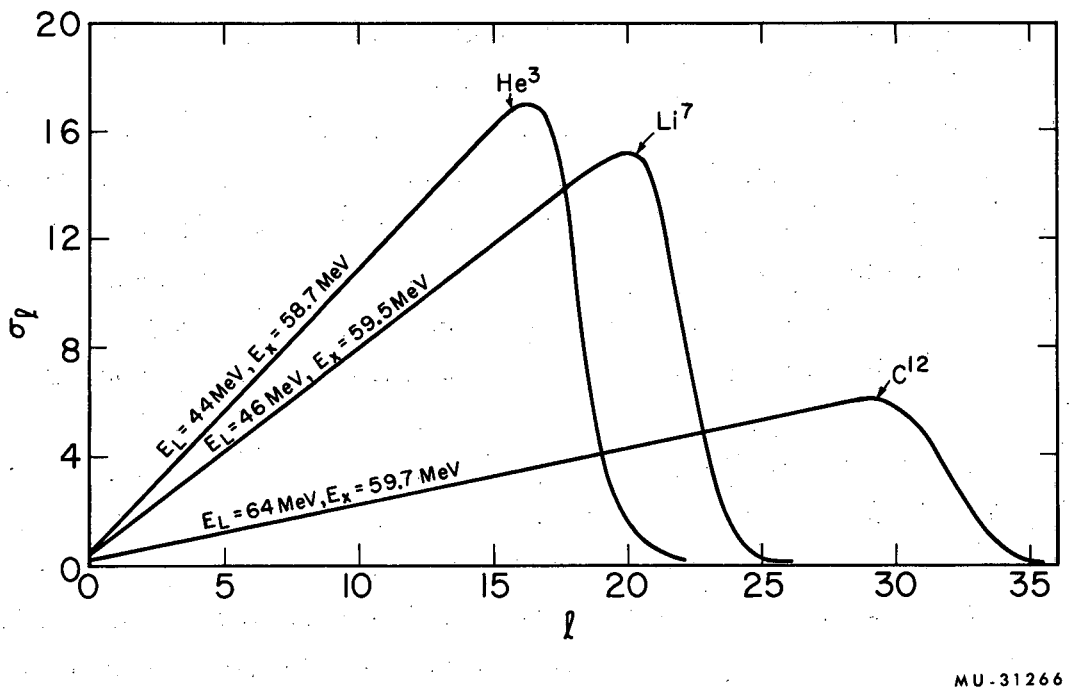

Fig. 31. Distribution of angular momentum as determined by the Bunthorne calculation for three compound systems, all at the same excitation energy. The distributions illustrate the effect of projectile energy and size on the angular momentum brought into the compound-nucleus system.

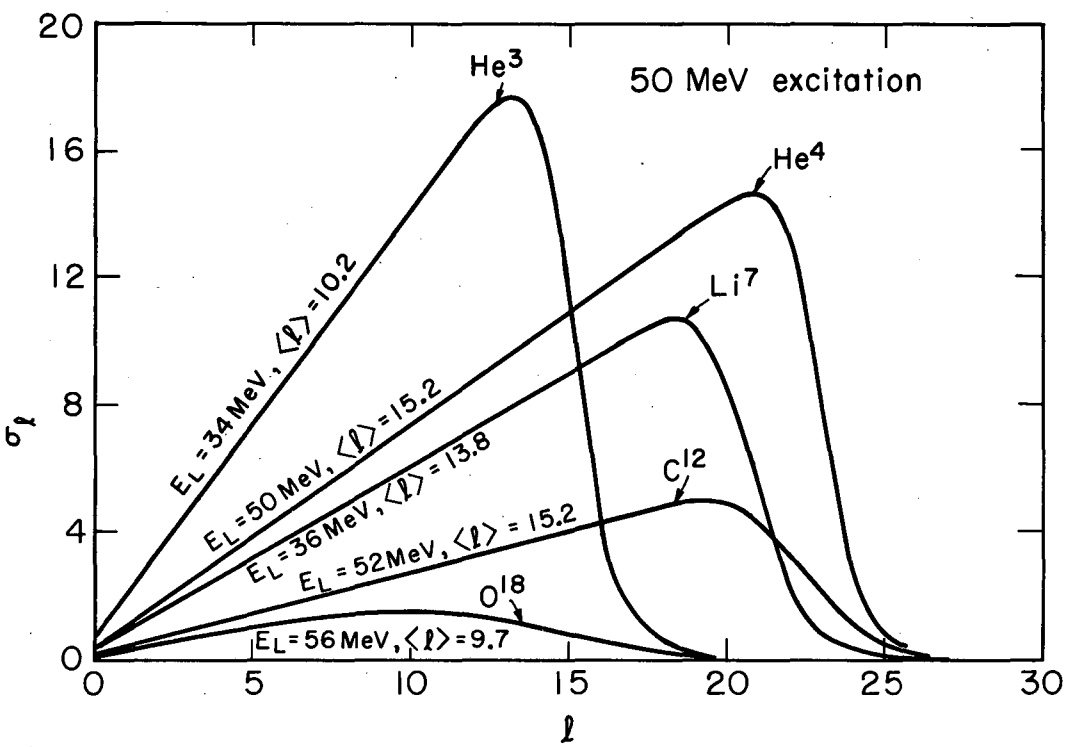

Fig. 32. Distributions in angular momentum of the compound nuclei produced by the five reactions yielding the compound nucleus Te^{122*}. The projectile energies were chosen so that the excitation energies of the compound systems were approximately equal (50 MeV).

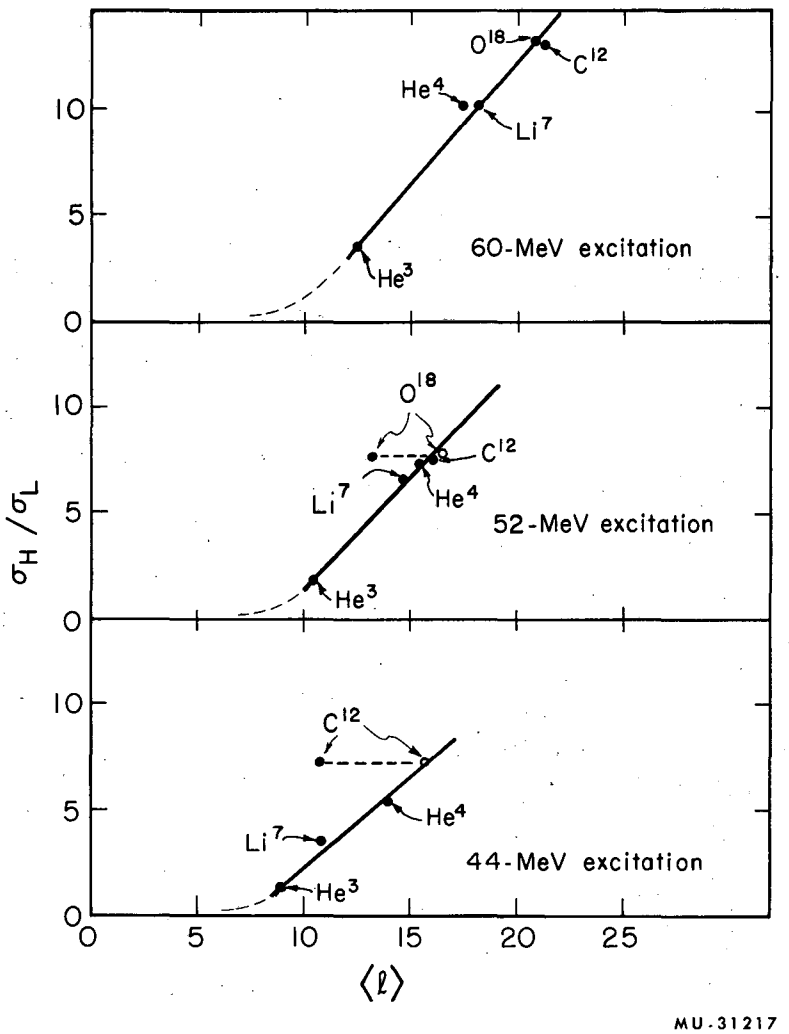

Fig. 33. Experimentally determined isomer ratios for the various reactions as a function of the average angular momentum of the compound nucleus.

momentum of the compound nucleus. Normalizing the reactions according to the amount of excitation energy in the compound nucleus, one sees that there is apparently a nearly linear relationship between the isomer ratio and the average angular momentum of the system over the range studied. In these plots, the He^3 ratios are extrapolated in a reasonable manner to the energies required for the comparison The Li^7 ratios are extrapolated with the assumption that no direct interaction occurs.

Since the ratio and $\langle \ell \rangle$ decrease together, the curve must in some way turn toward the origin, possibly as indicated by the dashed line extension. However, from an experimental standpoint, it is probably impossible to produce a system with a very small average angular momentum at the excitation energies listed.

At excitation energies of 44 and 52 MeV, the C^{12} and O^{18} reactions are respectively very near the Coulomb barrier. The solid points in Fig. 33 are the experimentally determined ratios corresponding to the the calculated average angular momenta. Again, the results indicate that the calculation underpredicts the average angular momentum of the system near the Coulomb barrier. The report by Viola, Thomas, and Seaborg contains a plot of angular momentum correction factors as a function of the energy above the Coulomb barrier.[78] When these factors are applied to the calculated $\langle \ell \rangle$ for the C^{12} and O^{18} reactions, the points fall precisely in line with the other reaction points (indicated by open circles). Thus, there seems to be good agreement between this work and that cited concerning the magnitude of error in the calculation for reactions taking place in the vicinity of the Coulomb barrier.

C. Prediction of the Isomer Ratio

Since there undoubtedly is a direct relationship between the angular momentum of the Te^{122*} compound nucleus and the relative amounts of the tellurium-119 isomers formed through its decay, one might hope to be able to make some prediction as to the ratios expected. The simplest course is to assume that there exists some sharp cutoff in the

angular momentum distribution such that all compound nuclei with angular momentum equal to or less than a chosen ℓ yield the ground-state isomer whereas all compound nuclei with angular momentum greater than the cutoff ℓ yield the upper-state isomer. This type of analysis was carried out for all the reactions studied. The cross sections for all angular momentum states up to and including the cutoff value were summed and assumed to lead to the ground-state isomer, Te^{119}. The cross sections for all angular momentum states greater than the cutoff were summed and assumed to yield Te^{119m}. The calculated ratio was then obtained by merely dividing the two summations,

$$\sigma_H/\sigma_L = \sum_{\ell=c+1}^{m} \sigma_\ell \Big/ \sum_{\ell=0}^{c} \sigma_\ell \ , \qquad (27)$$

where c is the cutoff point and m is the maximum value of ℓ provided by the calculation.

The above procedure was carried out with different values for the cutoff point and over the range of energies used in the calculations. Each reaction thereby yielded a family of curves of predicted isomer ratios based upon the chosen cutoff points. The experimentally determined isomer ratios were then superimposed upon the calculated curves. Figures 34 through 38 show the calculated and experimentally determined ratios for the various reactions yielding the compound nucleus Te^{122*}. The significance of the analysis lies in the fact that all the experimentally determined ratios can be correctly predicted by choosing a cutoff angular momentum of approximately 8. Except in the vicinity of the Coulomb barrier, over all the energies studied, the experimental ratios for the five reactions are within the area difined by cutoff value of between 7 and 9. Figure 39 illustrates this procedure for the C^{12} reaction. For the angular momentum distributions shown, the correct isomer ratio at each energy can be approximated by dividing the area under the appropriate curve for all values $\ell>8$ by the area under the same curve for values $\ell\leqslant 8$.

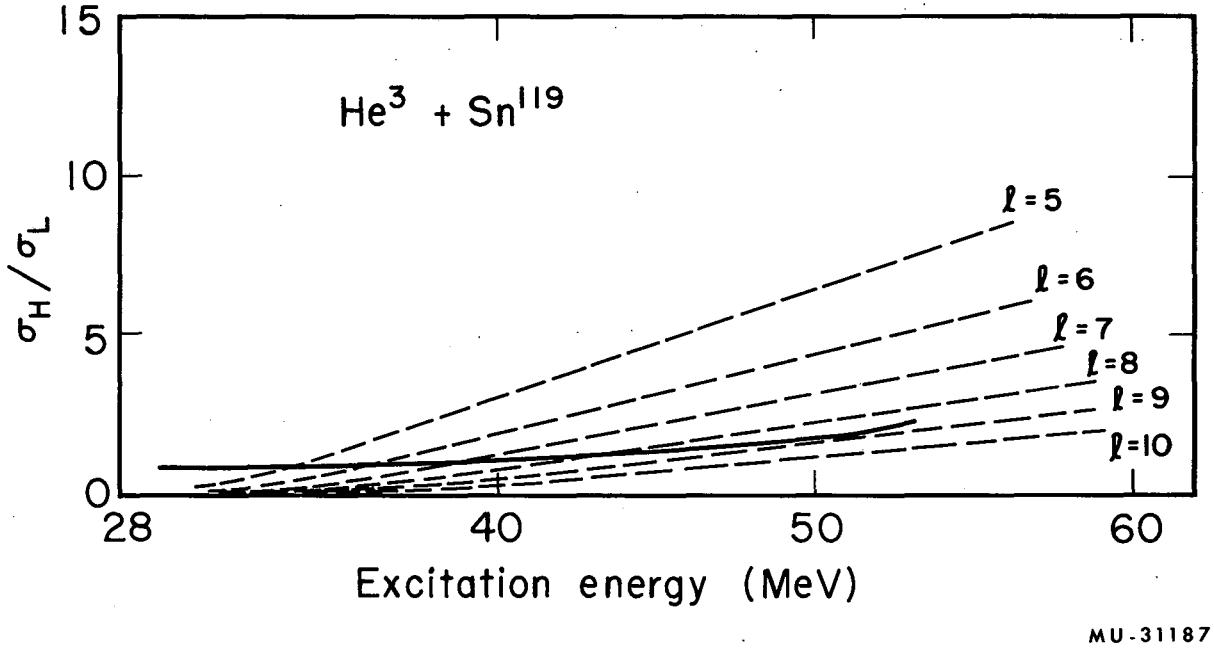

Fig. 34. Comparison of experimentally determined and calculated isomer ratios for the reaction $He^3 + Sn^{119} \longrightarrow Te^{119, 119m} + 3n$. The solid line is the experimental data and the broken lines are the ratios calculated on the assumption that all nuclei of ℓ greater than the value shown for each curve populate the high-spin isomer, while all nuclei with an angular momentum of ℓ or less yield the low-spin isomer.

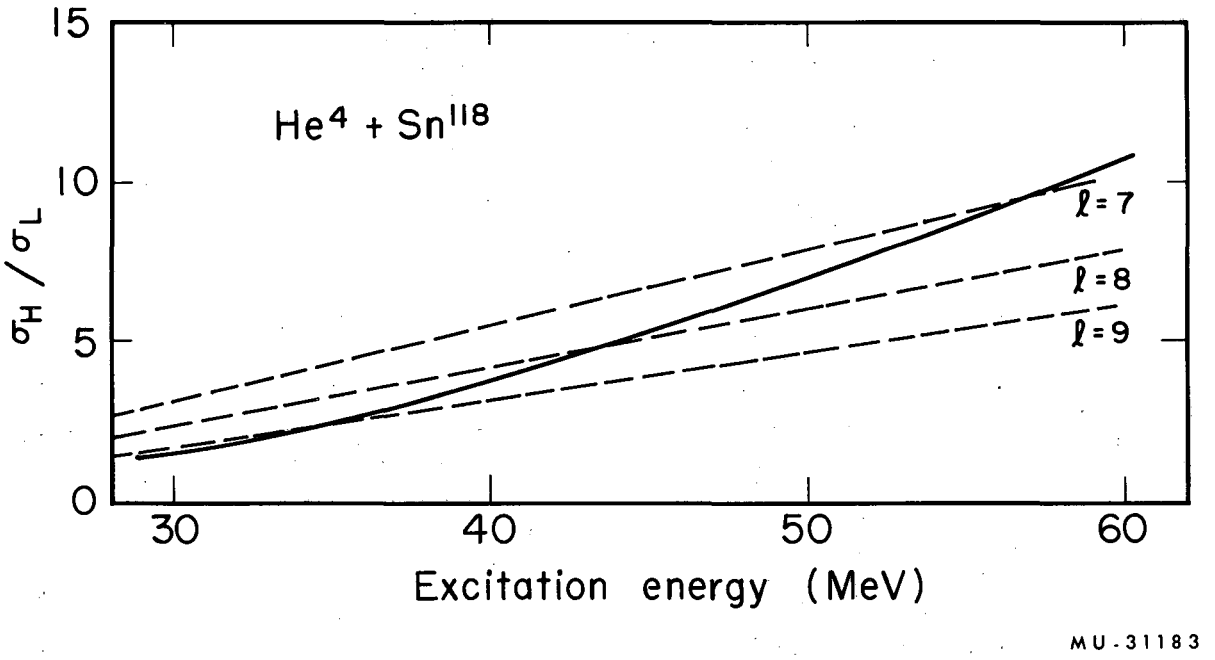

Fig. 35. Comparison of experimentally determined and calculated isomer ratios for the reaction $He^4 + Sn^{118} \longrightarrow Te^{119, 119m} + 3n$. (Explanation of the figure is the same as for Fig. 34.)

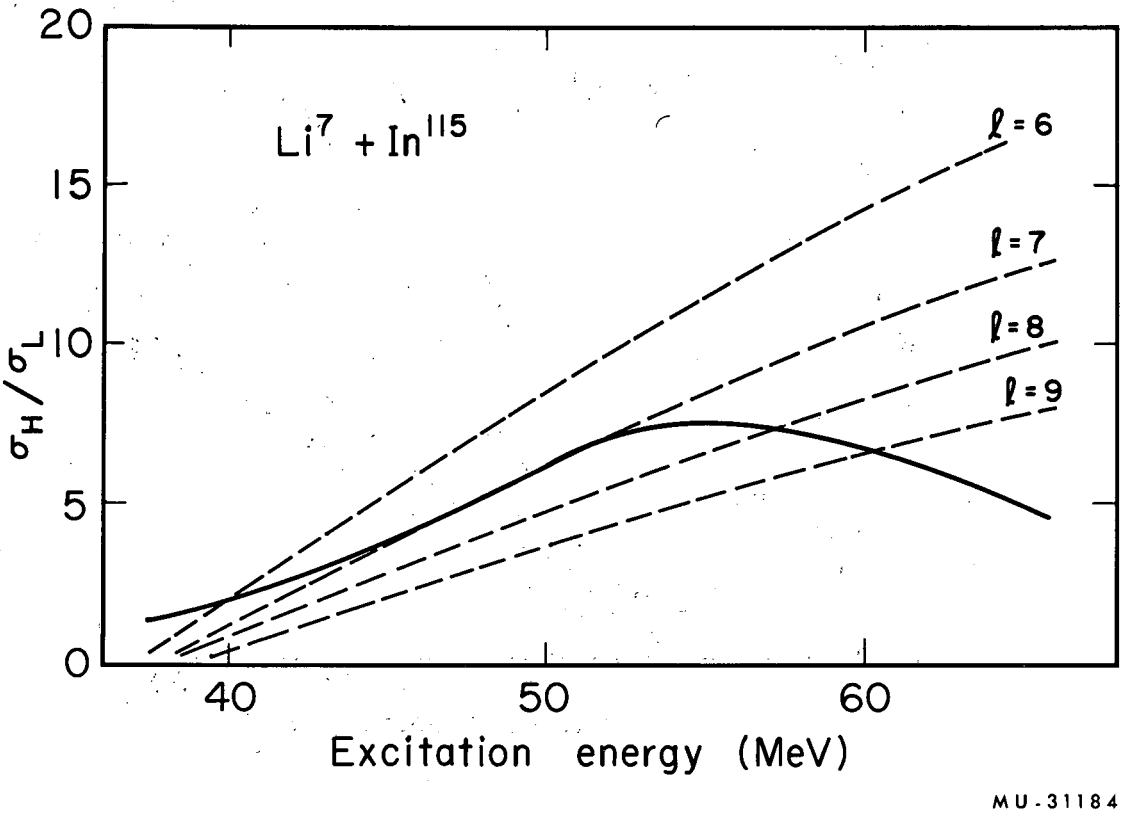

Fig. 36. Comparison of experimentally determined and calculated isomer ratios for the reaction $Li^7 + In^{115} \longrightarrow Te^{119, 119m} + 3n$. (Explanation of the figure is the same as for Fig. 34.)

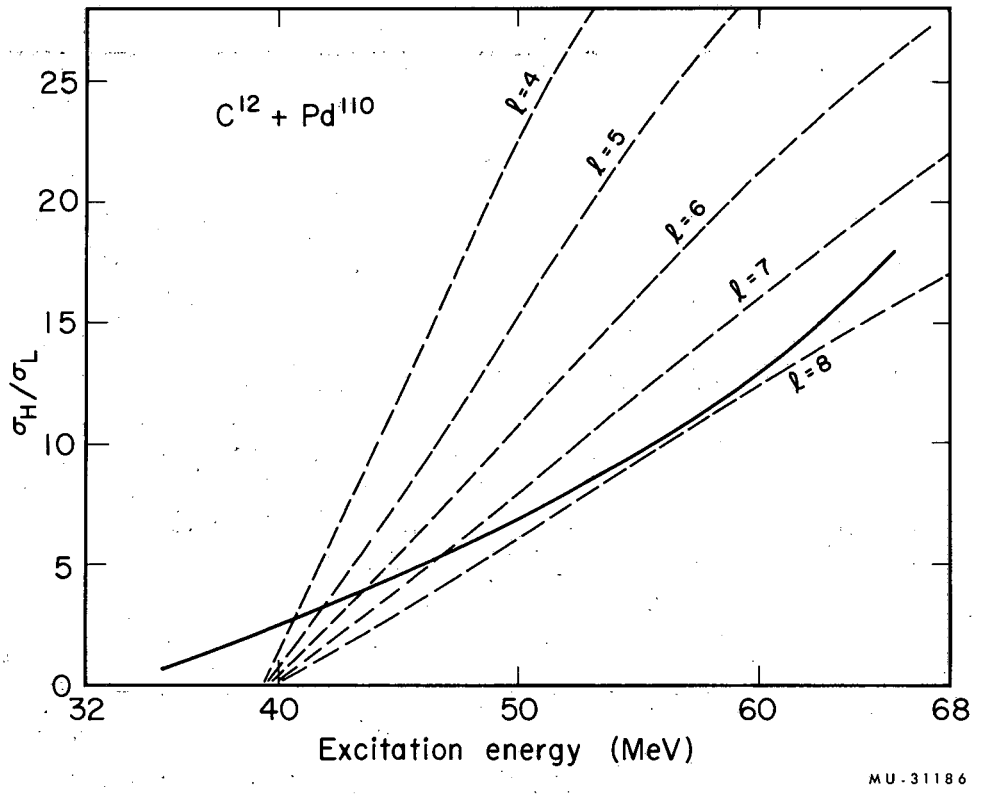

Fig. 37. Comparison of experimentally determined and calculated isomer ratios for the reaction $C^{12} + Pd^{110} \longrightarrow Te^{119, 119m} + 3n$. (Explanation of the figure is the same as for Fig. 34.)

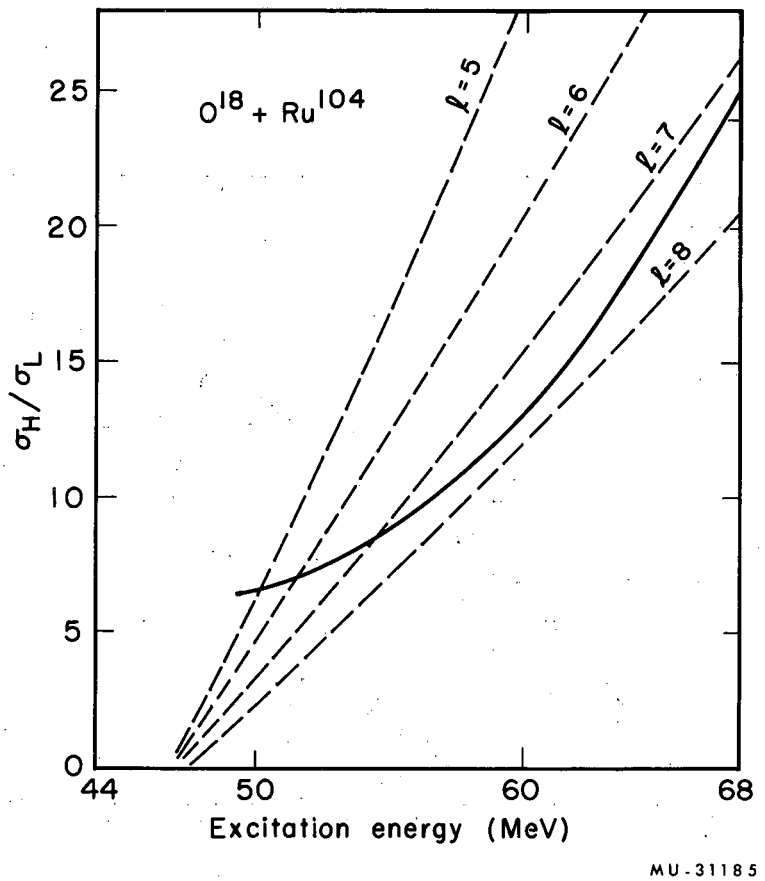

Fig. 38. Comparison of experimentally determined and calculated isomer ratios for the reaction O^{18} + Ru^{104} ⟶ $Te^{119, 119m}$ + 3n. (Explanation of the figure is the same as for Fig. 34.)

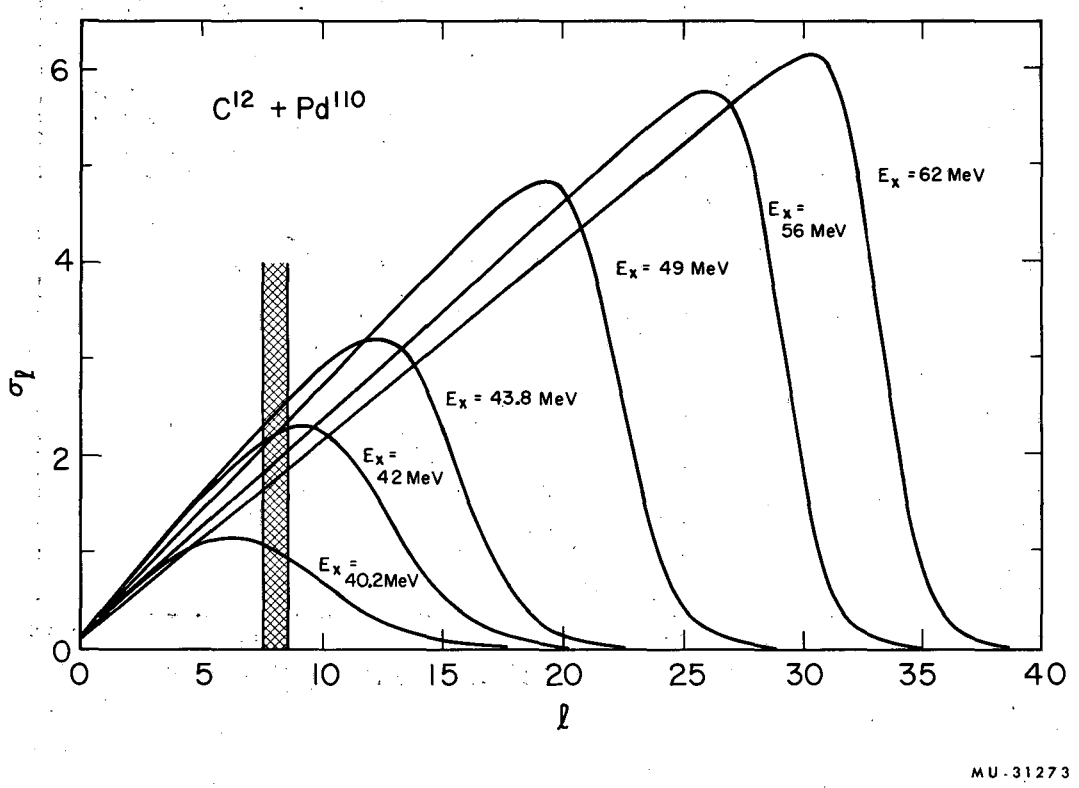

Fig. 39. Angular momentum distributions of the compound nuclei produced at different energies by the reaction $C^{12} + Pd^{110} \longrightarrow Te^{122*}$. The hatched area at $\ell = 8$ represents the zone of the angular momentum cutoff that yields reasonable agreement between calculated and experimentally determined ratios.

The analysis appears to break down in the vicinity of the Coulomb barrier. At about 6 to 8 MeV above the barrier the experimental curves are observed to break away and become greater than the values predicted by a cutoff value of about 8. In terms of the excitation energy, which is used in the plots, the Coulomb barrier for the O^{18} reaction occurs at about 44 MeV, for the C^{12} reaction at 36 MeV, for the Li^{7} reaction at 37 MeV, and for the He^{3} reaction at 32 MeV. The barrier for the He^{4} reaction is lower than any of the energies considered, and it is notable that only for this reaction is there no breaking away from the predicted ratios. As discussed previously, it appears that the compound-nucleus calculation underpredicts the amount of angular momentum transferred to the compound nucleus when the reaction occurs at energies only slightly above the Coulomb barrier.

Figures 40 through 43 show similar plots for the Te^{121*} and Te^{123*} compound nuclei systems. Although the cutoff values are not much different from that of the Te^{122*} system, it appears that the Te^{121*} compound nucleus, which yields the isomers by emission of two neutrons, requires a cutoff point at somewhat lower angular momentum (about 6); and the Te^{123*} system, which yields the isomers by a 4n reaction, a somewhat higher value (about 9).

The assumption that there is a sharp cutoff point such that all compound nuclei with angular momentum greater than the point yield the high-spin isomer and all compound nuclei with angular momentum less than or equal to the cutoff point yield the low-spin isomer, is undoubtedly a very crude approximation. The upper-state isomer is surely produced by compound nuclei with angular momentum less than the cutoff value and the inverse is true for the ground-state isomer. However, on the basis of the consistency of results, it is probably reasonable to conclude that the critical area in angular momentum that determines which isomer is produced must be in the vicinity of an angular momentum of 8.

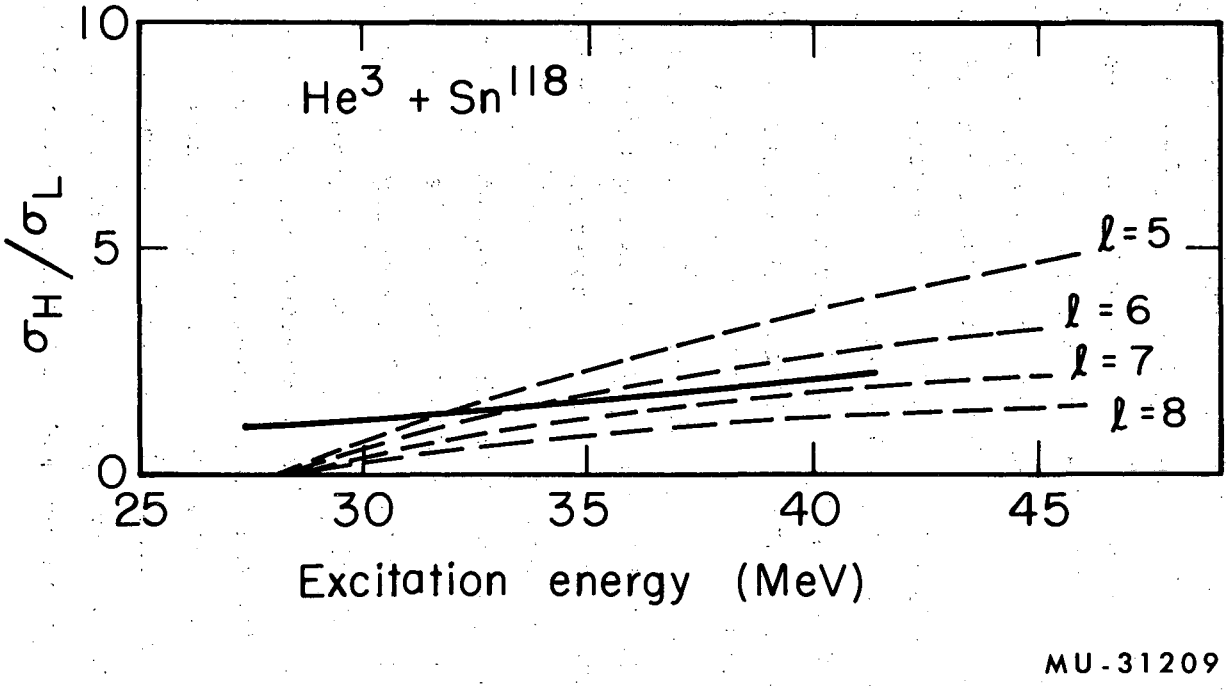

Fig. 40. Comparison of experimentally determined and calculated isomer ratios for the reaction $He^3 + Sn^{118} \longrightarrow Te^{119, 119m} + 2n$. (Explanation of the figure is the same as for Fig. 34.)

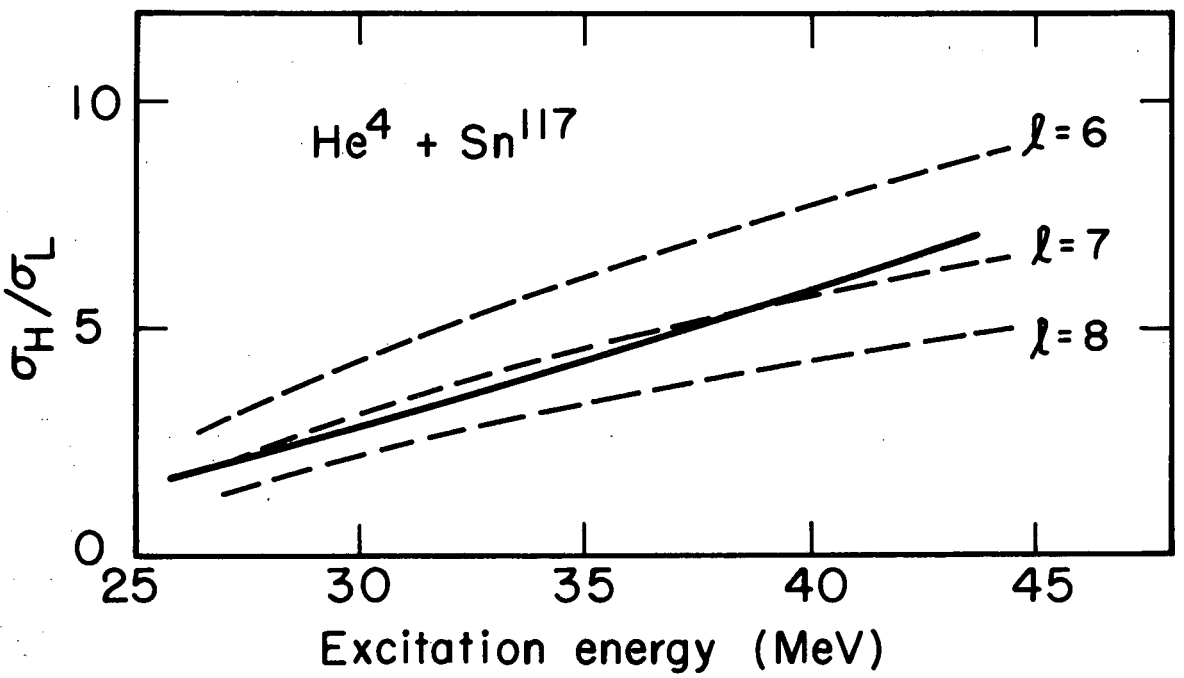

Fig. 41. Comparison of experimentally determined and calculated isomer ratios for the reaction $He^4 + Sn^{117} \longrightarrow Te^{119, 119m} + 2n$. (Explanation of the figure is the same as for Fig. 34.)

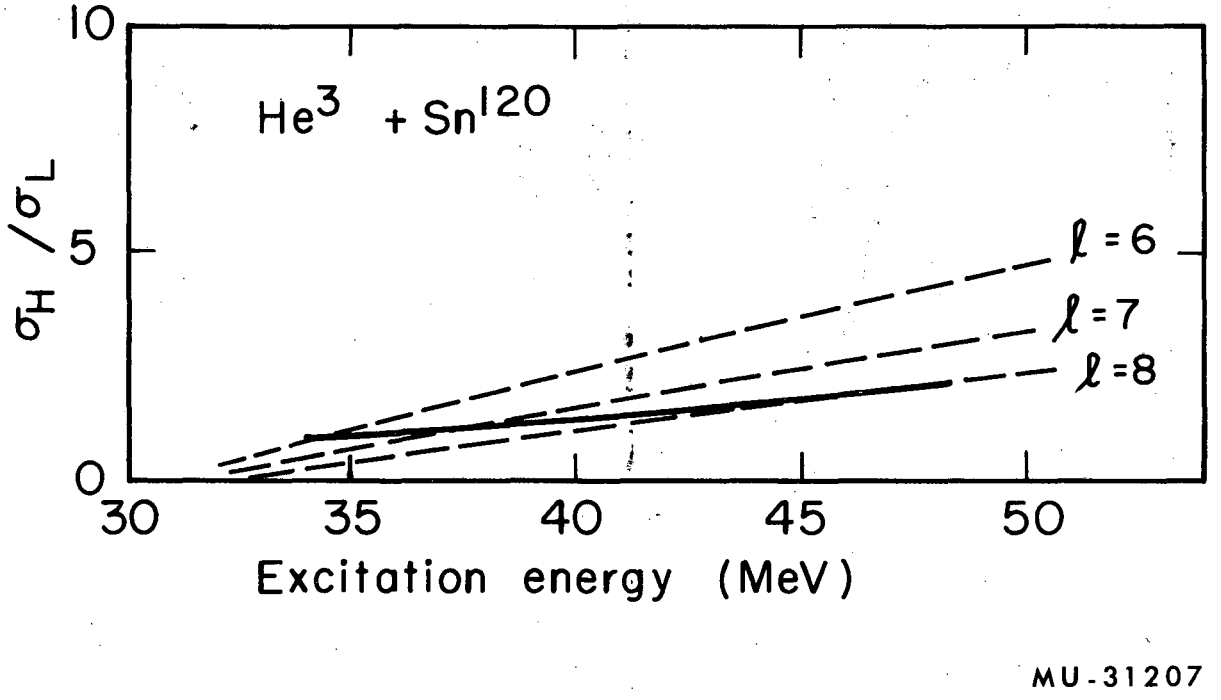

Fig. 42. Comparison of experimentally determined and calculated isomer ratios for the reaction $He^3 + Sn^{120} \longrightarrow Te^{119, 119m} + 4n$. (Explanation is the same as for Fig. 34.)

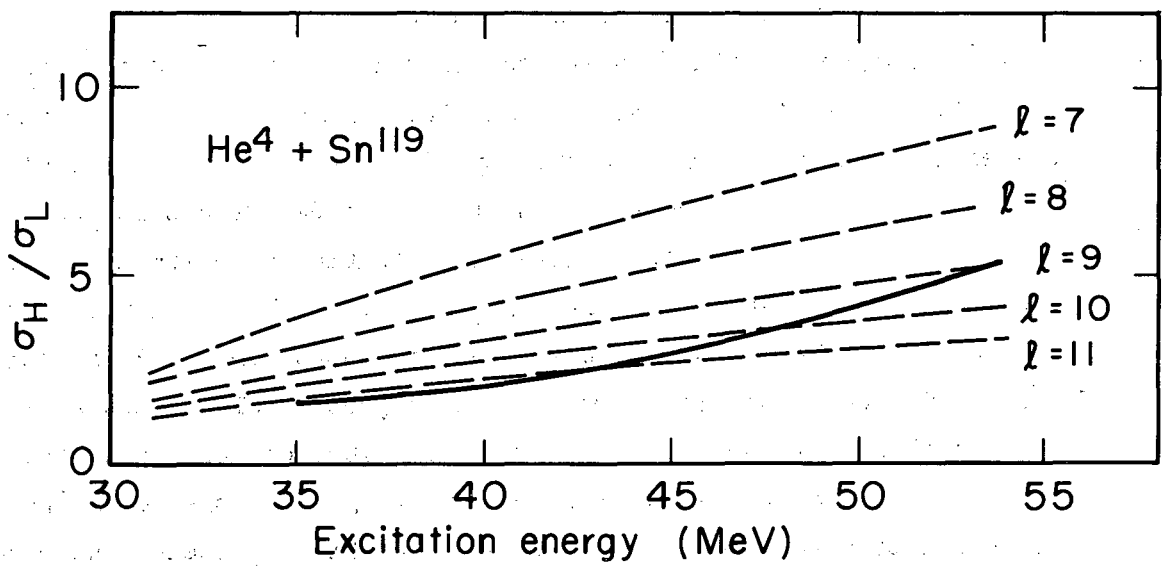

Fig. 43. Comparison of experimentally determined and calculated isomer ratios for the reaction $He^4 + Sn^{119} \longrightarrow Te^{119, 119m} + 4n$. (Explanation is the same as for Fig. 34.)

Recent work by Simonoff and Alexander indicates that the fractionation of the total reaction cross section into the individual reactions may have some angular momentum dependence.[8] The conclusion they reach is that neutron emission is favored from compound nuclei of low angular momentum. Therefore for compound nuclei at an energy which corresponds to de-excitation by either a 3n or a 4n reaction, the nuclei with low angular momentum will favor the 4n process while those with high angular momentum will favor the3n reaction.

In the calculations it was assumed that the fractionation was strictly a statistical phenomenon and the angular momentum distribution played no part in determining which product was formed. In considering the 3n reaction, to correct for angular momentum effects it would be necessary to weight the compound-nucleus angular momentum distribution toward the high ℓ values for all energies at which the 4n reaction competes and toward smaller ℓ values at all energies at which the 2n reaction can occur. The only energies at which the compound-nucleus angular momentum distribution would be the same as the distribution leading to the 3n reaction would be those at which no competing reactions occur (peak of the excitation function). If the above weighting procedure were carried out, it would have the effect of making the slopes of the calculated ratio curves (assuming the sharp cutoff point) to become steeper. For the heavy-ion reactions this would cause the calculated ratio curves to become more similar in slope to the experimental curves.

VI. ISOMER RATIO CALCULATIONS

The considerations of this section are somewhat more sophisticated and quantitative than those presented in the preceding section. Attempts are made to calculate the isomer formation cross section ratios according to the method of Vandenbosch and Huizenga.[10,18] The computations are performed with an IBM 7094 computer using a program provided by the above authors.[41] The calculation takes into account the intrinsic spins of the target and projectile, the emission of neutrons, and the γ-ray cascade. Proton emission is neglected, and it is assumed that all neutrons are emitted before the γ-ray cascade begins.

A. Theory of the Calculation

This subsection discusses the theoretical aspects of computing the relative formation cross sections of isomers produced in nuclear reactions.

Since high-energy projectiles can carry into a nucleus various amounts of angular momentum, the compound system produced in such reactions contains a wide distribution of spins. This distribution is calculated according to the following equation, which gives the formation cross section for a compound nucleus of spin J_c produced by a projectile of energy E:[6,79]

$$\sigma(J_c,E) = \pi\lambda\!\!\!^{-2} \sum_{S=|I+s|}^{I+s} \sum_{\ell=|J_c-S|}^{J_c+S} \frac{2J_c+1}{(2s+1)(2I+1)} T_\ell(E) \,. \tag{28}$$

$\lambda\!\!\!^{-}$ = de Broglie wavelength of the incoming projectile,
I = intrinsic spin of the target nucleus,
s = intrinsic spin of the projectile, and
$T_\ell(E)$ = barrier transmission coefficient for a projectile of angular momentum ℓ and energy E.

The maximum angular momentum of the system is $J_{c,max} = \ell_{max} + s + I$, and is either integral or half integral, depending upon the intrinsic spins.

For all the reactions considered, except those of He^3 and Li^7, the intrinsic spins of both target and projectile are zero, and Eq. (28) reduces to

$$\sigma(J_c, E) = \pi \lambda^2 (2J_c + 1) T_{J_c}(E) . \qquad (29)$$

The first part of the program computes the normalized initial compound-nucleus spin distribution according to Eq. (28). The input parameters that must be provided are

(a) target spin = I,

(b) projectile spin = s,

(c) proportionality constant = $\pi \lambda^2$
(In this work the absolute cross sections as a function of J_c were not required and the constant was set equal to 1. Such a procedure yields only a normalized spin distribution, P_{J_c}),

(d) transmission coefficients as a function of ℓ for the desired reaction (These were obtained from the Bunthorne calculation discussed in the preceding section).

The output quantities of the program at this point are the partial cross sections $\sigma(J_c, E)$, P_{J_c} (the probability that the compound nucleus has spin J_c), given by

$$P_{J_c} = \sigma(J_c, E) \Big/ \sum_{J_c=0}^{\infty} \sigma(J_c, E) , \qquad (30)$$

a running sum of P_{J_c}, and $\langle J_c^2 \rangle_{av}$.

The program next computes the normalized spin distribution of the system following neutron emission. The distribution depends upon two factors: the density of available levels having a final spin J_f,

and the amount of angular momentum carried away by the neutron (ℓ'). A particular state of spin J_c can decay by neutron emission to a variety of states, and the relative probability of population of state J_f is given by

$$P(J_f)_{J_c} \propto \rho(J_f) \sum_{S = |J_f - s'|}^{J_f + s'} \sum_{\ell' = |J_c - S|}^{J_c + S} T'_{\ell'}(E) \; ; \qquad (31)$$

where s' is the intrinsic spin of the emitted particle (1/2 for neutrons), and $T'_{\ell'}(E)$ is the transmission coefficient of the emitted particle of energy E and angular momentum ℓ'; $\rho(J_f)$ is the density of levels of spin J_f, and is predicted theoretically to be of the form[80,81]

$$\rho(J_f) \propto (2J_f + 1) \exp[-(J_f + 1/2)^2/2\sigma^2] \; . \qquad (32)$$

The σ is called the spin cutoff factor, and should not be confused with the same symbol used to represent the cross section. The context in which it is used will normally serve to differentiate between the two. The value of the spin cutoff factor is one of the results sought by this investigation.

The normalized yield of spin J_f, produced from an initial spin J_c, is the product of the initial normalized yield of J_c (Eq. 30) and the probability for an initial state J_c to emit a particle to yield a final state of spin J_f (Eq. 31):

$$\text{Normalized yield } (J_c \rightarrow J_c) = P_{J_c} \rho(J_f) \sum_{S = |J_c - s'|}^{J_c + s'} \sum_{\ell' = |J_c - S|}^{J_c + S} T'_{\ell'} \; . \qquad (33)$$

The total normalized yield of J_f is computed by summing over all values of J_c, and is given by the following equation:

$$P_{J_f} = \sum_{J_c = \begin{cases} J_{c_I} \text{ for } (J_f - \ell_{max} - s') \leq 0 \\ J_f - \ell_{max} - s' \text{ for } (J_f - \ell_{max} - s') > 0 \end{cases}} \left[P_{J_c} \; \rho_{J_F} \sum_{S=|J_f - s'|}^{J_f + s'} \sum_{\ell'=|J_c - S|}^{J_c + S} T'_{\ell'} \right]$$

$$J_c = \begin{cases} J_{c_{max}} \text{ for } (J_f + \ell'_{max} + s') \geq J_{c_{max}} \\ J_f + \ell_{max} + s' \text{ for } (J_f + \ell'_{max} + s') < J_{c_{max}} \end{cases}$$

$$J_f = \sum_{J_f = J_c + \ell'_{max} + s'}^{\begin{cases} J_{f_I} \text{ for } (J_c - \ell_{max} - s') \leq 0 \\ J_c - \ell_{max} - s' \text{ for } (J_c - \ell'_{max} - s') > 0 \end{cases}} \left[\rho_{J_f} \sum_{S=|J_f - s'|}^{J_f + s'} \sum_{\ell'=|J_c - S|}^{J_c + S} T'_{\ell'} \right]$$

where $\rho(J_f)$ is defined as in Eq. (32) for $J_f = J_{f_I}, J_{f_I} + 1, \cdots J_{f_{max}}$,

$J_{f_{max}}$ is $\ell_{max} + s' + J_{c_{max}}$,

$J_{c_{max}}$ is the maximum value of the index J_c from the input P_{J_c},

J_{c_I}, J_{f_I} are initial values of the indices J_c and J_f (i.e., if $J_{c_{max}}$ is integer, then $J_{c_I} = 0$; if $J_{c_{max}}$ is half integer, then $J_{c_I} = 1/2$; J_{f_I} behaves similarly with respect to $J_{f_{max}}$,

P_{J_c} is the normalized initial spin distribution from the initial compound nucleus,

$T'_{\ell'}$ are the transmission coefficients,

s' is the outgoing particle intrinsic spin,

ℓ'_{max} is the maximum value of the index ℓ' for the input $T'_{\ell'}$.

The portion of the numerator in brackets represents the relative probability of populating a final spin J_f after emission of a neutron from a compound nucleus of spin J_c. The bracketed denominator sums the relative probabilities of a nucleus of spin J_c leading to a final spin J_f over all possible values of the final spin. The quotient of the two bracketed portions then represents the absolute probability of populating a particular spin state J_f from an initial spin state J_c. The summation outside the brackets then sums the probability over all possible values of the initial spin J_c and thereby yields the absolute probability that a particular final spin J_f is produced from any compound nucleus spin J_c.

The input parameters for the second portion of the program are:

(a) normalized compound-nucleus spin distribution (output of the first part of the computation),

(b) spin of the emitted particles (1/2 in this investigation, since the only particles considered are neutrons),

(c) transmission coefficients of the emitted particles, $T'_{\ell'}$,

and

(d) the value of the spin cutoff factor σ.

The third and final portion of the computation involves the calculation of the spin distribution following γ-ray emission. It is assumed that no gamas are emitted until particle evaporation is complete, and that the probability of decaying from a state J_i to a state J_f is proportional to the density of states of spin J_f. According to this assumption the total normalized yield of state J_f is given by

$$F_{J_f} = \sum_{J_i = |J_f - \ell|}^{J_f + \ell} \frac{F_{J_i}\, \rho(J_f)\, \delta J_i, J_f}{\sum_{J_f = |J_i - \ell|}^{J_i + \ell} \rho(J_f)} \qquad (35)$$

where $\rho(J_f)$ is defined by Eq. (32)

$J_{f_{max}} = J_{i_{max}} + \ell$,

$\delta J_i, J_f = 1$ for $|J_i - J_f| \leq \ell \leq |J_i + J_f|$,

$\delta J_i, J_f = 0$ for all other conditions due to selection rules,

ℓ = multipolarity of gamma emission,

σ = spin cutoff factor

F_{J_i} = normalized initial spin distribution following the evaporation of last particle (output of the second portion of the computation).

The input for this portion of the calculation consists of the three parameters immediately above.

According to Eq. (35), upon emission of a γ ray each spin-state population of the excited nucleus redistributes itself among a number of new spin states, and a new distribution results. The number of states involved in the redistribution depends upon the multipolarity of the γ ray emitted. Depending upon the level of excitation of the nucleus,

various numbers of γ rays are emitted. The redistribution calculation is repeated for each emission.

Figures 44 through 46 illustrate the redistribution of spins that occurs on emission of neutrons and γ rays from a compound-nucleus system. These distributions were obtained by means of the computation discussed in the foregoing pages. For these calculations "equal energy neutrons," 1.5 MeV dipole γ rays, and a spin cutoff parameter of $0.5\ \sigma_{rigid}$ were employed. The significance of these parameters is treated in detail in the following section.

Figure 44 shows the broadening effect of the de-excitation on a single nuclear spin value. The illustration represents the results of a calculation for the reaction $He^4 + Sn^{118} \longrightarrow Te^{122*}$ in which both projectile and target nuclei have zero intrinsic spin. A single angular momentum value ($\ell = 15$) for the incoming projectile was fed into the program and the plot therefore shows the redistribution effects of the neutron emission and γ-ray cascade for a single spin state. Along the abscissa are plotted the various spin values, J, and the ordinate represents the probability P_J of the various values. Note that the original compound nucleus has a spin of 15 with unit probability.

Figure 45 illustrates the same type of calculation as Fig. 44 except that the reaction considered is $Li^7 + In^{115} \longrightarrow Te^{122*}$. Again a single angular momentum value ($\ell = 15$) was assigned to the projectile, but in this case the intrinsic spins of the projectile and target are not zero. The Li^7 spin is 3/2 and that of the In^{115} 9/2. Because of these intrinsic spins, a compound nucleus with a single spin value is not formed as it was for the He^4 reaction.

Figure 46 is a plot of the distributions resulting from a more realistic situration. The reaction considered is again that of He^4 and Sn^{118}. However, in this case angular momenta (a wide range of values, obtained from the Bunthorne calculation) and the corresponding transmission coefficients are fed into the program. This, then, represents the type of distributions considered in a typical isomer ratio calculation. The average value of the angular momentum of the compound nucleus as determined by the Bunthorne calculation is 15. This corresponds to the single angular-momentum value used in the first two calculations.

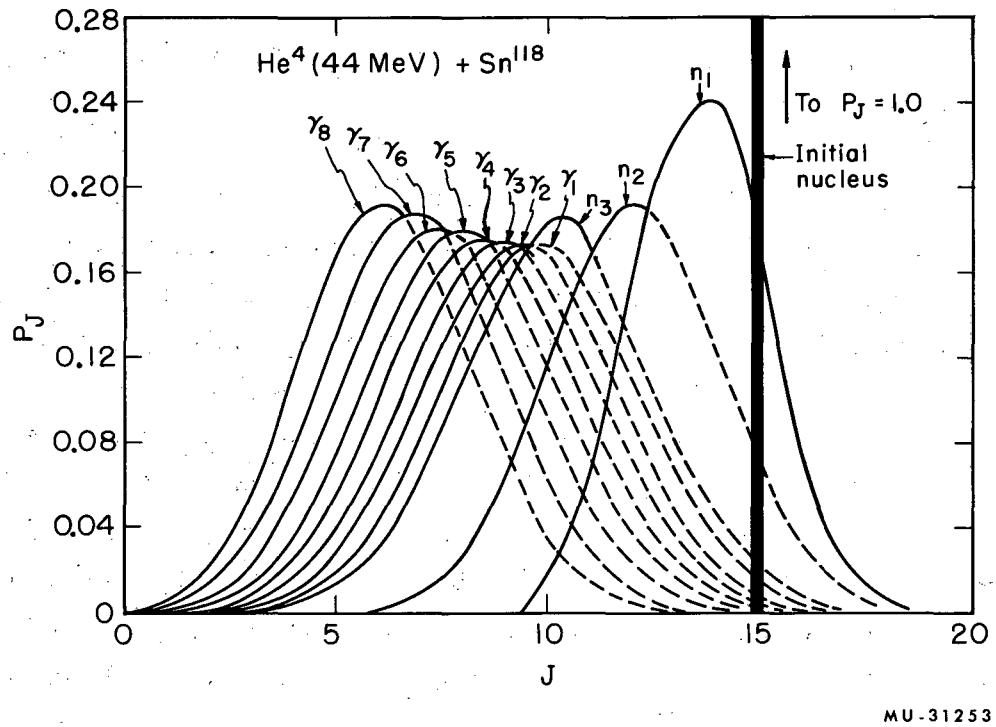

Fig. 44. Redistribution of spins occurring in a compound nucleus following neutron evaporation and γ-ray emission. The target and projectile had zero intrinsic spins, and a single angular momentum value (ℓ = 15) was assigned to the incoming projectile.

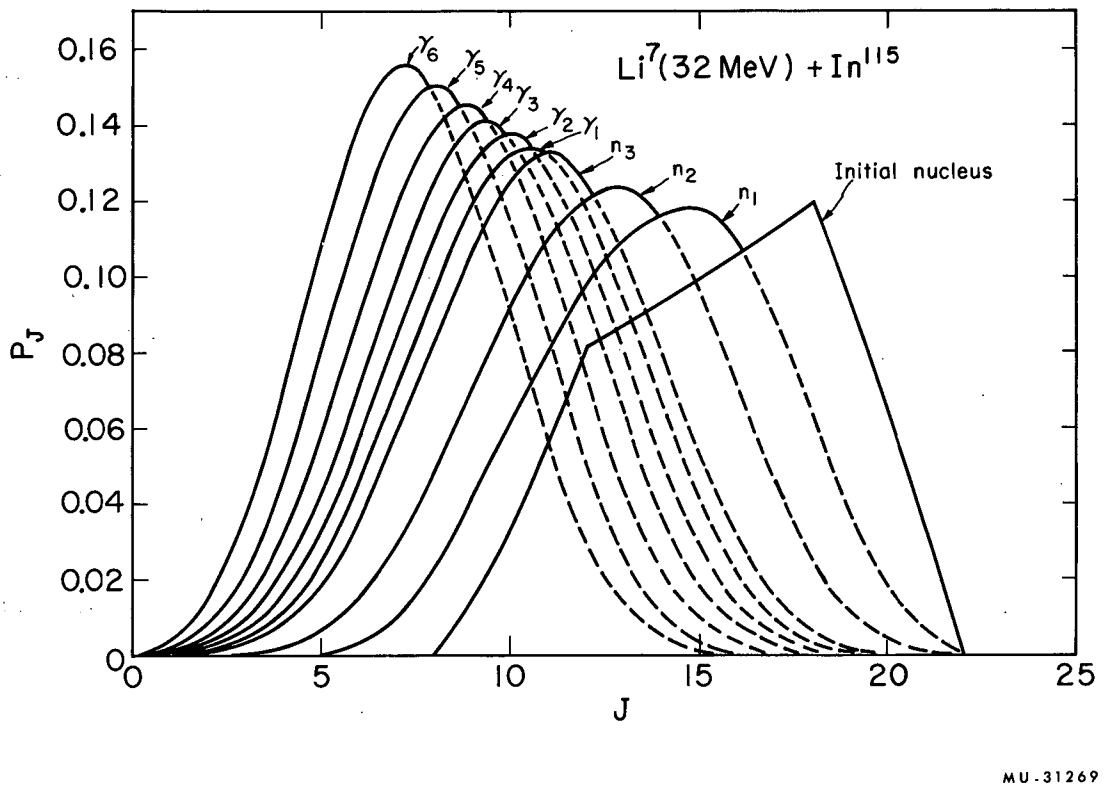

Fig. 45. Redistribution of spins occurring in a compound nucleus following neutron evaporation and γ-ray emission. The target and projectile had intrinsic spins of +9/2 and +3/2 respectively. A single angular momentum value (ℓ = 15) was assigned to the incoming projectile.

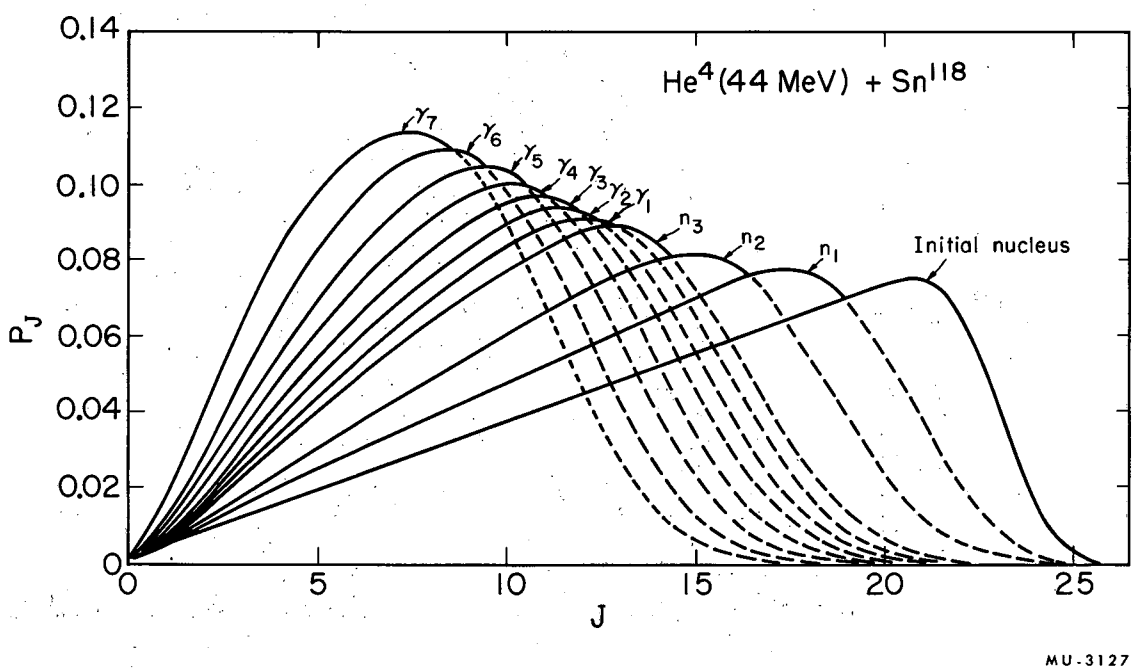

Fig. 46. Redistribution of spins occurring in a compound nucleus following neutron evaporation and γ-ray emission. The target and projectile spins were zero but a complete distribution of angular momentum, as determined by the Bunthorne calculation, of $\langle \ell \rangle = 15$ was assumed to be carried in by the projectile.

Normally it is assumed that, upon emission of the next-to-last γ ray, only two states are available for population, these states being the upper and lower isomeric states of the isotope being studied, and that the isomer populated is that involving the smallest spin change. Thus for the isomers studied in this investigation, the division would occur at a spin of 5/2. All excited nuclei of spin 5/2 or less would be assumed to populate the + 1/2 ground state and those of spin 7/2 or greater would populate the - 11/2 upper state. However, in the tellurium-119 isomers it is likely that a + 3/2 state also competes. Such a state, if populated, would lead directly to the ground-state isomer. No data are presently available on the low-lying states of tellurium-119, but a good analogy can probably be drawn from the levels of tin-117, which contains the same number of neutrons.[82]

In tin-117 the + 7/2 level lies in the vicinity of 1 MeV excitation, and a + 3/2 level lies between a low-lying -11/2 state and the + 1/2 ground state. If the same arrangement were present in tellurium-119, the + 7/2 state could populate either the - 11/2 isomeric state or the + 3/2 state by the same spin change. The first possibility, however, would be an M2 transition, whereas the second would be an E2 transition. Since the E2 transition is much faster, it is assumed in these calculations that the division in spins determining which isomer is produced occurs at the 7/2 level. All spins of 7/2 or less are assumed to populate the ground-state isomer and those above 7/2 the upper-state isomer.

The calculated isomer ratio is influenced rather strongly by the chosen point of division. For a typical calculation, a division at spin 5/2 yields a ratio approximately twice as large as a division at spin 7/2. Table XXII shows this effect for the reaction $C^{12} + Pd^{110} \longrightarrow Te^{122*}$.

Table XXII. Comparison of the calculated isomer ratios obtained by a division at spin 5/2 with that obtained by a division at spin 7/2.

Projectile energy (MeV)	Calculated isomer ratios	
	Division at 5/2	Division at 7/2
64	27.6	14.0
56	16.0	8.1
48	7.5	3.7
40	1.7	0.7

B. Parameters Necessary for the Calculation

A number of parameters must be determined in order to carry out the computation. Unfortunately most of these parameters have not been experimentally determined and the various theoretically predicted values are not always in good agreement. The parameters that must be determined are as follows.

(a) The angular momentum brought into the system by the incoming projectile and the associated transmission coefficients.

(b) The angular momentum carried off by the neutrons and the associated transmission coefficients. In order to determine these values it is necessary to know the energies of the emitted particles. Fortunately experimental results and theoretical predictions are in fairly good agreement and the values used are considered to be quite reliable.

(c) The number and multipolarity of the γ rays emitted. This is one of the weakest aspects of the calculation, since what little experimental evidence is available in this area does not show good agreement with the theoretical predictions.

(d) The spin cutoff factor (σ). The caluclations are very sensitive to this parameter and are actually used to estimate what its value must be.

Each of these four types of input parameters is dealt with in detail in the following subsections.

1. The Angular Momentum Brought into the System by the Incoming Projectile and the Associated Transmission Coefficients

These values are taken from the Bunthorne calculation described in the Section V, and appear to be quite good at energies corresponding to the peak of the excitation function. As previously discussed, the transmission coefficients for large spins are apparently too low when the incoming projectile energy is only slightly above the Coulomb barrier.

An additional complication arises as one leaves the vicinity of the peak of the excitation function. The transmission coefficients provided by the calculation are for compound-nucleus formation and should probably be corrected for any angular momentum effects involved in the fractionation of the compound nucleus into the various products. On the high-energy side of the excitation function of the reaction being considered, the distribution of compound-nucleus angular momentum should be weighted in favor of high spin states, since the low spin states favor neutron emission and thus yield a product containing one less neutron. On the low-energy side of the excitation function the opposite modification would be required. No attempt has been made to carry out such an analysis because no information is available on the magnitude of the effect.

2. Angular Momentum Carried Off by the Neutrons

The angular momentum carried off by the neutrons and the associated transmission coefficients are a function of the neutron velocity. The velocities are in turn a function of the nuclear excitation energy or temperature. The energy distribution of neutrons emerging from an excited nucleus is predicted theoretically to be of the form[6]

$$N(E_n) \propto E_n \exp(-E_n/T) , \qquad (36)$$

where $N(E_n)$ is the relative number of neutrons of kinetic energy E_n; T is the nuclear temperature of the residual nucleus, and is defined by

$$1/T = d \ln [\rho(A,E)] / dE , \qquad (37)$$

$\rho(A,E)$ is the level density, and is related to the excitation energy and the number of nucleons within the nucleus. It is approximated by the expression[6]

$$\rho(A,E) = C \exp\left(2\sqrt{aE}\right) , \qquad (38)$$

where C and a are dependent upon the mass number A, and the energy dependence of C has been neglected. Substituting Eq. (38) into Eq. (37) and carrying out the differentiation yields

$$T = \sqrt{E/a} , \qquad (39)$$

which shows the relationship between the nuclear temperature and the excitation energy.

According to Eq. (36), the neutrons are emitted over a wide range of energies, therefore to treat the problem in all exactness it would be necessary to assign a different set of transmission coefficients to each neutron according to its energy and to weight the various assignments according to the calculated distribution. Bishop has approximated this by dividing the energy distribution into selected bins and assigning sets of transmission coefficients corresponding to the average energy of each bin.[15] The isomer ratio calculation was carried out for each bin and the final results weighted according to the relative numbers of neutrons contained within the bins.

Bishop also did calculations in which he used only a single set of transmission coefficients, which were associated with the average energy of the evaporated neutrons.[15] This average neutron kinetic energy is equal to 2T if the distribution is of the form given by Eq. (36), and if the E in the equation represents the residual excitation energy after the evaporation. He found that so far as the isomer ratio calculations are concerned, the results obtained by the simpler method of using only the average kinetic energy of the neutrons was in good agreement with those obtained by dividing the neutron spectrum into various bins. In this work the average energy of the particles is used and, hence, only a single set of transmission coefficients is necessary for each evarporation.

The residual energy, E_r, of an excited nucleus after emission of a neutron must equal the original excitation energy of the compound nucleus, E_c minus the binding energy B_n and the kinetic energy E_n of the emitted neutron. Or, expressed mathematically,

$$E_r = E_c - B_n - E_n = E_c - B_n - 2T , \qquad (40)$$

where 2T has been substituted for the neutron kinetic energy. Defining the excitation energy in Eq. (39) as that of the residual nucleus and substituting in Eq. (40), one obtains

$$T = \sqrt{[\underline{a}\,(E_c - B_n) - 2\underline{a}T] \,/\, \underline{a}} . \qquad (41)$$

Solving Eq. (41) for T yields

$$T = [-1 \pm \sqrt{1 + \underline{a}(E_c - B_n)}] \,/\, \underline{a} . \qquad (42)$$

The positive root must be selected, since a negative temperature T is not allowed. Once the parameter $\underline{a}$ is known, Eq. (42) can be solved to yield the nuclear temperature of the residual nucleus, and the average neutron energy, $E_n = 2T$, can then be determined. Neutron binding energies were taken from Seeger's masses,[63] and the excitation energies were calculated as discussed in Section IV. The constant $\underline{a}$ is not unambiguously defined, but recent work indicates that its value lies in the range of A/12 to A/8 MeV^{-1}.[38,83,84] The calculations done in this work use a value of A/8 MeV^{-1}. Bishop has shown that the calculation is quite insensitive to this parameter and another choice would yield practically the same results.[15]

Recent experimental evidence indicates that setting the average neutron energy equal to 2T is a good approximation.[8] Simonoff and Alexander have determined average neutron kinetic energies for various xn reactions and plotted them as a function of the total energy available.

The residual energy left in the nucleus after the emission of three neutrons as calculated by using their data, is in very good agreement with that calculated by using the $E_n = 2T$ assumption. Table XXIII shows the close correspondence. Some calculations were performed in which it was assumed that all the neutrons were of equal energy (using the average energies indicated by Simonoff and Alexander's work) and the same set of transmission coefficients was therefore used for each evaporation. The results did not differ appreciably from those obtained by the same type of analysis but assuming the energy of the three neutrons to be different and to be given by the 2T relationship.

Bishop[15] and Vandenbosch[39] have both performed calculations employing the square well neutron transmission coefficients of Feld et al.[85] and the optical model coefficients of Campbell.[86] The results obtained from the two sets of coefficients were almost identical.

The neutron transmission coefficients used in this work are the square well coefficients of Feld. The coefficients are given in graphical form as a function of the parameter X, which is defined in terms of the nuclear radius R and the neutron kinetic energy E_n:

$$X = 0.22\, R\sqrt{E_n} \quad . \tag{43}$$

The square well radius of tellurium-120 is 7.4×10^{-13} cm. The transmission coefficients used in the calculations are for a well radius of 8.0×10^{-13} cm.

Table XXIII. Residual nucleus energy (E_r) after neutron emission; comparison of Simonoff's and Alexander's data with results obtained by assuming $E_n = 2T$

Reaction $He^4 + Sn^{118} \longrightarrow Te^{122*}$

Projectile energy (MeV)	Original nucleus excitation energy (MeV)	Neutron	Neutron kinetic energy (MeV)		Residual nucleus energy (MeV)	
			$E_n=2T$	Exp[a]	$E_n=2T$	Exp[a]
50	49.6	n_1	3.14	2.9	36.9	37.1
		n_2	2.74	2.9	26.6	26.6
		n_3	1.98	2.9	14.6	13.7
44	43.9	n_1	2.88	2.6	31.4	31.7
		n_2	2.38	2.6	21.1	21.5
		n_3	1.60	2.6	9.5	8.9
38	38.3	n_1	2.62	2.2	26.1	26.5
		n_2	2.06	2.2	16.4	16.7
		n_3	1.18	2.2	5.2	4.5
32	32.5	n_1	2.34	1.6	20.8	21.3
		n_2	1.74	1.6	11.5	12.1
		n_3	0.50	1.6	1.0	0.5

[a]The columns labeled Exp. refer to the average neutron energies as determined by Simonoff and Alexander (reference 8).

3. Number and Multipolarity of the Gamma Rays Emitted

The number of γ rays involved in the de-excitation is probably the least satisfactory parameter applied in the calculation. Two basically different methods are employed in determining this quantity, and they give rather widely differing results. The multipolarity is probably not as critical as the number of γ rays emitted, but it does have an appreciable effect. In general, to fit the data, if the multipolarity goes up the multiplicity must come down. For most of the calculations it is assumed that dipole transitions occur. It has been assumed by other investigators[38] that although some quadrupole emission undoubtedly occurs, it is primarily attributable to states of high spin that are forced to emit the higher-multipolarity gammas in order to rid themselves of large amounts of angular momentum. Such a process would not be important in predicting isomer ratios, since such high spin states would populate the high-spin isomer anyway.

The methods employed in this investigation for estimating the number of γ rays emitted in the de-excitation process are discussed in the following paragraphs.

Assuming the relationship between level density and excitation energy given in Eq. (38), one can show that the expected γ-ray energy distribution should be of the form[87]

$$N(E_\gamma) \propto E^3 \exp\left[2\sqrt{\underline{a}\,(E_c - E_\gamma)}\right], \qquad (44)$$

where $N(E_\gamma)$ is the relative number of γ rays having an energy E_γ. Using this distribution and assuming that only single-particle states were involved, Strutinsky et al. were able to obtain, for the average number of γ rays emitted from an excited nucleus of energy E_c,[88] the approximate relationship

$$\overline{N}_\gamma(\ell+1) = \sqrt{\underline{a}\,E_c}\,. \qquad (45)$$

The average number of γ rays emitted is $\bar{N}_\gamma$, the multipolarity of the emission is ℓ, and $\underline{a}$ is the constant defined by Eq. (38).

Strutinsky et al. have also shown that the average energy, $\bar{E}_\gamma$, of the γ rays emitted from a nucleus of temperature T can be expressed as

$$\bar{E}_\gamma \approx (2\ell + 2)T, \tag{46}$$

and since $T = \sqrt{E_c/\underline{a}}$, the equation can be rewritten as

$$\bar{E}_\gamma \approx (2\ell + 2)\sqrt{E_c/\underline{a}}\,. \tag{47}$$

Vandenbosch and Haskin have modified the quation slightly and for dipole radiation propose that the average γ-ray energy may be expressed by[38]

$$\bar{E}_\gamma = 4\sqrt{(E_c - 1)/\underline{a}}\,, \tag{48}$$

where E_c is the excitation energy of the nucleus before the γ ray is emitted.

The remaining source of information on γ-ray energies is the work of Mollenauer,[7,89] whose experiments on the angular distribution of γ rays indicate a large amount of quadrupole radiation of average energy 1.2 ± 0.3 MeV. His work also indicates that compound-nuclei systems produced in heavy-ion bombardments may dissipate as much as 25 MeV of their energy in the γ-ray cascade. The large amount of energy carried away by the γ rays is in agreement with the results obtained by Simonoff and Alexander, whose angular correlation experiments indicated that as much as 30 MeV may be removed from the compound system by means of γ rays.[8] However, most of Mollenauer's bombardments were at energies approximately twice as high as those employed in this investigation, and

it was necessary for him to propose collective modes of de-excitation to account for the angular distributions. A number of calculations were performed in which it was assumed that each γ ray had an energy of 1.5 MeV (corresponding to the upper limit of the Mollenauer data). At low excitation energies this is about the same as the energy predicted by the theoretical equations, but at high energies it is much less and consequently requires that a rather large number of γ rays be emitted (as many as 17 for the higher-energy carbon reactions).

The number of γ rays emitted, as predicted by the above methods, depends upon the excitation energy left in the nucleus after evaporation of the last neutron. Equation (45) yields the number directly, and the energy of each γ ray is taken as the excitation energy at the beginning of the cascade divided by the number of γ rays emitted.

When Eq. (48) was used to determine the number of γ rays emitted, the procedure was as follows: After emission of a γ ray of energy E, the excitation energy remaining in the nucleus is $E_c - E$. This value is used to predict the energy of the second γ ray, and the procedure is continued until the excitation energy remaining in the nucleus is less than 2 MeV. For remaining energies of 1 to 2 MeV it is assumed that two more equal-energy γ rays are emitted, and for energies of less than 1 MeV it is assumed that a single additional γ ray is emitted.

When it was assumed that each γ ray carried off 1.5 MeV, the number of γ rays emitted was calculated by merely dividing the total available energy by 1.5. For all the methods it was normally assumed that only one γ ray was emitted when the excitation energy remaining after the last neutron evaporation was less than 1 MeV.

Table XXIV compares the number of γ rays expected for a given excitation energy according to the three methods described. It is seen that Eqs. (46) and (48) predict practically the same number; however, when Eq. (46) is used the γ rays are all assumed to be of the same energy. Use of Eq. (48) predicts γ rays whose energy decreases with the remaining excitation energy.

Table XXIV. Comparison of the number of γ rays predicted for a given excitation energy as determined by three independent methods.

Excitation energy after last neutron (MeV)	Number of γ rays emitted[a]			
	Method #1 (dipole)	Method #1 (quadrupole)	Method #2	Method #3
23.4	9.4	6.2	9.0	15.6
17.4	8.1	5.4	8.0	11.6
14.6	7.4	4.9	7.0	9.7
10.7	6.3	4.2	6.0	7.1
9.5	6.0	4.0	5.0	6.3
5.2	4.4	2.9	4.0	3.5
3.4	3.6	2.4	3.0	2.3
1.0	1.0	1.0	1.0	1.0

[a]Method #1 makes use of Eq. (45).

Method #2 uses Eq. (48).

Method #3 assumes that each γ ray has an energy of 1.5 MeV.

Equation (48), as explained, leads to integral numbers for the multiplicity of the cascade but the other two procedures do not. Since the calculation is rather sensitive to the number of γ rays, whenever the predicted number was nonintegral the ratio calculation was performed for the two nearest whole numbers and the ratio was assumed to vary linearly between the two. The ratio was thus adjusted for any fractional number of γ rays. For example: if it was predicted that 7.6 γ rays would be emitted, the ratio calculation was performed for 7 γ rays and for 8 γ rays. The difference in the ratio obtained by the two calculations was multiplied by 0.6 and the result subtracted from the ratio calculated for the 7-γ-ray cascade (the number was subtracted, since the ratio decreases with the number of γ rays emitted).

Table XXV shows the sensitivity of the isomer ratio calculation to the number of γ-rays emitted and their multipolarity. Equation (45) predicts that the number of γ rays emitted should go down as the multipolarity goes up. However, for sake of comparison, the number was assumed to be the same. The calculation data shown are for the $He^4 + Sn^{118}$ reaction at 44 MeV (projectile energy). The energy of each γ ray was assmed to be 1.5 MeV.

Table XXV. Sensitivity of the calculated isomer ratio to the number and multipolarity of the γ rays emitted.

Number of γ rays emitted	Isomer ratio (dipole)	Isomer ratio (quadrupole)
0	18.7	18.7
1	18.0	16.4
2	17.0	14.0
3	16.0	11.6
4	14.9	9.3
5	13.6	7.2

According to Eq. (45), in order to achieve the same amount of nuclear de-excitation, only about 2/3 as many quadrupole as dipole γ rays are required. The results shown in Table XXV show that even if such a correction were applied, the quadrupole emission would yield a smaller calculated ratio than the dipole emission.

4. The Spin Cutoff Parameter, σ

Once the energy of the neutrons and the multiplicity and multipolarity of the γ rays have been decided upon, the one remaining parameter that must be supplied for the computation is the spin-cutoff or spin density parameter, σ. This parameter must be supplied for each event, whether it be the evaporation of a neutron or the emission of a γ ray.

A number of investigators have assumed constant values for σ in calculations of this type and have obtained reasonable results for σ values ranging from about 3 through 5.[10,15,18,90] Such a procedure is probably quite useful at low energies at which the number of neutrons and γ rays emitted is quite small. However, when the neutron and γ-ray emission occur over a fairly wide range of energies, the variation of σ with energy must be considered.

Erickson has shown that the spin density parameter, σ, is related to the moment of inertia of the nucleus, $\mathcal{I}$ through the relationship[91]

$$\sigma^2 = cT = \mathcal{I}T/\hbar^2 , \qquad (49)$$

where T is the nuclear temperature as defined in Eq. (39), which, when substituted into Eq. (49), yields

$$\sigma^2 = (\mathcal{I}/\hbar^2)\ (\sqrt{E_c/a}) . \qquad (50)$$

It has also been shown by Erickson[92] that at high excitation energies the moment of inertia, $\mathcal{I}$, of the nucleus should become equal to that of a rigid sphere,

$$\mathcal{I}_{rigid} = (2/5)mAR^2 . \qquad (51)$$

In this equation, m is the nucleon mass, A is the mass number of the particular isotope considered, and R is the nuclear radius. Assuming that the moment of inertia is equal to the rigid value and substituting Eq. (51) into Eq. (49) yields

$$\sigma^2 = (2/5)\ (mAR^2/\hbar^2)(\sqrt{E_c/a}) . \qquad (52)$$

This equation has been used to construct a plot of σ vs the excitation energy. Since $\mathcal{I} = \mathcal{I}_{rigid}$ is assumed, all σ's obtained from this equation are designated σ_r.

A number of investigations have been carried out in which σ_r has been used in calculations similar to those described in this work[15,38,93] The results have invariably been too high, and usually a value of about 0.3 to 0.6 of the rigid value is necessary in order to obtain agreement between experiments and calculations.

The reduction of the moment of inertia from that predicted by the rigid-body assumption is usually attributed to pairing interactions. Lang,[94] Erickson,[95] and LeCouteur[96] have all considered such interactions in detail, and have derived the formulae as given below.

In order to account for the pairing interaction the simple formula relating the excitation energy and the nuclear temperature ($E_c = \underline{a}T^2$) is replaced by

$$E_c = \underline{a}T^2 - T - (1/12)g\Delta^2 - (1/2)\epsilon\Delta \ , \qquad (53)$$

where Δ is defined as[95]

$$\Delta \approx 3.36 - 0.008 \ A \ \text{MeV} \ , \qquad (54)$$

and ϵ takes the values 0,1,2 for even-even, even-odd, and odd-odd nuclei respectively. Equation (51) is considered to be accurate at all energies above that given by $T \approx \Delta/3$, and for the tellurium isotopes this is equivalent to about 0.8 MeV.

By use of Eq. (53) as the definition of the nuclear temperature, and other equations provided by Lang,[94] the nucleus level density parameter, σ, may be evaluated as follows:

$$\sigma^2 = c''T,$$

where c'' is given by $c'' = (c')^{1/3}(c/2 + c'/2)^{2/3}$, (55)

and c' is in turn defined by

$$T\,c' = [cT \exp(-0.44\ \Delta/T)] + \epsilon \langle m^2 \rangle [1-\exp(-0.44\ \Delta/T)];$$

c is the constant defined by Eq. (49) and may be thought of as a moment of inertia. It is evaluated in terms of $\mathcal{J}_{rigid}$.

The only term in the above expressions that has not been discussed is $\langle m^2 \rangle$. Here m represents the magnetic quantum number and is the projection of J upon some selected axis of the nucleus; $\langle m^2 \rangle$ is the mean square of m for single-particle states of energy close to the Fermi level. It is evaluated through the relationship $c = \langle m^2 \rangle g$. The c is determined as discussed in the preceding paragraph, and g, which depends upon the density of the single-particle states, is given by

$$\underline{a} = (1/6)\pi^2 g \ . \qquad (57)$$

Because of the ϵ term is Eq. (53), three values of σ are obtained for any given excitation energy. For tellurium, however, no odd-odd isotopes are possible, and the equation therefore yields only two values of σ. In considering the neutron evaporation and the γ-ray cascade leading from Te^{122*} to the isomers of tellurium-119, only one even-even nucleus is encountered, namely, Te^{120}.

Values of σ were calculated according to the above discussion and plotted as a function of the excitation energy. In the following sections the σ's obtained from the pairing consideration are labeled σ_p, and those obtained from assumption of a rigid moment of inertia are labeled σ_r.

Figure 47 is a plot of σ_p, σ_r, and various fractions of σ_r. It will be noted that the pairing correction yields values of the cutoff parameter that are considerably lower than those obtained by assumption of a rigid moment of inertia.

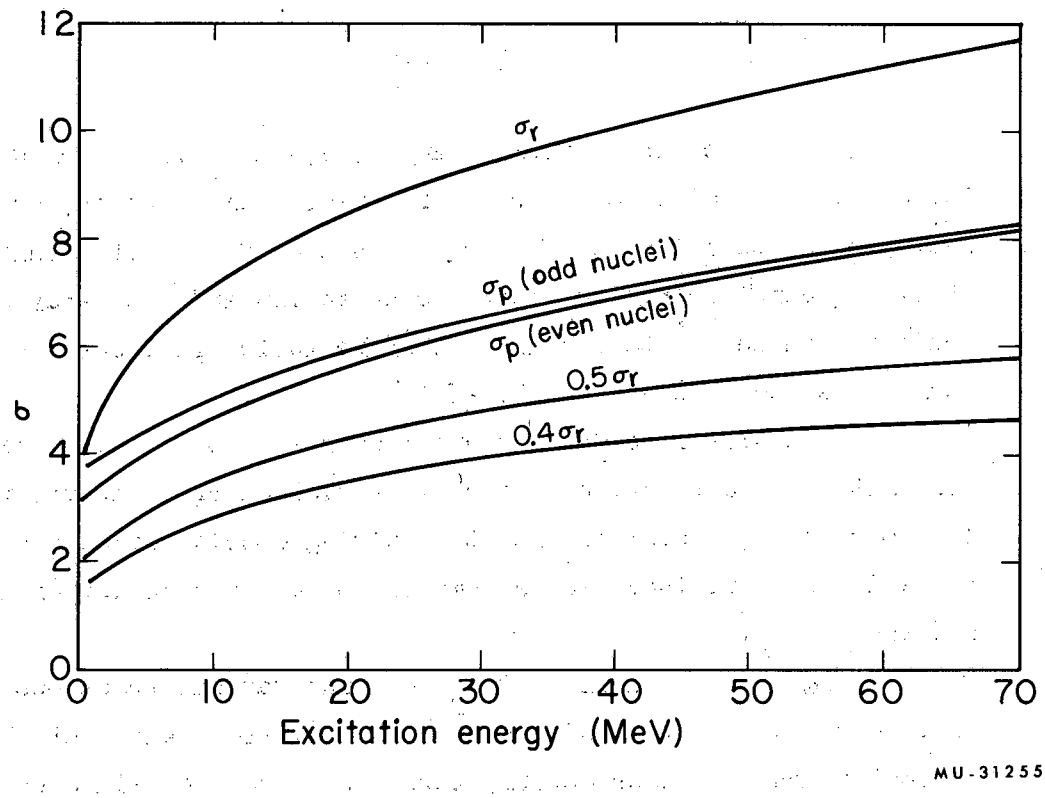

Fig. 47. Spin cutoff parameters as a function of the excitation energy of the excited nucleus.

C. Calculation Results

Because of the number of parameters involved in the calculation, and the various means for determining their values, numerous combinations are possible. Each combination normally leads to a different calculated isomer ratio.

The purpose of the calculations was to determine a particular set of parameters (actually the means of determining them) that would give good agreement with the experimental results for all the reactions studied. It is recognized that any such set of parameters is not mutually exclusive, and that other sets that might be just as successful in matching the experimental results may be possible.

With the above purpose in mind, calculations were undertaken in which the same methods were employed to determine the input parameters for both the $He^4 + Sn^{118}$ and $C^{12} + Pd^{110}$ reactions. These two reactions were chosen because they represent both a heavy and a light projectile, and because the experimental results are considered to be quite reliable. Approximately 20 calculations were performed for this pair of reactions, and the results are given in graphical form in Figs. 48 through 55. In the plots, the heavy solid line represents the experimental results and the other lines, labeled alphabetically, represent the results of the various calculations.

Note that the figures are given in pairs (one for the C^{12} reaction and one for th He^4 reaction) and that curves with the same alphabetic designation for both reactions represent calculations using the same methods for determining the input parameters.

For convenience sake in discussing the individual calculations, the various means employed for determining the input parameters will be reviewed here. The previous section treats these methods in detail.

Two theoretical equations were employed for determining the number of γ rays emitted:

$$\overline{N}_\gamma = \frac{\sqrt{aE_c}}{\ell+1} , \qquad (45)$$

$$\overline{E}_\gamma = 4\sqrt{(E_c - 1)/a} \qquad (48)$$

In the following discussion they are referred to by equation number.

A third method was also employed in which it was assumed that all γ rays were of the same energy (1.5 MeV), corresponding to the γ-ray energies determined by Mollenauer (1.2 ± 0.3 MeV).[7,89]

The multipolarity of the γ rays was assumed to be either dipole or quadrupole. A statement as to the assumption used is included in each description.

The energy of the neutrons, which determines the transmission coefficient assigned, is listed in each description as being "equal-energy neutrons" or "average-energy neutrons". The expression "equal-energy neutrons" refers to neutron energies taken from the work of Simonoff and Alexander, and an identical set of transmission coefficients was used for each neutron.[8] "Average-energy neutrons" means that the neutron energies were calculated in terms of the nuclear temperature as discussed in the preceding section. Such a procedure yields neutron energies that decrease from the first through the last emitted, and consequently a different set of transmission coefficients is required for each.

The final input parameter is the spin-cutoff factor, σ. This is referred to as σ_p or σ_r, as defined in the preceding section. Fractions of these values, such as $0.5\ \sigma_r$, are also used.

On the basis of the above definitions, the methods employed in calculating the various isomer ratio curves are discussed in the following paragraphs. The individual calculations are referred to in terms of their alphabetical designations.

Figures 48 and 49 represent a series of calculations (except for calculation A) which use σ_p as the spin cutoff parameter.

Calculation A: Equation (45) was used to determine the number of dipole γ rays emitted. Average neutron energies were assumed and the spin cutoff parameter was taken as σ_r. The results are too high by approximately a factor of six.

Calculation B: This is identical to calculation A except that σ_p was used as the cutoff parameter instead of σ_r. The results are moved in the right direction, but are still much too high.

Calculation C: Equation (45) was used to determine the multiplicity of the γ rays, and all were assumed to be quadrupole. Average neutron energies were used and the spin cutoff parameter was σ_p. The calculation gives poor results for the He^4 reaction, the γ rays appearing to carry away too much angular momentum at the higher energies.

Calculation D: This uses Eq. (48) to determine the number of γ rays emitted, otherwise it is identical to calculation B. The results indicate that the two methods of calculating the γ-ray multiplicity are more or less equivalent, so far as isomer ratio calculations are concerned.

Calculation E: Equal neutron energies were used. Otherwise the calculation is identical to calculation B. The results do not differ greatly from calculation B and it may therefore be concluded that the two methods of choosing neutron energies lead to the same results.

Calculation F: Equal neutron energies were used. The γ rays were of energy 1.5 MeV and dipole in nature; σ_p was used as the spin cutoff parameter.

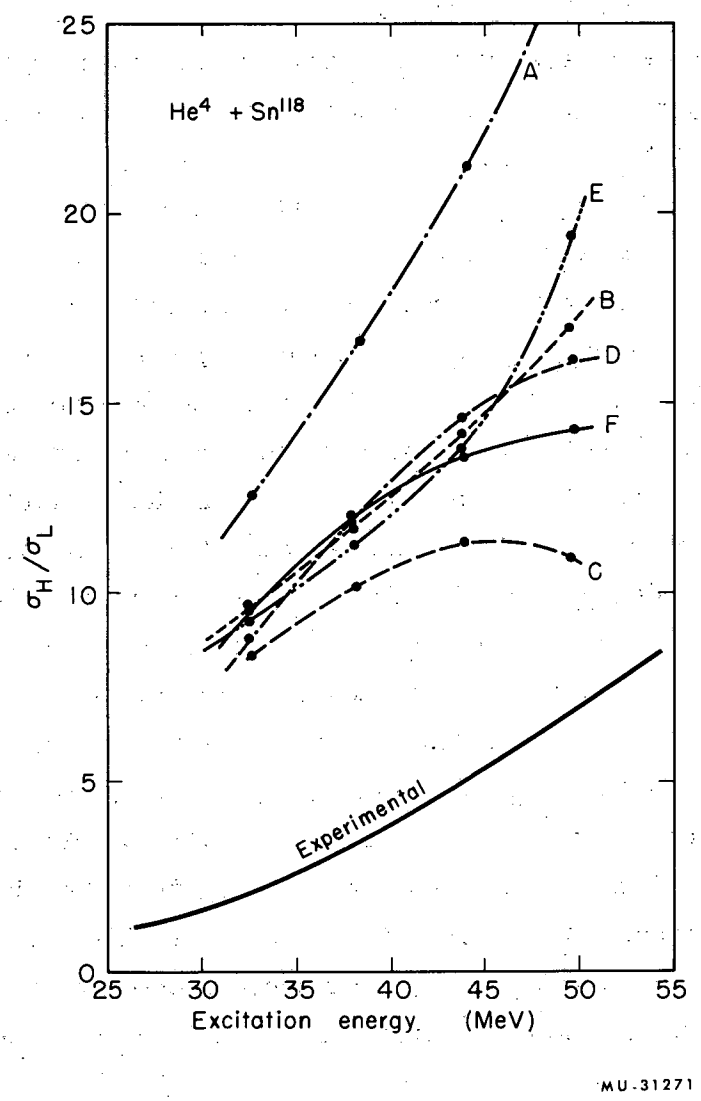

Fig. 48. Comparison of calculated and experimentally determined ratios for the reaction $He^4 + Sn^{118} \longrightarrow Te^{119, 119m} + 3n$. The heavy solid line represents the experimentally determined values, and the various other lines represent the calculated ratios obtained by use of different sets of input parameters.

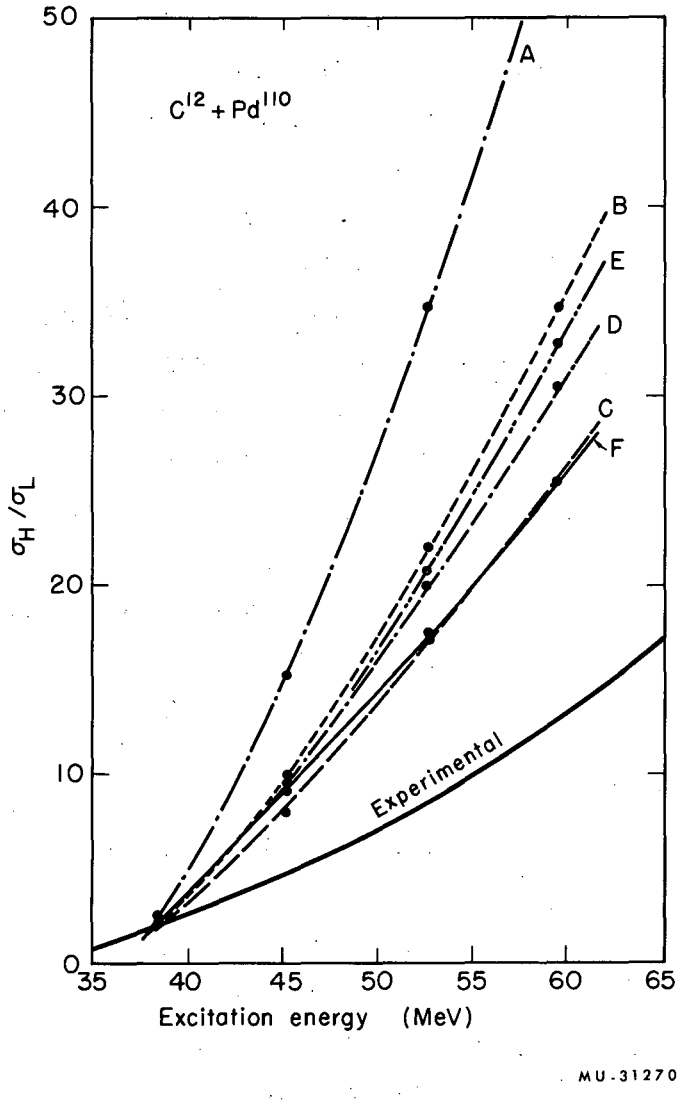

Fig. 49. Comparison of calculated and experimentally determined ratios for the reaction $C^{12} + Pd^{110} \longrightarrow Te^{119, 119m} + 3n$. (Explanation is the same as for Fig. 48.)

Figures 50 and 51 illustrate a series of calculations in which σ_p was used as the spin cutoff parameter and it was assumed that after the neutron evaporation no more than 12 MeV excitation energy could remain for the γ rays to carry away. Therefore, 12 MeV plus the sum of the neutron binding energies was subtracted from the total excitation energy of the initial compound nucleus and the energy remaining was divided equally among the neutrons as their kinetic energy. The procedure actually affects the first calculated point for the He^4 reaction only slightly (because the total excitation energy after the neutron evaporation only slightly exceeds the 12 MeV selected as the cutoff point), but does affect rather drastically the first two point (highest energy) for the C^{12} reaction. The effect is to increase the neutron energies and decrease the number of γ rays emitted.

Calculation G: Equal neutron energies were used and 1.5-MeV dipole γ rays were assumed to be emitted. The spin cutoff parameter was σ_p. For He^4 the calculation is practically identical to calculation F, and for C^{12} the last two points are the same.

Calculation H: This is identical to calculation G except that the γ rays are assumed to be quadrupole. The results for the He^4 reaction indicate that if the multipolarity of the γ rays is allowed to increase, the multiplicity must decrease. Equation (45) would predict such a conclusion.

Calculation I: This is identical to calculation G except that the multipolarity of the γ rays is allowed to alternate between dipole and quadrupole, starting with a quadrupole emission. The results show fair agreement with the experimentally determined results of the C^{12} reaction, but poor agreement for the He^4 reaction.

Calculation J: This is identical to calculation G except that $2/3\ \sigma_p$ is used in place of σ_p. The combination of the smaller spin cutoff parameter and the large number of γ rays predicted by the 1.5-MeV assumption yield calculated ratios that are too low.

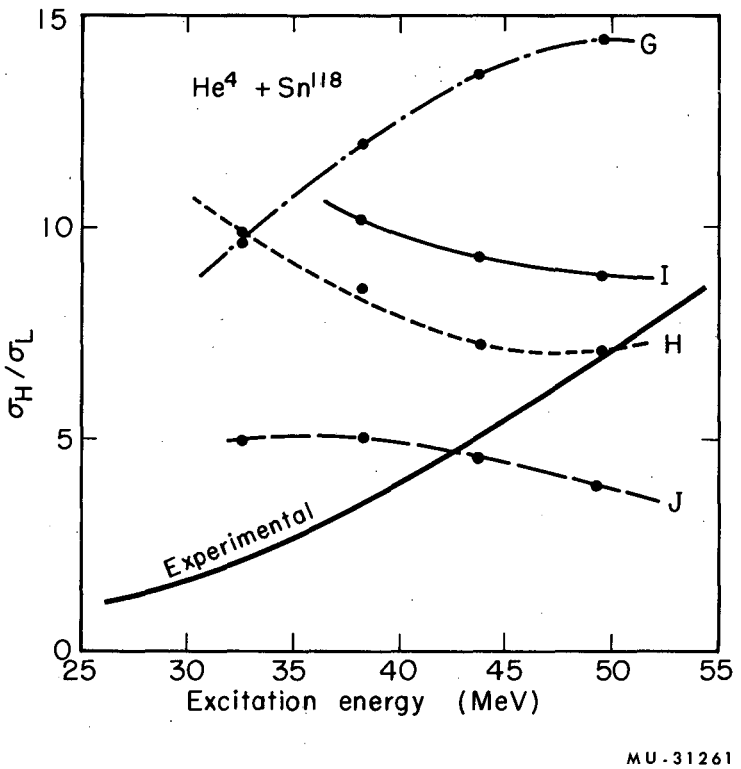

Fig. 50. Comparison of calculated and experimentally determined ratios for the reaction $He^4 + Sn^{118} \longrightarrow Te^{119, 119m} + 3n$. (Explanation is the same as for Fig. 48.)

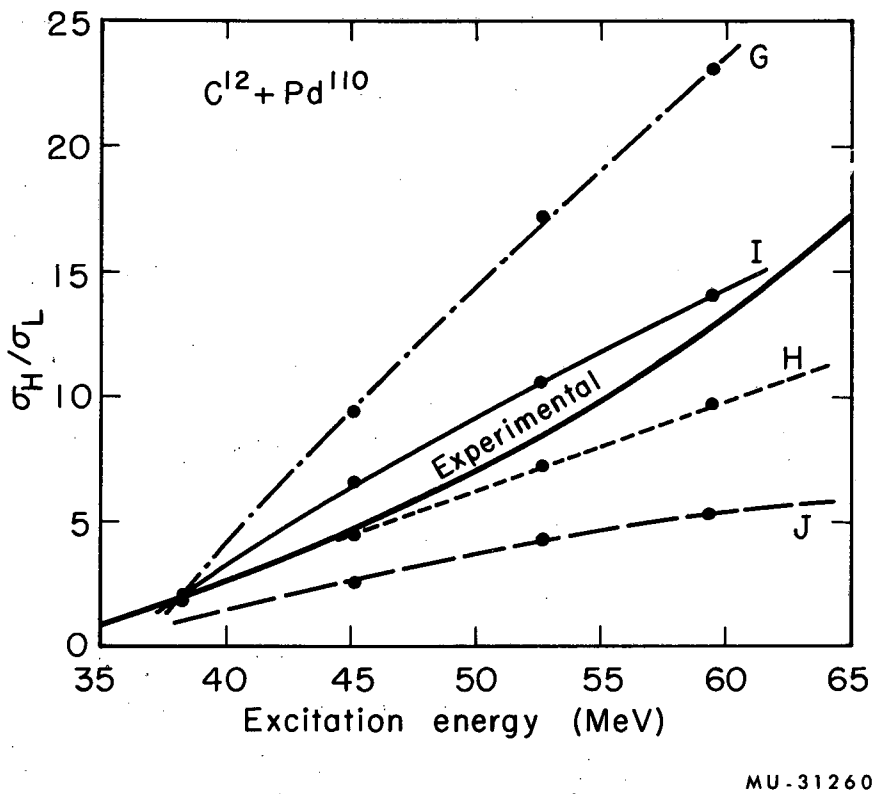

Fig. 51. Comparison of calculated and experimentally determined ratios for the reaction $C^{12} + Pd^{110} \longrightarrow Te^{119, 119m} + 3n$. (Explanation is the same as for Fig. 48.)

On the basis of the preceding calculation it can probably be justifiably argued that although consideration of the pairing interaction definitely adjusts the spin cutoff parameter in the right direction, the correction is simply not enough to yield agreement of theory and experiment as far as calculations of the isomer ratio are concerned.

Figures 52 and 53 illustrate a series of calculations in which the spin cutoff parameter has the value $0.5\ \sigma_r$.

Calculation K: This uses a spin cutoff parameter of $0.5\ \sigma_r$. The γ rays are considered to be dipole and the number is calculated according to Eq. (45). Average neutron energies are used. The calculation is seen to give quite good agreement with the experimental results of both the He^4 and C^{12} reactions. This calculation undoubtedly represents the best combination of parameters found in this investigation.

Calculation L: This uses $0.5\ \sigma_r$, equal neutron energies, and 1.5-MeV dipole γ rays. It is also assumed that a maximum of 12 MeV excitation energy remains after the neutron evaporation. The results are not particularly good.

Calculation M: This is identical to calculation K except that Eq. (45) was used to calculate the number of γ rays emitted, assuming that they were all quadrupole. As indicated before, quadrupole radiation appears to carry off too much angular momentum at the high energies, at which a rather large number of γ rays must be assumed.

Calculation N: This is identical to calculation K except that Eq. (48) was used to determine the number of γ rays emitted. The results are not as satisfactory as those obtained by using Eq. (45) to determine this parameter.

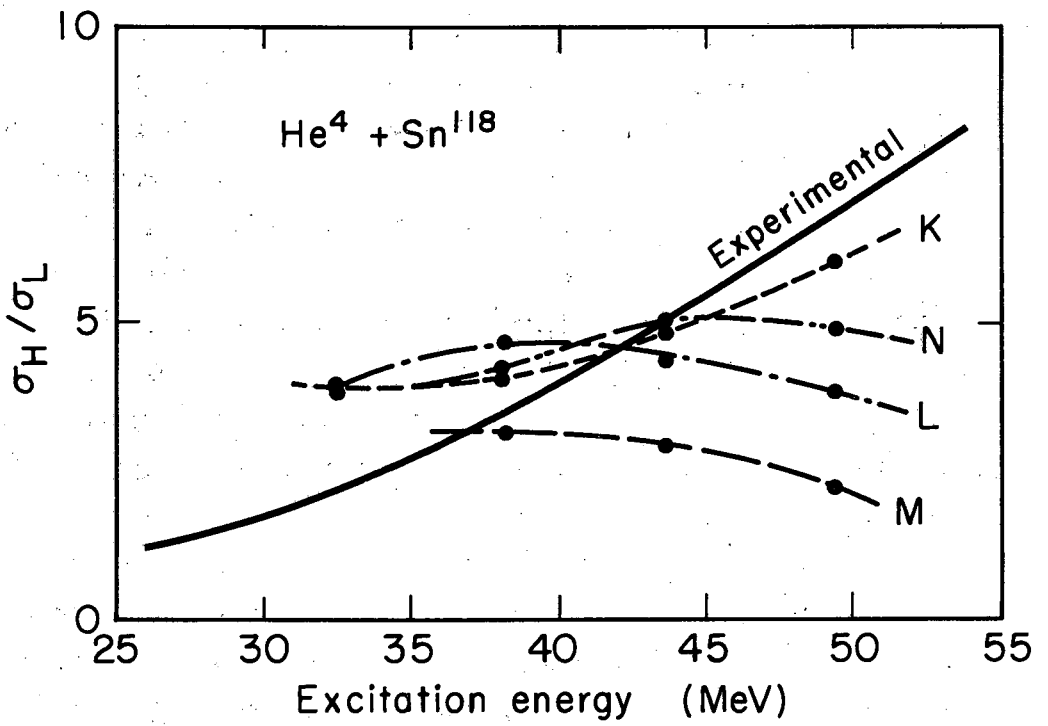

Fig. 52. Comparison of calculated and experimentally determined ratios for the reaction $He^4 + Sn^{118} \longrightarrow Te^{119, 119m} + 3n$. (Explanation is the same as for Fig. 48.)

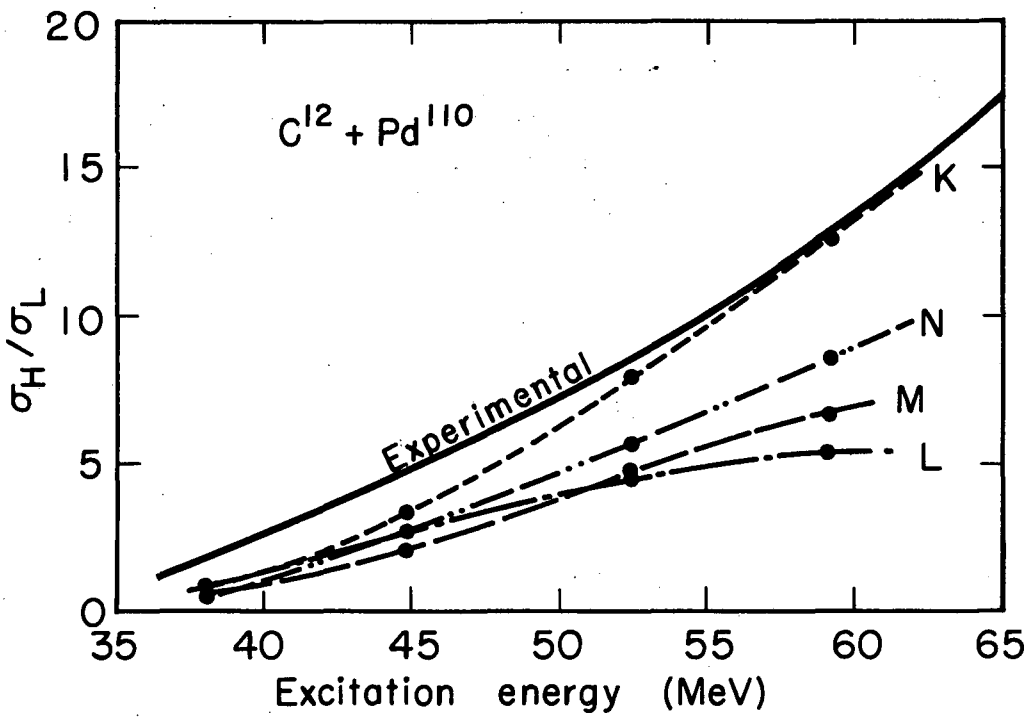

Fig. 53. Comparison of calculated and experimentally determined ratios for the reaction $C^{12} + Pd^{110} \longrightarrow Te^{119, 119m} + 3n$. (Explanation is the same as for Fig. 48.)

Figures 54 and 55 illustrate two calculations for a spin cutoff parameter of 0.5 σ_r and two for 0.4 σ_r. The calculations indicate that 0.5 σ_r is probably the smallest value of the spin cutoff parameter that can be used to obtain agreement between experiments and calculations.

Calculation O: Equal neutron energies were used, and the γ rays were assumed to be dipole. Their number was calculated by Eq. (48). The spin cutoff parameter values was 0.5 σ_r.

Calculation P: Equal neutron energies and 1.5-MeV dipole γ rays were assumed. The spin cutoff parameter value was 0.5 σ_r.

Calculation Q: Equal neutron energies and a spin cutoff parameter of 0.4 σ_r were employed. The number of dipole γ rays was calculated according to Eq. (45).

Calculation R: This is identical to calculation Q except that average neutron energies were assumed.

D. Conclusions

A few of the principal conclusions that can be drawn from the calculations are as follows:

(a) The use of σ_r yields calculated ratios that are almost an order of magnitude too high.

(b) The pairing-interaction consideration adjusts the spin cutoff parameter in the right direction but not far enough. The results are consistent with those of Carver et al., who were required to use a value of 0.6 σ_s, where σ_s is a spin cutoff parameter related to the σ_p used in this work.[90]

(c) The use of a spin cutoff parameter equal to 0.5 σ_r seems to fit the experimental results reasonably well. Calculations that yield very poor slopes for the curves still fall in the correct region with this value of the parameter. It should be mentioned that the calculation is most sensitive to the spin cutoff parameter in the region where most of

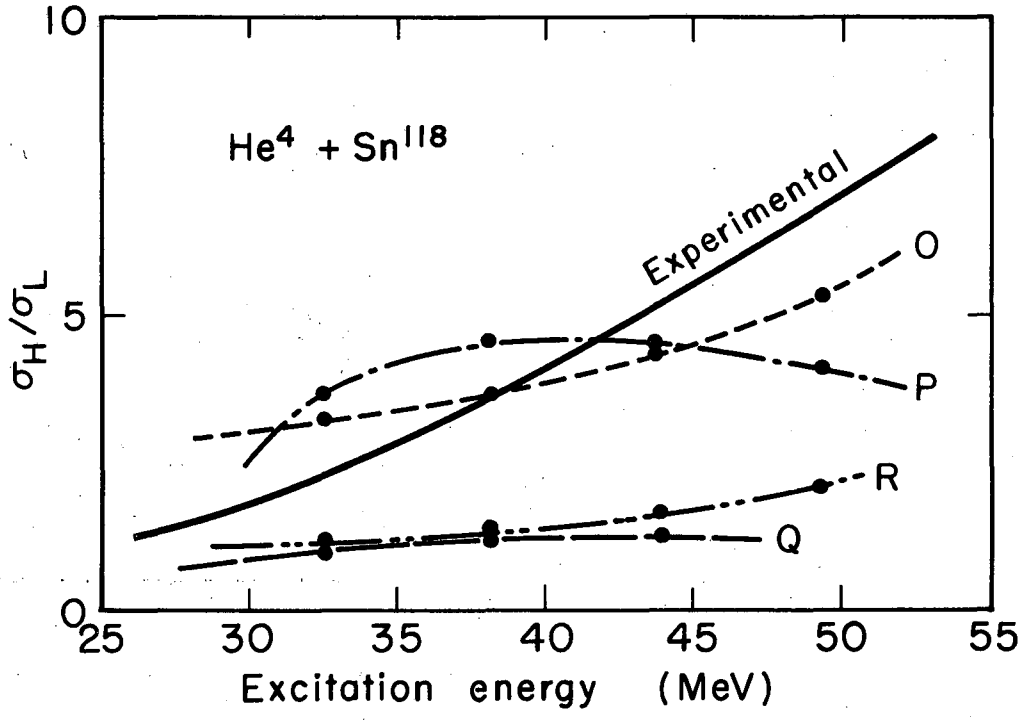

Fig. 54. Comparison of calculated and experimentally determined ratios for the reaction $He^4 + Sn^{118} \longrightarrow Te^{119, 119m} + 3n$. (Explanation is the same as for Fig. 48.)

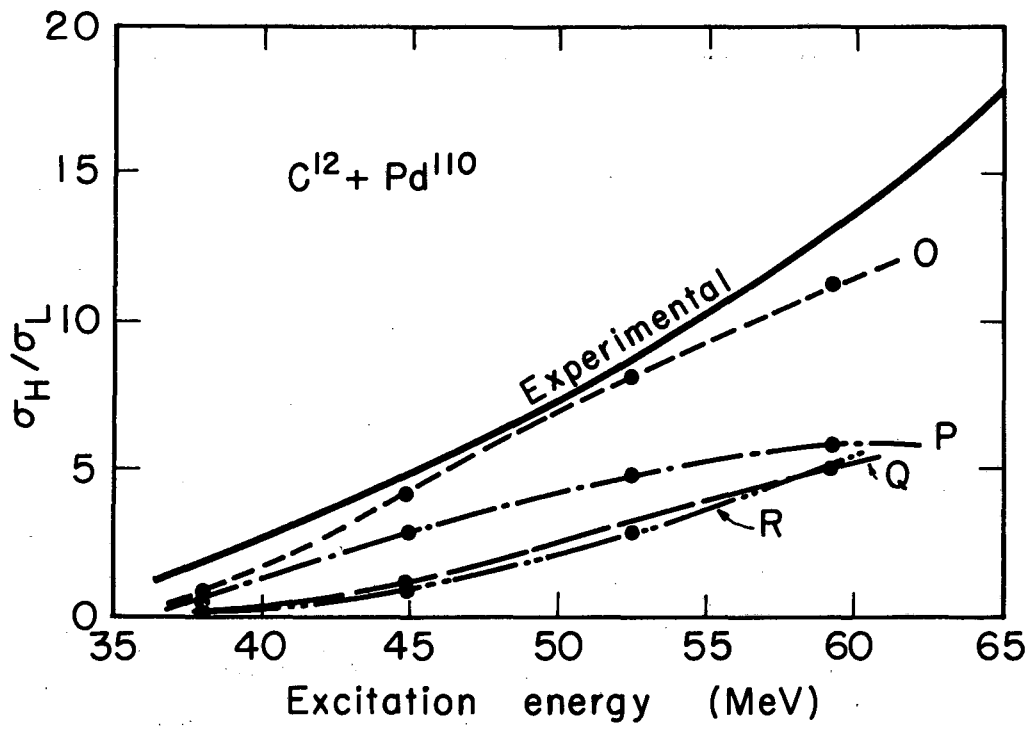

Fig. 55. Comparison of calculated and experimentally determined ratios for the reaction $C^{12} + Pd^{110} \longrightarrow Te^{119, 119m} + 3n$. (Explanation is the same as for Fig. 48.)

the transitions occur, or in the area below an excitation energy of approximately 20 MeV at which the γ ray cascade takes place. It is probably possible to obtain reasonable results by using a σ that agrees fairly well with 0.5 σ_r at low energies but has a different slope at higher energies. Theoretically, at sufficiently high energies, the spin cutoff parameter should become equal to the rigid value, and perhaps the slope of the curve (Fig. 47) should increase with energy until it becomes equal to σ_r. The calculation unfortunately does not give much information in this respect, since the important σ's are those at the lower energies. Calculations using 0.4 σ_r yielded results that were undoubtedly too low.

(d) The calculations indicate that dipole radiation is more important than quadrupole in determining which isomer is populated. Usually the slopes of the calculated curves, assuming quadrupole radiation, were quite unsatisfactory and indicated -- especially at higher energies, where the γ rays emitted were numerous -- that too much angular momentum was carried away. The results strongly indicate that Eq. (45) correctly predicts that a quadrupole γ-ray de-excitation process requires fewer γ rays than a dipole γ-ray process.

(e) Use of an average γ-ray energy of 1.5 MeV was not very successful. The calculations yielded ratio curves whose slopes decreased with energy instead of increasing. The results indicate that the procedure predicts too many γ rays at the higher energies. Even the assumption that no more than 12 MeV excitation energy remained after the neutron emission did not correct the effect. The higher-energy neutrons required by this assumption apparently carry away too much angular momentum.

(f) Equations (45) and (48), used to determine the number of γ rays emitted, both gave fairly satisfactory results. As shown before, they both predict practically the same number. However, Eq. (48) assigns much higher energies to the first few γ rays emitted, with the effect that the nucleus quickly loses its excitation energy and most of the γ rays

therefore require σ's from the low-energy end of the curve. Use of Eq. (45) assumes equal-energy γ rays and the nucleus is not de-excited as quickly. The average spin cutoff parameter assigned by Eq. (48) is therefore lower than that assigned by Eq. (45). The effect is that Eq. (48) yields a somewhat lower calculated ratio. This equation, used with a somewhat larger spin cutoff parameter -- say 0.6 σ_r -- might produce satisfactory results.

(g) The use of "average-energy neutrons" or "equal-energy neutrons" was more or less equivalent, although the "average energy" assumption is probably more realistic. The "equal energy" assumption uses the same transmission coefficients for all three neutrons. When "average-energy neutrons" are assumed, the transmission coefficients for the first neutron are larger, for the second about equal, and for the third smaller than those used in the "equal energy" assumption. The effects apparently about cancel out.

The most successful calculation performed was that designated calculation K. The calculation represents the best method found in this investigation for the determination and combination of the various required parameters. The same methods, which assumed average neutron energies, dipole γ rays of multiplicity determined by Eq. (45), and a spin cutoff parameter of 0.5 σ_r, were applied in the calculation of the isomer ratios for the other seven reactions. The results of these calculations are illustrated in Figs. 56 through 60.

In general the results are quite satisfactory, especially in the region of the excitation-function peaks. The heavy ions show an appreciable Coulomb barrier effect, which results from the Bunthorne calculation predicting too low an angular momentum.

If consideration was given to the competition of other xn reactions, the result would be to increase the calculated ratio at energies above the excitation-function peak and to lower it for enrgies on the low-energy side of the peak. Such an adjustment would provide better agreement for the He^4 3n and 4n reactions. In view of the omission of

these correction factors, the calculation can be expected to give good results only in the vicinity of the peak of the excitation function energy (assuming the peak is sufficiently removed from the Coulomb barrier region). In this respect the calculations are very satisfactory.

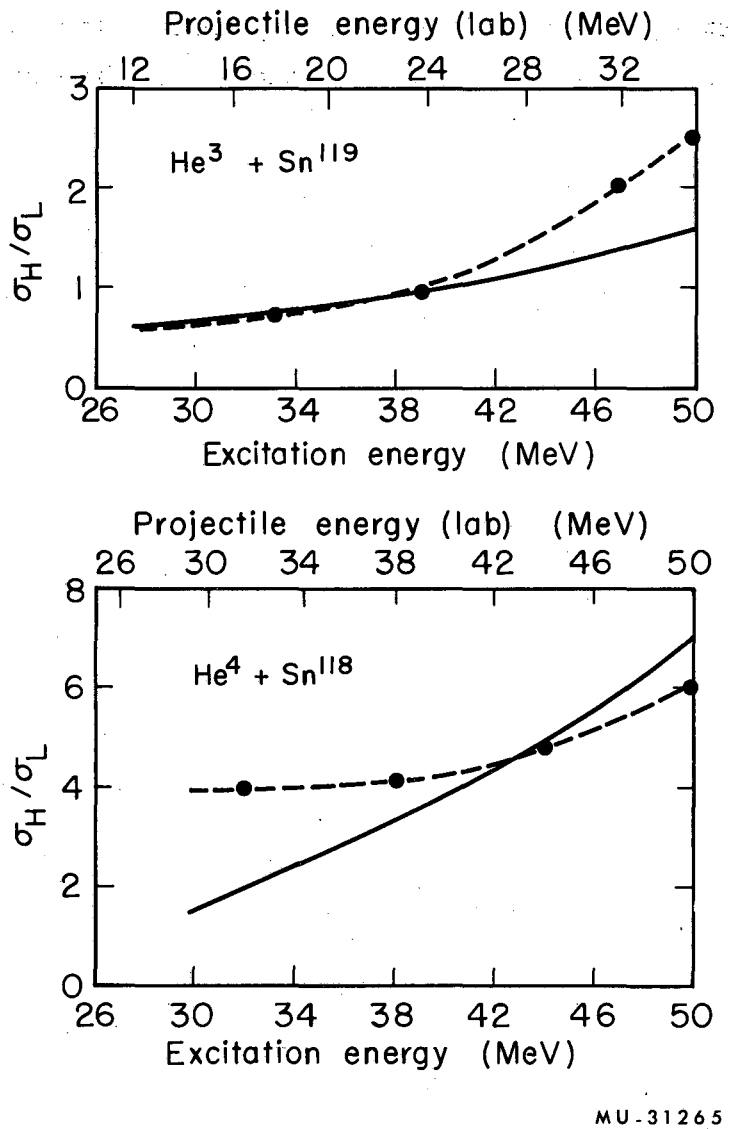

Fig. 56. Comparison of calculated and experimentally determined isomer ratios for the reactions $He^3 + Sn^{119} \longrightarrow Te^{119, 119m} + 3n$ and $He^4 + Sn^{118} \longrightarrow Te^{119, 119m} + 3n$. The solid line represents the experimentally determined ratios and the broken line represents the calculated values.

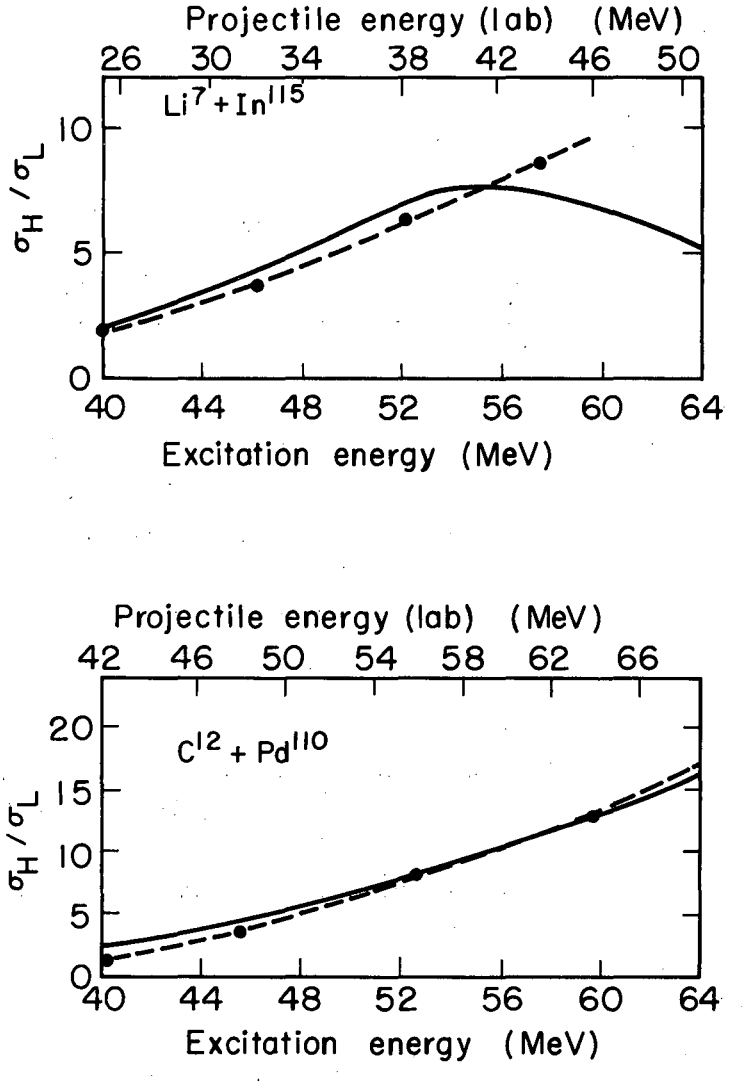

Fig. 57. Comparison of the calculated and experimentally determined isomer ratios for the reactions $Li^7 + In^{115} \longrightarrow Te^{119, 119m} + 3n$ and $C^{12} + Pd^{110} \longrightarrow Te^{119}, + 3n$. (Explanation is the same as for Fig. 56.)

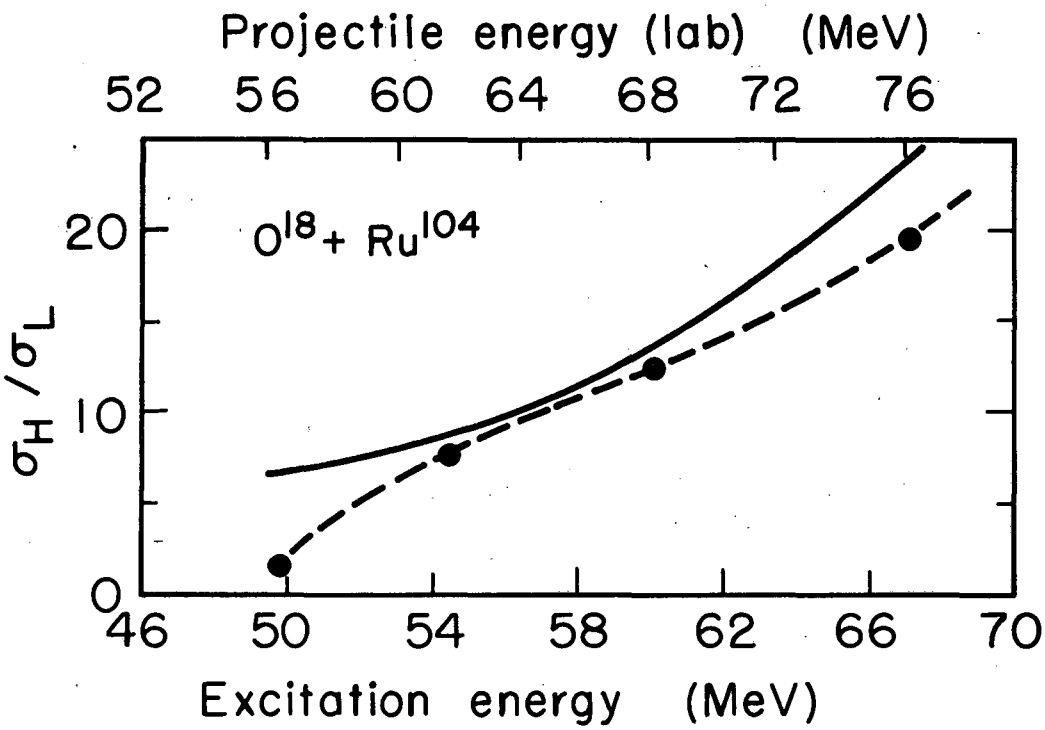

MU-31263

Fig. 58. Comparison of the calculated and experimentally determined isomer ratios for the reaction O^{18} + Ru^{104} ⟶ $Te^{119, 119m}$ + 3n. (Explanation is the same as for Fig. 56.)

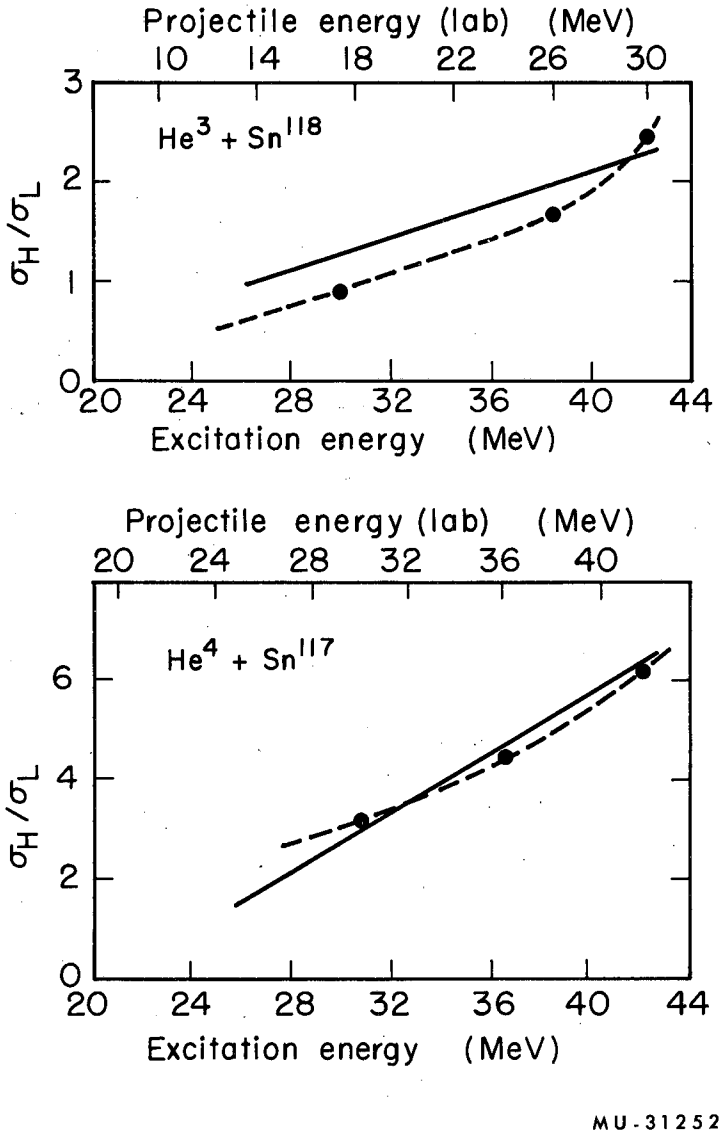

Fig. 59. Comparison of calculated and experimentally determined isomer ratios for the reactions yielding the compound nucleus Te^{121*}. (Explanation is the same as for Fig. 56.)

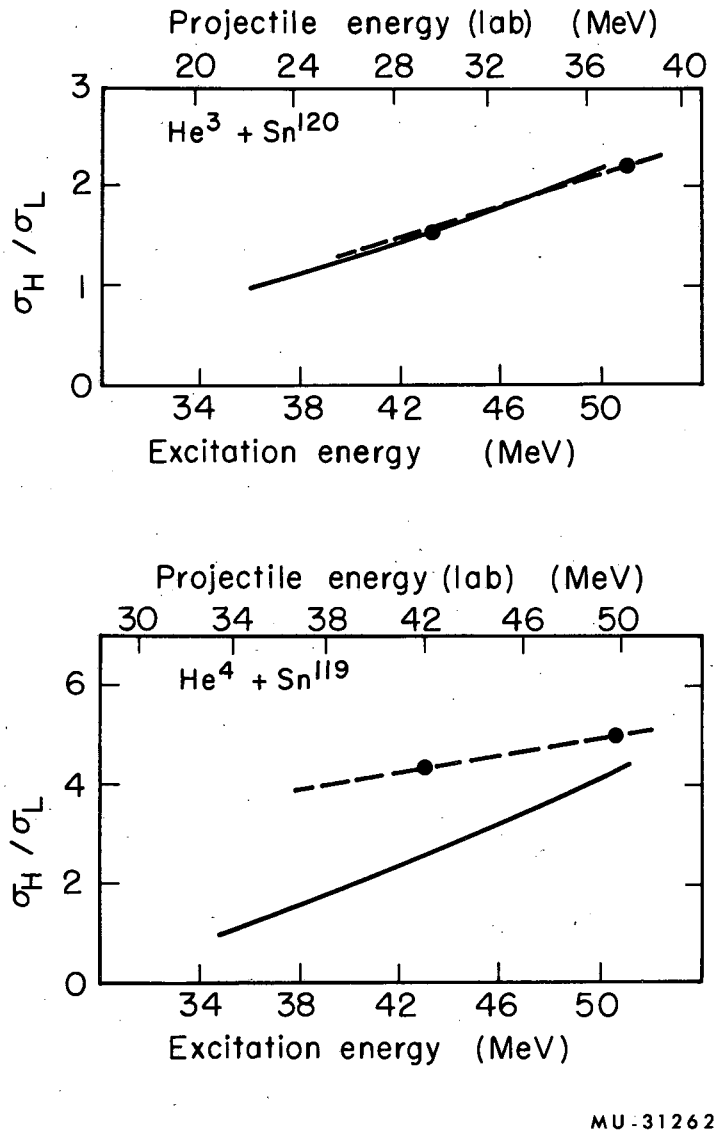

Fig. 60. Comparison of calculated and experimentally determined isomer ratios for the reactions yielding the compound nucleus Te^{123*}. (Explanation is the same as for Fig. 56.)

VII. SUMMARY

1. The effects of angular momentum on compound-nucleus reactions was investigated by measuring the formation cross-section ratios of a pair of isomers produced by compound nuclei through xn reactions.

The compound nucleus Te^{122*} was produced by five different reactions using projectiles ranging in size from He^3 to O^{18}. The Te^{122*} then yielded by the 3n reaction the pair of isomers Te^{119} and Te^{119m}.

The compound nuclei Te^{121*} and Te^{123*} were also produced by using both He^3 and He^4 projectiles. The de-excitation through a 2n and a 4n reaction, respectively, yielded the same tellurium isomer pair.

2. A method was devised and used for determining the isomer ratios that was independent of any decay scheme. The uncertainties inherent in branching ratio, conversion coefficients, etc. were thereby eliminated.

The ratios determined (upper-state isomer to lower-state isomer) varied from a low of approximately 0.75 to a high of approximately 25. The expected increase of ratio with energy and projectile size was confirmed. An apparent direct interaction was observed for Li^7 projectiles.

3. Excitation functions were obtained for the reactions yielding the Te^{122*} compound nucleus. The expected shift in peak position with projectile size was clearly demonstrated.

4. Compound-nucleus calculations were performed assuming a rounded nuclear potential approximated by a parabola (Bunthorne). Good agreement was obtained between experimentally determined isomer ratios and predictions based upon the calculated average angular momentum of the compound nucleus.

The prediction of too low an angular momentum by the model in the vicinity of the Coulomb barrier, as reported by others, was verified.

It is also shown that a reasonable estimate of the isomer ratio can be obtained by assuming that all compound nuclei with a spin greater than 8 populate the high-spin isomer whereas those with a spin of 8 or less yield the low-spin isomer.

5. Calculations of the Vandenbosch - Huizenga type were performed for the various reactions.[41] The projectile transmission coefficients were taken from the Bunthorne calculation. Average neutron energies were defined in terms of the nuclear temperature, and square-well neutron transmission coefficients of Feld et al. were employed. Various combinations of input parameters were investigated and the best results were obtained by assuming equal-energy dipole γ rays of multiplicity defined by

$$\bar{N}_\gamma = (\sqrt{aE_c})/2$$

and a spin cutoff parameter of $0.5\ \sigma_r$. The σ_r represents the spin cutoff parameter calculated by assuming that the nucleus has a moment of inertia equivalent to that of a rigid sphere.

ACKNOWLEDGMENTS

I wish to acknowledge the guidance and assistance throughout this work of Dr. Kenneth Street, who proposed the problem.

I wish to thank Dr. John O. Rasmussen for many helpful discussions and for reading of the manuscript.

Appreciation is extended to Dr. John Alexander and Dr. Ronald D. Macfarlane for numerous helpful discussions and suggestions.

I am grateful to Dr. Robert Vandenbosch for supplying the computer program by which the calculations were performed.

I am grateful to Eileen Carson for obtaining the various separated isotopes employed in the investigation.

I have appreciated many useful discussions with Mr. Richard Kiefer.

I wish to thank the various accelerator crews and the Health Chemistry Group for their valuable assistance.

The educational program of the U.S. Air Force which allowed me to do this work is gratefully acknowledged.

The work was performed under the auspices of the U. S. Atomic Energy Commision.

APPENDICES

A. Range-Energy Relationships

As mentioned in Section IV.A, almost no range-energy data were available for the various projectile-target combinations employed in this work. It was therefore necessary to calculate such curves. The basis of these calculations was the proton range-energy data of Sternheimer[60] and the heavy-ion range-energy data of Hubbard[58] and Northcliffe.[59] The calculations were accomplished as described in the following.

He^4 ranges

Sternheimer provides the range-energy relations for protons in Be, C, Al, Cu, Pb, and air. Some of these ranges are illustrated in Fig. A-1. From these data the ranges of He^4 in Al and Cu were calculated by means of:

$$R_{He^4, E} = R_{p, E/4} \tag{48}$$

The equation reads: the range of He^4 ions of energy E in a given material is equal to the range of protons of energy E/4.

An equation provided by Friedlander and Kennedy was then used to calculate the range of He^4 in other materials such as Ni and Sn[57]. The equation that provides the relationship between the range of a projectile of charge Z_p and energy E in two materials of different Z is

$$\frac{R_{Z_1}}{R_{Z_2}} \quad \frac{0.90 + 0.0275Z_1 + (0.06 - 0.0086Z_1)\log(E/Z_p)}{0.90 + 0.0275Z_2 + (0.06 - 0.0086Z_2)\log(E/Z_p)} . \tag{49}$$

The results of the calculations are given in Fig. A-2.

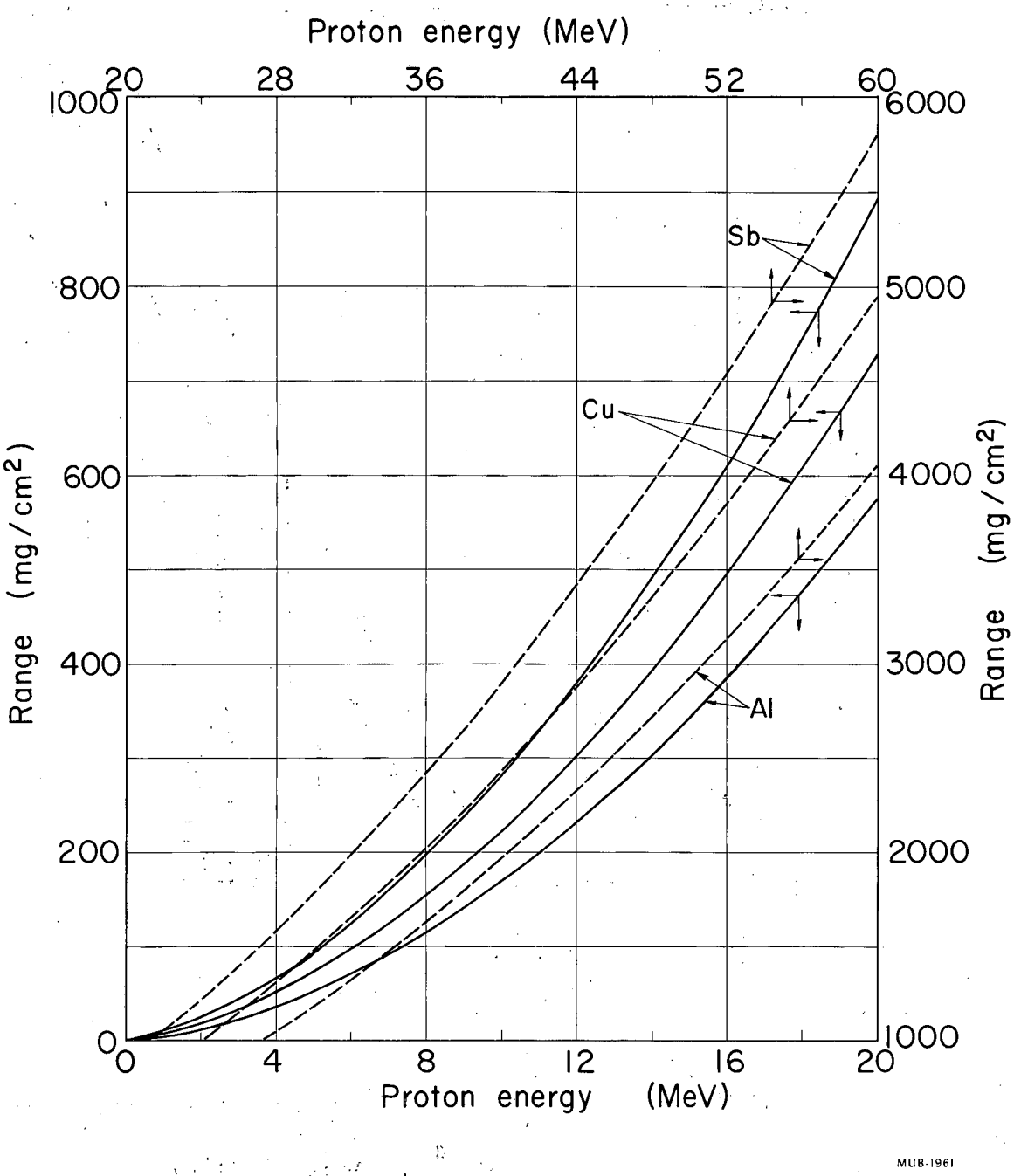

Fig. A1. Range-energy curves for protons in various materials.

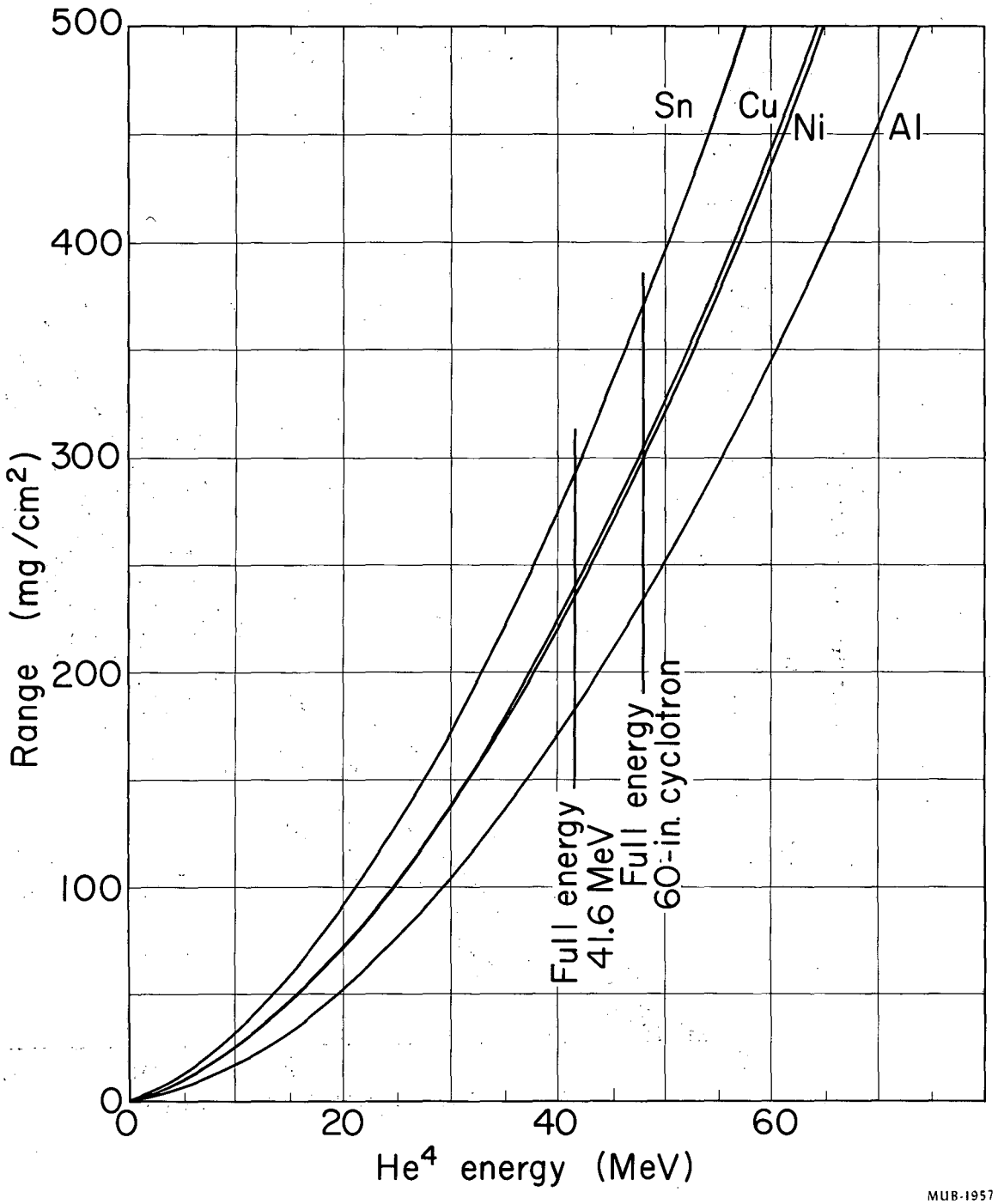

Fig. A2. Range-energy curves for He^4 ions in various materials.

He^3 ranges

The same target and backing materials were used for the He^3 and He^4 bombardments. The He^3 ranges were calculated from the He^4 data by the following equation, which describes the relative ranges, in a particular target material, of two projectiles of equal charge but different mass:

$$R_{He^3}(E) = \frac{3}{4} R_{He^4}(E') , \qquad (50)$$

where $E' = 4/3\ E$.

The He^3 range-energy relations are illustrated in Fig. A-3.

Li^7 ranges

The data of Northcliffe,[59] which give the range of various lithium isotopes in aluminum, were used to calculate the range of Li^7 in In^{115}. Equation (49) was used for this calculation. The extrapolation is admittedly a long one, but should introduce little error into the experimental data since the backing foils (where most of the degradation occurs) used were aluminum, and the data of Northcliffe could be applied directly. The range-energy curves used are given in Fig. A-4.

C^{12} ranges

Hubbard gives the ranges of C^{12} in Al, Ni, Cu, Ag, Au, and Pb.[58] The materials used in the bombardments were Al, Ni, Cu, Au, and Pd. Therefore most of the ranges necessary were directly available. The range of C^{12} in Pd was calculated from the silver range by means of Eq. (49). The extrapolation in this case is a very small one and the calculated data should be quite good. The range-energy relationships are shown in Fig. A-5.

O^{18} ranges

The O^{16} range-energy data of Hubbard was used for these calculations.[58] An equation similar to Eq. (50) was used to determine the O^{18} ranges from the O^{16} data. By this means the range of O^{18} was determined for Al, Cu, and Ag. The silver data thus obtained were then used to calculate the range of O^{18} in Ru^{104} by means of Eq. (49). The results are plotted in Fig. A-6.

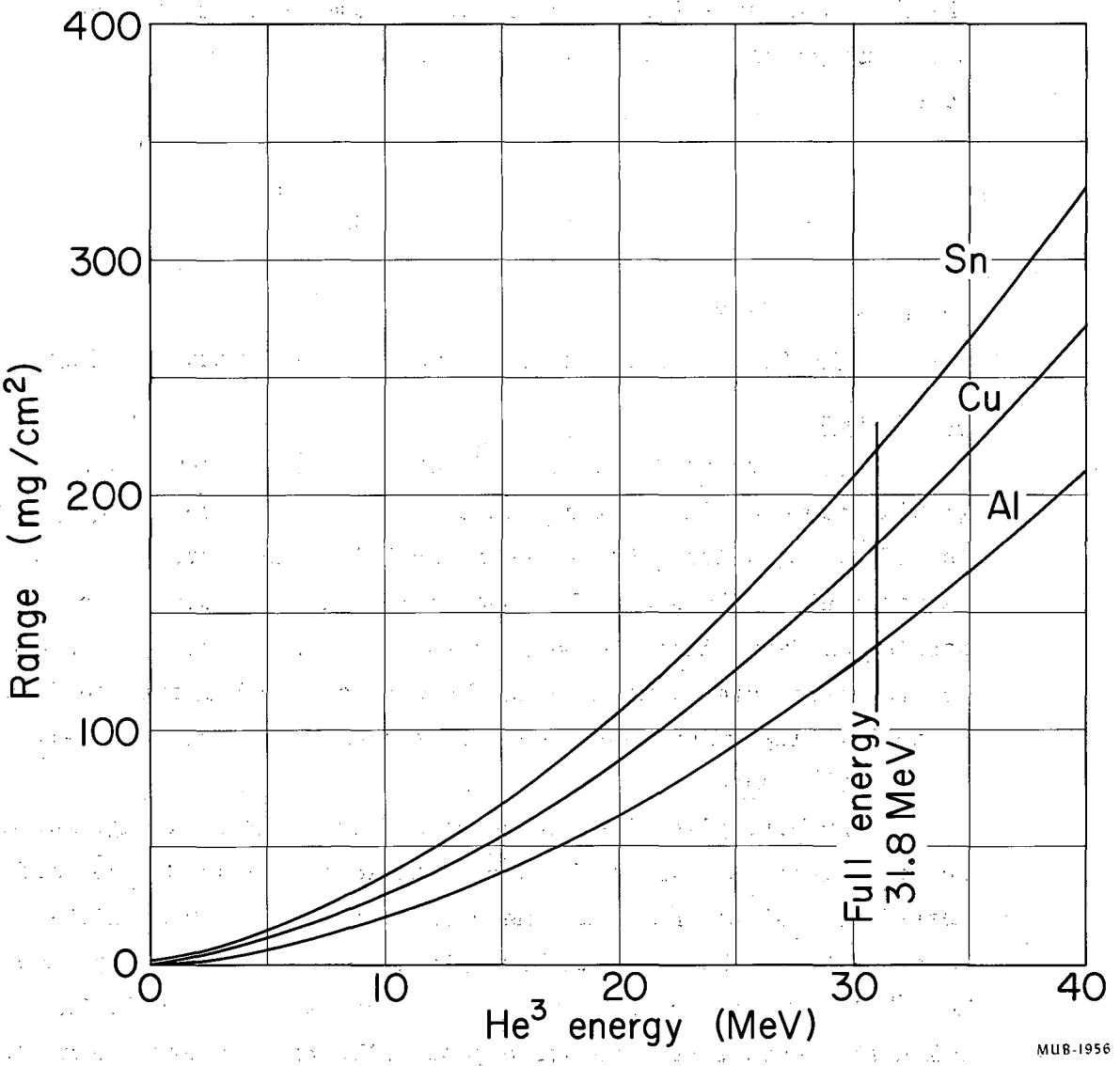

Fig. A3. Range-energy curves for He^3 ions in various materials.

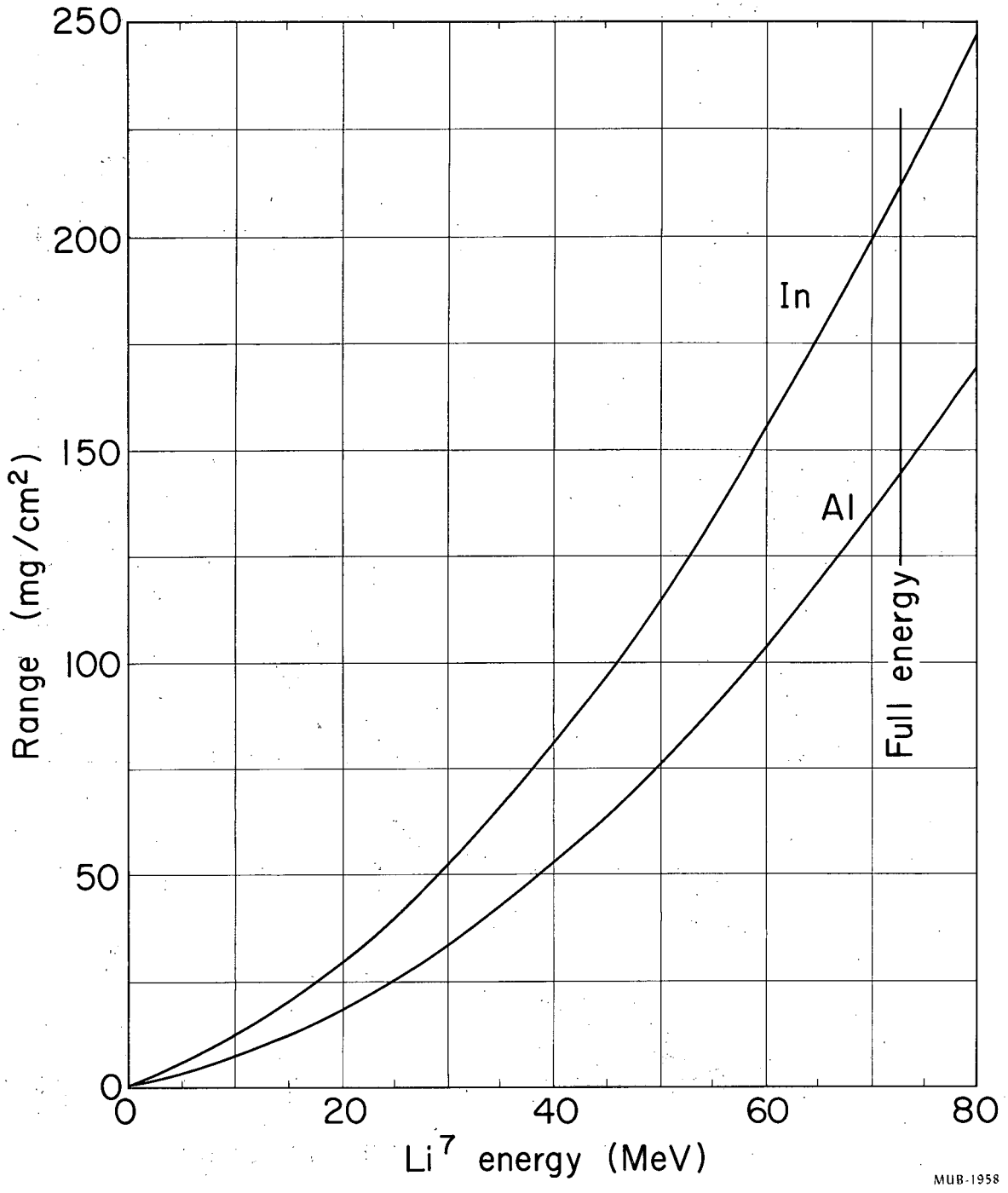

Fig. A4. Range-energy curves for Li^7 ions in various materials.

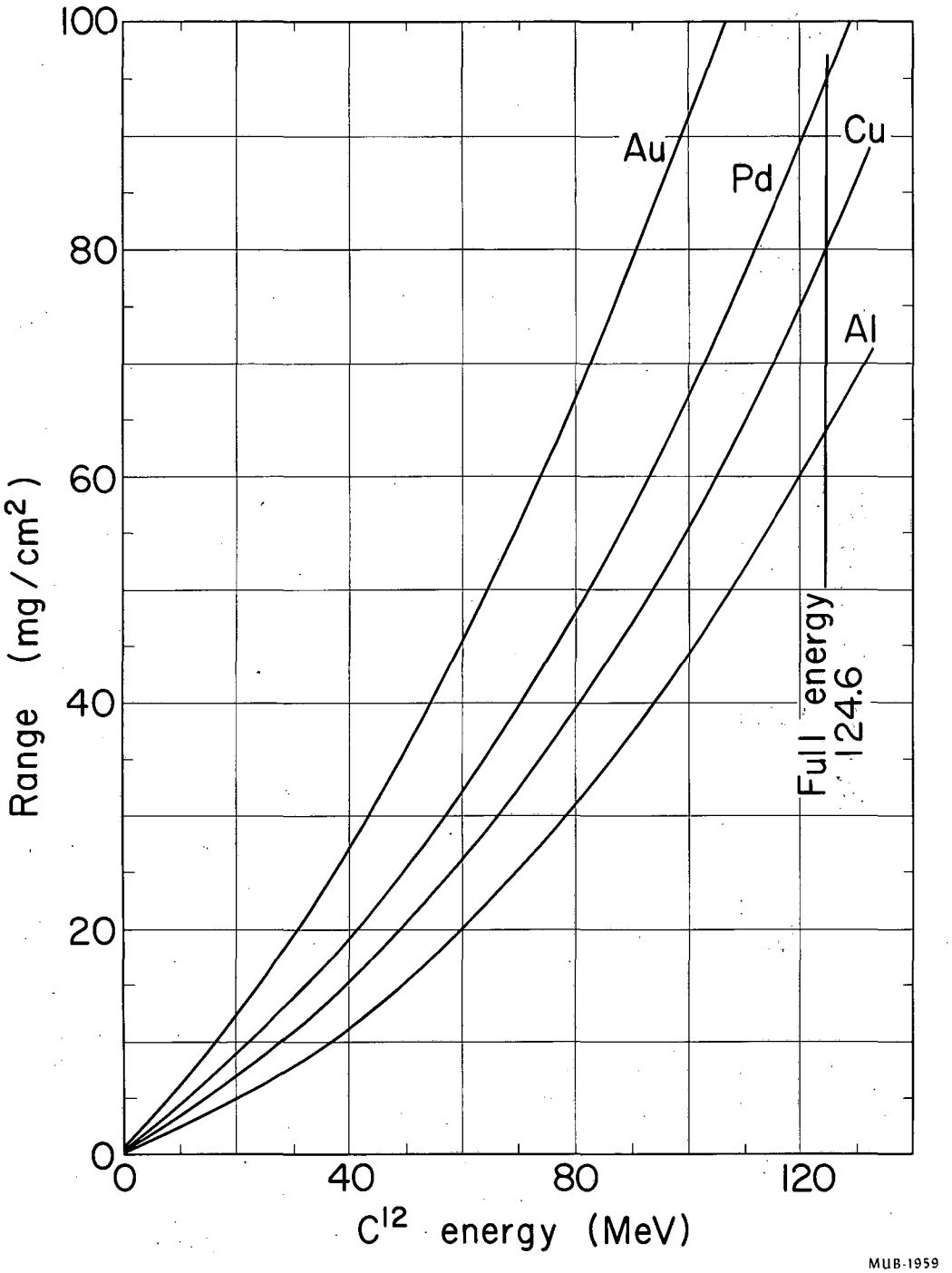

Fig. A5. Range-energy curves for O^{18} ions in various materials.

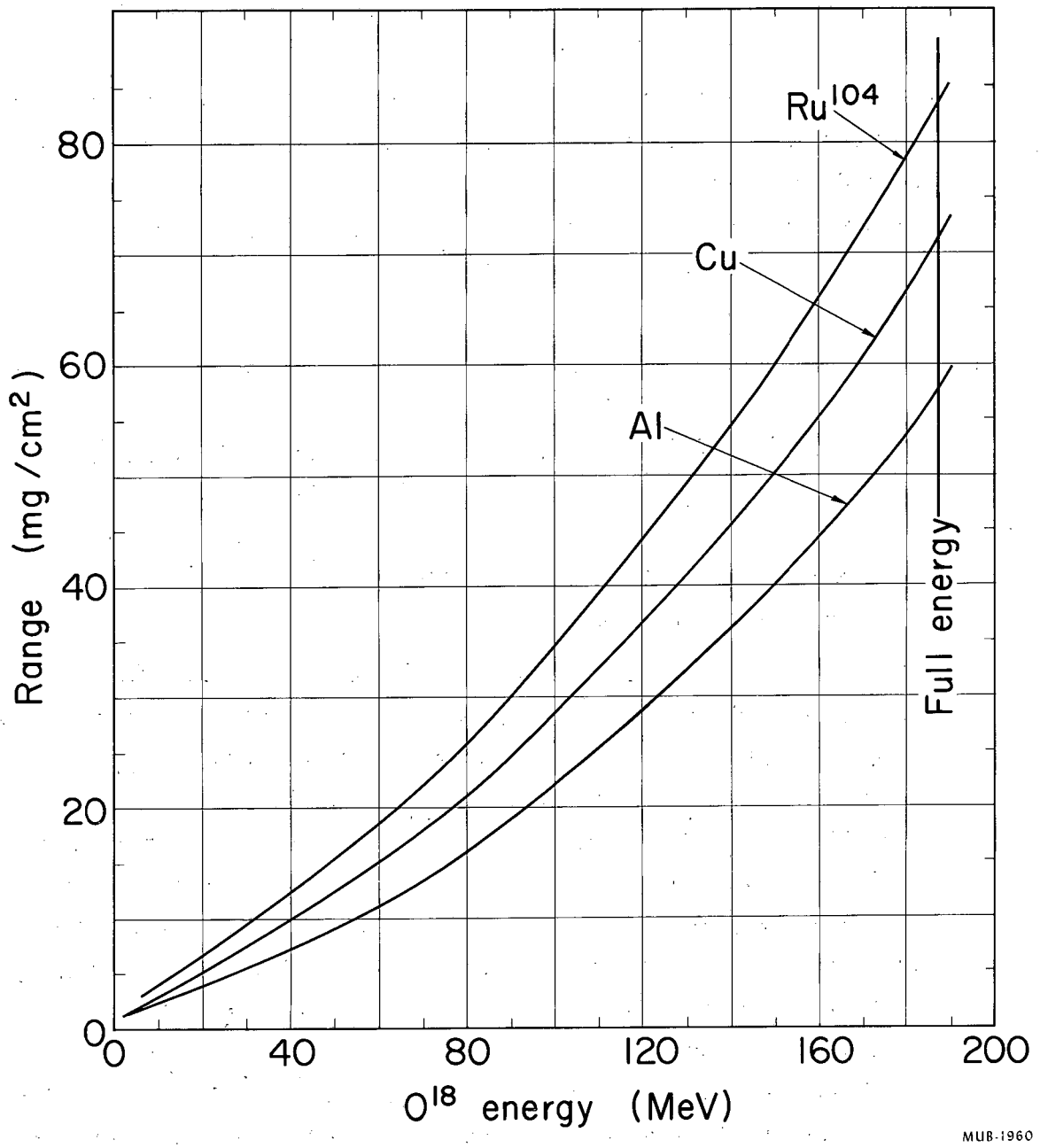

Fig. A6. Range-energy curves for O^{18} ions in various materials.

B. Relationship Between Projectile Energy and the Excitation Energy of the Compound System.

The excitation energy brought into the compound-nucleus system by the various projectiles was calculated according to the method outlined in Section IV A. Plots giving the conversion from the projectile laboratory energy to the excitation energy of the compound nucleus are given in Figs- A-7 through A-10.

C. Target Preparation and Chemical Purification Employed for the Various Bombardments.

1. The Reaction $He^3 + Sn^{119} \longrightarrow Te^{119,119m} + 3n$

a. Target Preparation

All tin targets were prepared by an electrolysis process. The procedure for making the targets was as follows: The enriched tin isotopes were obtained as the oxide from Oak Ridge National Laboratory.[66] The oxide of tin is very resistant to practically all chemical reagents and it was necessary to carry out a sodium fusion in order to put the tin into solution. The oxide was placed in the bottom of a silica evaporation dish and a small piece of sodium placed over it. The dish was heated over a burner until the sodium melted and the reaction began to take place. The reaction yielded a mass of white-yellow crystals consisting of sodium stannate and sodium peroxide. Water was cautiously added to the solid and the material transferred to a 40-ml Pyrex centrifuge cone. The evaporation dish was then washed with a few ml of 6 M HCl and the wash added to the solution in the cone. The solid material usually dissolved without too much trouble. The addition of the acid to the solution often resulted in the precipitation of gelatinous silica (dissolved from the evaporation dish) and stannic acid. The mixture was centrifuged and the decantate poured into a second centrifuge cone. The gelatinous mixture was washed repeatedly with both HCl and NH_4OH solutions to remove all tin, and the

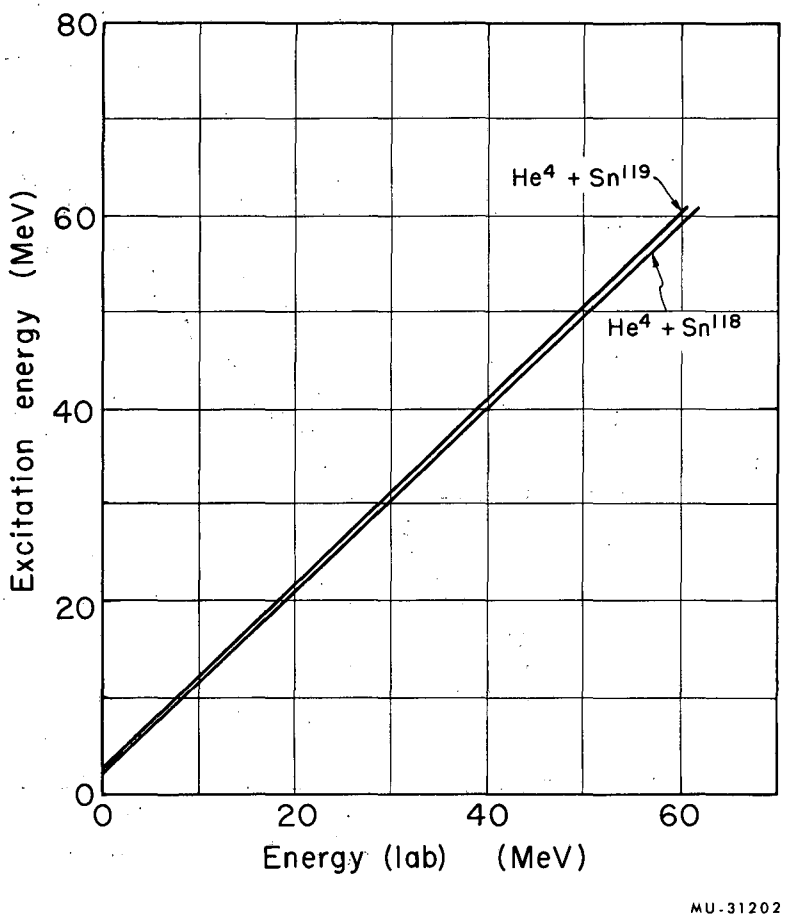

Fig. A7. Excitation energy of the compound nucleus as a function of the laboratory-system projectile energy for the reactions $He^4 + Sn^{119} \longrightarrow Te^{123*}$ and $He^4 + Sn^{118} \longrightarrow Te^{122*}$.

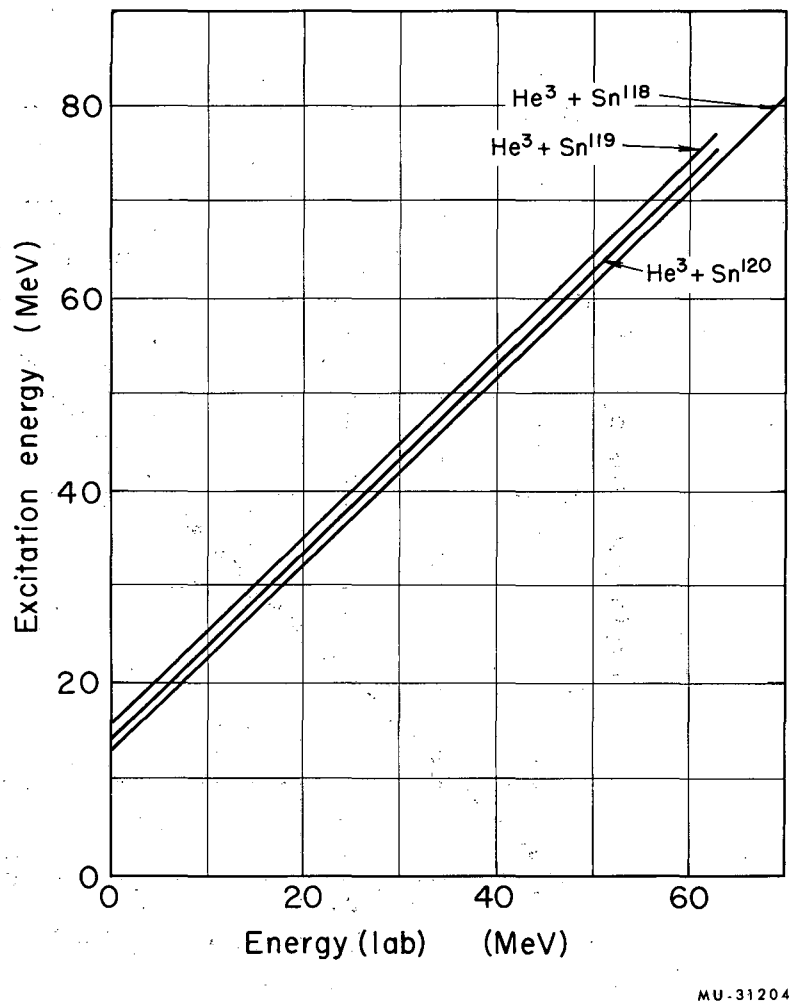

Fig. A8. Excitation energy of the compound nucleus as a function of the laboratory-system projectile energy for the reactions $He^3 + Sn^{119} \longrightarrow Te^{122*}$, $He^3 + Sn^{118} \longrightarrow Te^{121*}$, and $He^3 + Sn^{120} \longrightarrow Te^{123*}$.

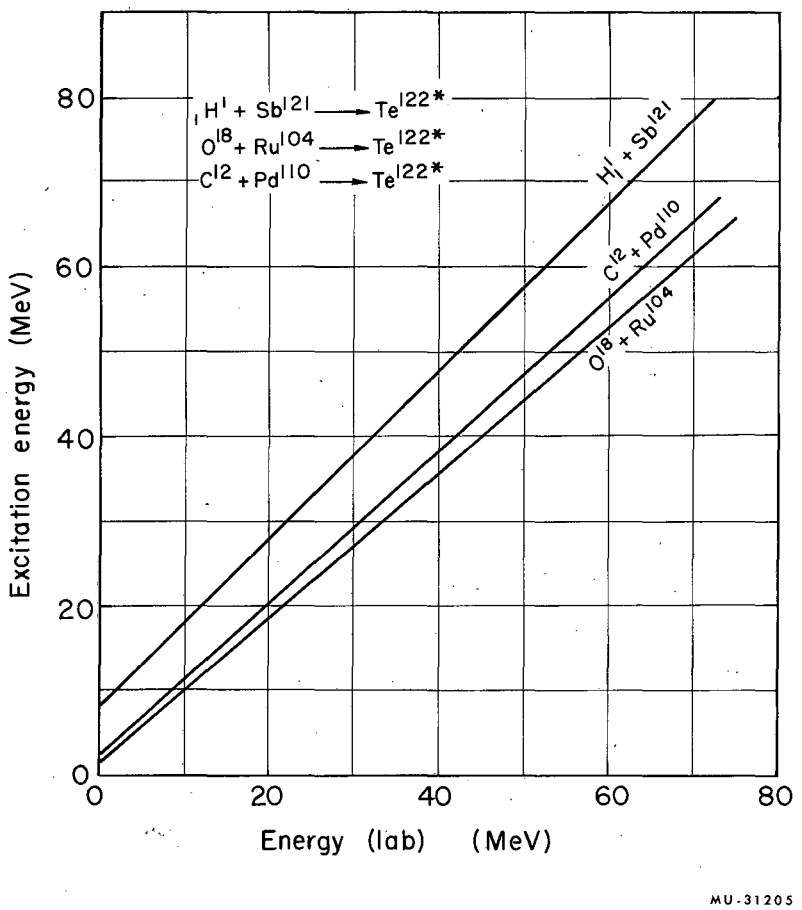

Fig. A9. Excitation energy of the compound nucleus as a function of the laboratory-system projectile energy for the reactions $H^1 + Sb^{121} \longrightarrow Te^{122*}$, $C^{12} + Pd^{110} \longrightarrow Te^{122*}$, and $O^{18} + Ru^{104} \longrightarrow Te^{122*}$.

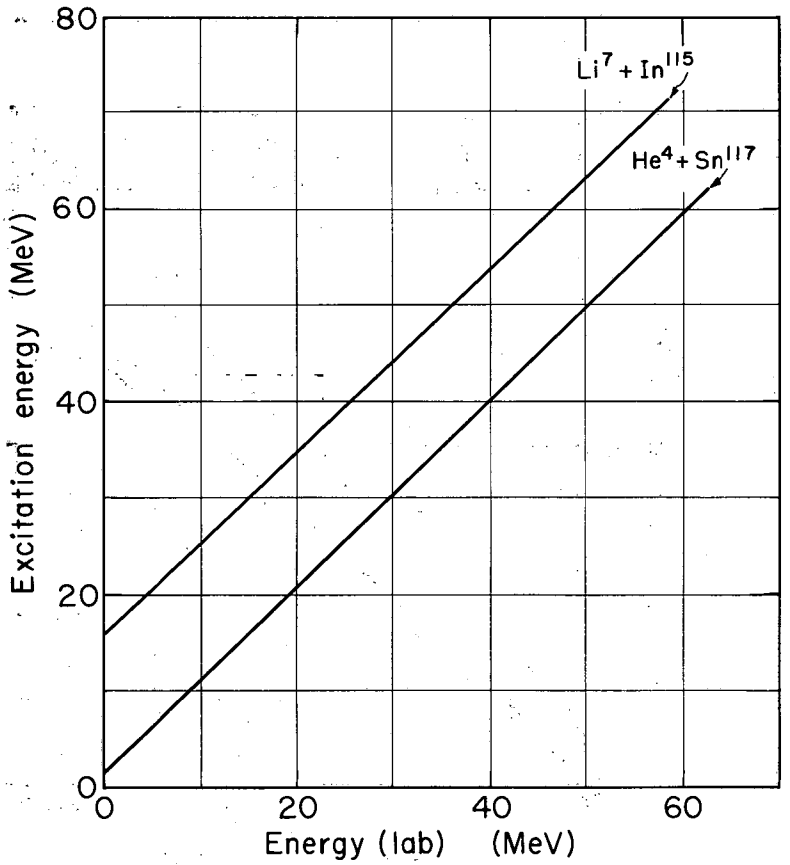

Fig. A10. Excitation energy of the compound nucleus as a function of the laboratory-system projectile energy for the reactions $Li^7 + In^{115} \longrightarrow Te^{122*}$ and $He^4 + Sn^{117} \longrightarrow Te^{121*}$.

washes were added to the original decantate. The pH of the solution was next adjusted so that it was weakly acidic and then the solution was saturated with H_2S. The tin immediately precipitated as the sulfide and was centrifuged to the bottom of the cone. The sulfide was next dissolved in 6 M HCl and the resulting solution boiled to expel the H_2S. A certain amount of silica which had followed through the procedure was usually present; it was discarded. The solution was next diluted to provide a stock solution with a Sn concentration of approximately 1 mg/ml.

The actual production of the tin targets was accomplished as follows: 1 to 2 ml of the solution containing up to 2 mg of Sn was placed in the electrolysis cell shown in Fig. 18. The cell was then filled to within about 0.5 in. of the top with a solution consisting of about 3% ammonium oxalate and 3% oxalic acid. The electrodes were attached and the solution electrolyzed for about 2 h or allowed to continue overnight. Most of the material was probably plated within the first hour. The 1-in.-square foils used for the backing were obtained from Chromium Corporation of America.[65] Cooper was normally used as the backing foil, but a few nickel foils were also employed. The foils used for the He^3 bombardments were about 5 mils thick. This provided a beam energy separation between the individual targets of slightly more than 1 MeV at the higher energies and about 2 MeV at the lower energies. Upon completion of the electrolysis the solution was removed and any Sn that had not been deposited was recovered. The backing foil containing the plate was washed in water and methanol and allowed to dry. The foils were always weighed before and after the plating process so that the thickness of both the foil and plate could be determined.

b. Chemical Procedures

After irradiation, the foils containing the target material were dropped into a 40-ml Pyrex centrifuge cone containing a known amount of tellurium carrier. The foils and target material were dissolved in a small amount of nitric acid. In the case of gold foils it was necessary to use aqua regia, and for the ruthenium targets a completely different scheme was required. The resulting solution was boiled for a few minutes to assure complete dissolution and to equilibrate the tellurium acitivity and carrier. About 10 ml of 6 M HCl was next added and the tellurium

extracted with methyl-isobutyl ketone.[54] The extraction step did not yield radiochemically pure tellurium, since antimony, tin, and a number of other elements also extract. It was found necessary to include the step, however, to remove the relatively large amounts of material due to the backing foil. This was particularly true when the backing foil was gold. If the step was omitted, the yields often came out greater than 100%, indicating that appreciable amounts of the backing foil had followed the tellurium through the chemistry.

In the presence of HCl, tellurium is extracted into the organic layer. The extraction apparatus was the same as that used in the iodine extractions discussed in an earlier section. The organic layer was washed several times with 6 M HCl and the tellurium was then removed by means of an extraction with water. The water containing the tellurium activity was made acidic with HCl and the tellurium precipitated as the metal with stannous chloride. The metallic tellurium was dissolved in a few drops of nitric acid and the solution boiled to dryness to expel the HNO_3. After cooling, the salt was dissolved in 3 M HCl and the tellurium was re-precipitated from the acid solution by saturation with H_2S. The sulfide was destroyed by boiling with HNO_3 and the resulting solution after dilution was filtered to remove traces of sulfur. The tellurium was again precipitated as the metal with $SnCl_2$. The metal was redissolved in HNO_3 and again boiled to dryness. The salt was dissolved in water and the solution made acidic with HCl. The metal was precipitated as the metal, but the final reduction was accomplished by using sulfurous acid and hydrazine hydrochloride. The resulting precipitate was washed with ethanol and mounted by suction filtration on a 7/8-in. tared filter paper. After drying for 10 min at 105°C the sample and paper were weighed in order to determine the yield. Yields were normally in the range of 60 to 70%. The samples were mounted for counting by Scotch taping them to aluminum plates previously described. Although the procedure was quite long, a stack of 10 foils could normally be ready for counting approximately 2 h after the chemistry was begun. The entire chemical procedure is outlined in Fig. A-11.

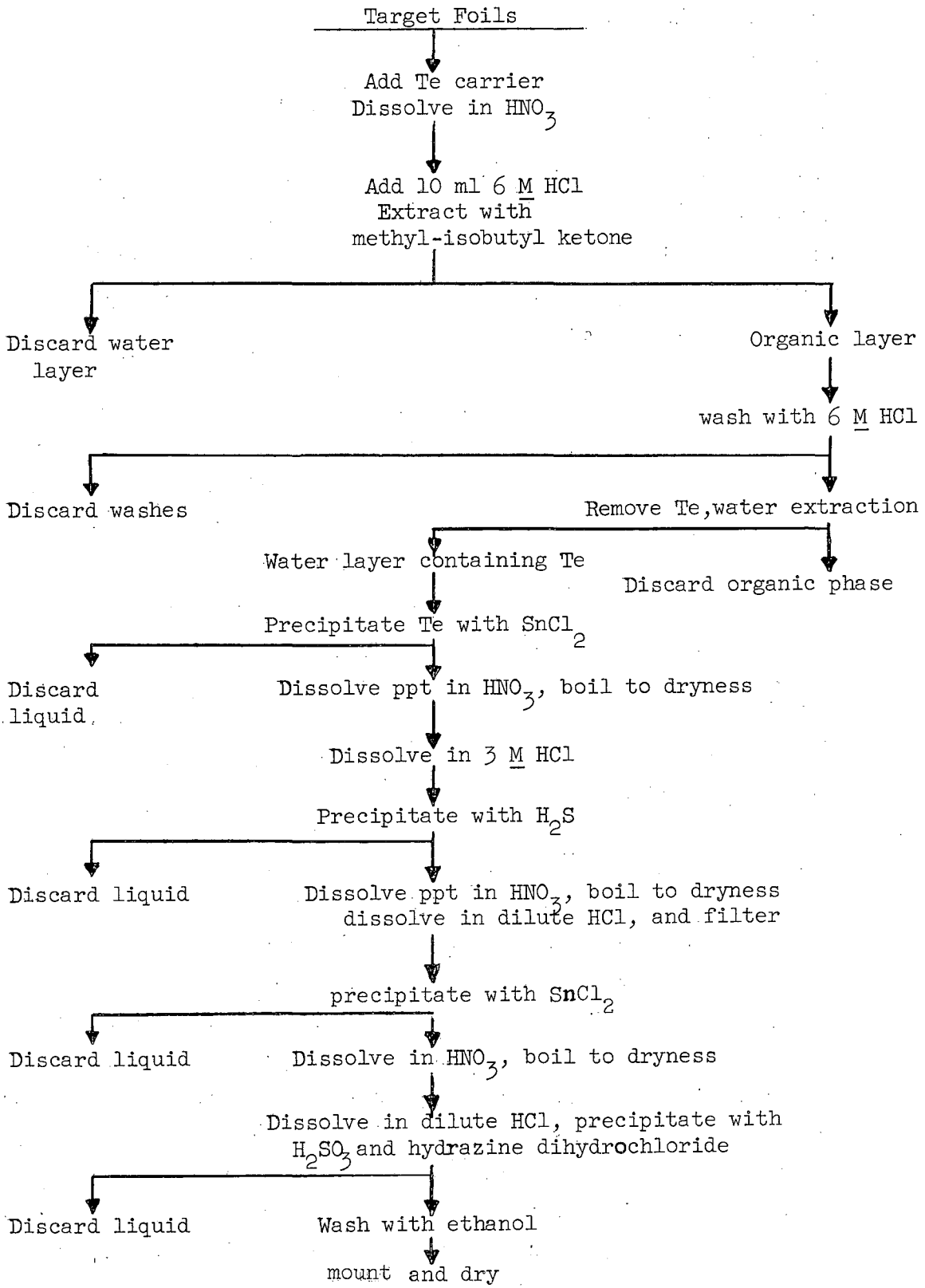

Fig. A-11. Chemistry flow sheet for purification of tellurium-119.

2. The Reaction $He^4 + Sn^{118} \longrightarrow Te^{119,119m} + 3n$

a. Target Preparation

The preparation of the Sn^{118} targets was practically identical to that of the Sn^{119} targets previously discussed. The only difference was that thicker backing foils were employed, since the maximum beam energy was higher than that available for the He^3 irradiations. The use of 1-mil backing foils resulted in an energy separation between samples of about 2 MeV at the highest energies and up to about 2.5 MeV at the lowest energies.

In one experiment, backing foils only 0.125 mil thick were employed. In this experiment aluminum degraders were placed between the foils. The aluminum degraders were checked to determine if any backward recoils occurred. The result was negative and it was concluded that all recoils were in the forward direction and were caught by the backing foil and the sample itself.

b. Chemical Procedures

The chemical purification employed on the targets for this reaction was the same as that used for the He^3 reaction.

3. The Reaction $Li^7 + In^{115} \longrightarrow Te^{119,119m} + 3n$

a. Target Preparation

The preparation of the indium targets was different from that of any of the other target materials. It was possible to use natural indium, which consists of 95.8% In^{115} and 4.2% In^{113}. The In^{113} does not interfere with the reaction, since at the energies employed it would be expected to produce tellurium isotopes of mass 118 or less.

Since natural material could be used, conservation of the indium was not so critical as when separated isotopes were used. The targets were prepared by an evaporation process. In the precess, the indium was contained in a tantalum boat suspended between two electrodes. One-inch-square aluminum backing foils (0.5 mil thick) were attached to larger aluminum plates by means of a small drop of rubber cement. The plates were in turn suspended above the electrodes within the evaporation chamber. The assembly was evacuated until the pressure within the chamber was

approximately 10 μ. The indium was then volatilized by heating the tantalum filament, and the condensation of the metal on the aluminum squares produced the targets. The process was normally repeated about three times in order to produce relatively thick coatings of indium. The beam current for Li^7 was always low and it was desirable to have targets as thick as possible. The thickness of the targets thus produced was about 4 mg/cm^2.

b. Chemical Procedures

The chemistry employed was the same as that described for the previous reactions, with one exception. Since aluminum was used as the backing foil, HCl instead of HNO_3 was used to dissolve the target. The regular procedure was then followed.

On one occasion the samples were counted without having been purified. Most of the activity that was created by the backing foil was rather short-lived and did not interfere seriously except that it was necessary to wait about 24 h before effective counting could be done. This was rather long, considering that the half life of one of the tellurium isomers is 16 h. It was undoubtedly preferable to do the chemistry so that counting could begin immediately.

4. The Reaction $C^{12} + Pd^{110} \longrightarrow Te^{119,119m} + 3n$

a. Target Preparation

The palladium separated isotope was obtained as the metal in granular form. It was easily dissolved by the addition of a small amount of nitric acid followed by gently heating. The resulting solution had a characteristic dark red color. To the red solution was added sodium phosphate and ammonium hydroxide. Upon boiling the palladium was complexed and the solution became colorless. The clear solution was diluted until the palladium content was about 1 mg/ml.

The backing foils used for the carbon bombardments were of copper or gold. A few nickel foils were used, but for some reason it was difficult to electroplate the palladium on the nickel and its use was therefore restricted. Since the range of heavy ions in matter is very

low compared with that of lighter projectiles, it was necessary to use foils that were very thin. The copper foils ranged in thickness from 0.075 to 0.2 mil. The gold backings were 0.1 mil thick. Foils of this thickness resulted in a beam energy degradation of approximately 5 MeV. It was therefore difficult to use more than about five foils in any one bombardment. Attempts were made to make thinner targets, but it was impossible to remove them from the electroplating apparatus without tearing. Often the time allowed for a bombardment was divided into two portions and two target assemblies were irradiated. For this reason some of the experiments indicate as many as 10 samples. Actually two separate bombardments were required to obtain them.

b. Chemical Procedures

The chemistry required was the same as that required for the tin targets.

5. The Reaction $O^{18} + Ru^{104} \longrightarrow Te^{119,119m} + 3n$

a. Target Preparation

Ruthenium is practically impossible to dissolve in any common reagent. Aqua regia has absolutely no effect on it. In order to get the material into solution it was necessary to perform a potassium hydroxide—potassium nitrate fusion. An approximately equal amount of each of the potassium compounds was mixed with the ruthenium in a silica evaporation dish. The mixture was heated to the fusion point by means of a Meeker burner and allowed to react in the molten state for several minutes. After cooling, the resulting solid would normally dissolve in water. Although several procedures were tried, the ruthenium was electroplated most successfully from the basic solution resulting from the fusion step. The concentration of the solution was adjusted to about 1 mg Ru per 20 ml solution for the electroslysis. The need for thin backing foils was even more critical for the ruthenium than for the palladium. The foils used were 0.05-mil copper. Great difficulty was encountered in removing the foils from the plating cell without tearing them. The thickness of the ruthenium plates deposited on the copper ranged from 0.2 to 0.5 mg per cm^2.

c. Chemical Procedures

The same problems were encountered in trying to purify the activity obtained from the bombardments as in preparation of the targets. The copper backing foil dissolved readily in nitric acid but the ruthenium was not affected. The solution was therefore boiled to dryness and a $KOH-KNO_3$ fusion performed. The salt thus obtained dissolved and the solution was made acidic. The tellurium was precipitated as the metal with $SnCl_2$ and the chemistry concluded as outlined previously. In one of the two experiments the yields were very low and the counting statistics consequently rather poor.

6. Reactions Yielding the Compound Nuclei Te^{121*} and Te^{123*}

The target preparation and chemical purification was the same as that described before for tin targets.

D. Absolute Counting Efficiency

In order to obtain the cross-section data presented in Section IV.D it was necessary to determine the absolute counting efficiency of the detector assembly.

Since the γ-ray peak used in determining the cross sections was the 648-keV peak of the 16-h isomer, it was necessary to determine the counting efficiency of a gamma peak of similar energy. With this in mind a Cs^{137} source of known disintegration rate was employed. Cs^{137} decays to 2.3-min Ba^{137}, which has a 661-keV γ ray. The peak-to-total ratios were taken from Health,[48] and the branching ratios, conversion coefficients, and other quantities for the Ba^{137} and Cs^{137} were taken from the compilation by Strominger, Hollander, and Seaborg.[4]

The absolute counting efficiencies thus obtained were in very good agreement with similar data provided by Heath.[48]

REFERENCES

1. N. Bohr, Science 86, 161 (1937).
2. N. Bohr, Nature 143, 330 (1939).
3. S. N. Ghoshal, Phys. Rev. 80, 939 (1950).
4. D. Strominger, J. M. Hollander, and G. T. Seaborg, Rev. Mod. Phys. 30, 585 (1958).
5. M. G. Mayer, Phys. Rev. 74, 235 (1948); 75, 1969 (1949); 76, 16 (1950).
6. J. M. Blatt and V. F. Weisskopf, Theoretical Nuclear Physics (John Wiley and Sons, Inc., New York, 1952).
7. J. F. Mollenauer, Effects of Angular Momentum on Gamma-Ray Production in Compound-Nucleus Reactions (Thesis), Lawrence Radiation Laboratory Report UCRL-9724, June 1960 (unpublished).
8. Gabriel N. Simonoff and John M. Alexander, Angular-Momentum Effects on Neutron Emission by Dy^{156}, Tb^{153}, and Tb^{157} Compound Nuclei, Lawrence Radiation Laboratory Report UCRL-10099, Feb. 1962 (unpublished).
9. John M. Alexander and Gabriel N. Simonoff, The Average Energy and Angular Momentum Removed from Dy Compound Nuclei by Neutrons and Photons, Lawrence Radiation Laboratory Report UCRL-10541, Jan. 1963 (unpublished).
10. R. Vandebosch and J. R. Huizenga, Phys. Rev. 120, 1313 (1960).
11. Fumio Fukuzawa, J. Phys. Soc. Japan 16, 2371 (1961).
12. E. Weigold and R. N. Glover, Nucl. Phys. 32, 106 (1962).
13. T. Erickson and V. M. Strutinsky, Nuclear Phys. 8, 284 (1958).
14. G. S. Pik-Pichak, Soviet Phys. JETP 11, 557 (1959).

15. Carl T. Bishop, Isomeric Cross-Section Ratios for Some (n, γ) and (α, xn) Reactions (Thesis), Argonne National Laboratory Report ANL-6405, Aug. 1961 (unpublished).

16. R. D. Macfarlane, Phys. Rev. 126, 274 (1962).

17. Sylvia M. Bailey, Independent Yields of Isomeric Pairs in Nuclear Reactions (Thesis), Lawrence Radiation Laboratory Report UCRL-8710, April 1959 (unpublished).

18. J. R. Huizenga and R. Vandenbosch, Phys. Rev. 120, 1305 (1960).

19. J. Wing and J. R. Huizenga, Phys. Rev. 128, 280 (1962).

20. L. F. Hansen, R. C. Jopson, H. Mark and C. D. Swift, Nuclear Phys. 30, 389 (1962).

21. P. Blaser, F. Boehm, P. Marimier, and P. Scherrer, Helv. Phys. Acta 24, 441 (1951).

22. B. Linder and R. A. James, Phys. Rev. 114, 332 (1959).

23. J. Wing, Isomeric-Yield Ratios in Nuclear Reactions (With a Compilation of Experimental Data), Argonne National Laboratory Report ANL-6598, Sept. 1962 (unpublished).

24. General Electric Chart of the Nuclides, Fifth Edition, Revised to April 1956.

25. The Nuclear Data Sheets, edited by C. L. McGinnis (Publications Office National Academy of Sciences, National Research Council, Washington D. C.).

26. M. Lindner and I. Perlman, Phys. Rev. 73, 1124 (1948); 78, 499 (1950).

27. R. H. Goeckermann and I. Perlman, Phys. Rev. 76, 629 (1949).

28. Bruce Dropesky, Nuclear Reactions of Iodine with 240-MeV Protons (Thesis), University of Rochester, 1953 (unpublished).

29. Richard W. Fink, Reactions of Cesium with High-Energy Protons (Thesis), University of Rochester, 1953 (unpublished).

30. R. W. Fink and E. O. Wiig, Phys. Rev. 96, 185 (1954).

31. C. W. Kocher, Allan C. G. Mitchell, C. B. Creager, and T. D. Nainan, Phys. Rev. 120, 1348 (1960).

32. R. W. Fink, G. Anderson, and J. Kantele, Arkiv Fysik 19, 323 (1962).

33. R. K. Gupta, G. C. Pramila, and R. Srinivasa Raghavan, Nucl. Phys. 32, 669 (1962).

34. A. A. Sorokin, A. Bedyesku, M. V. Klimentovskaya, L. N. Kryukova, K. P. Mitrofanov, V, V. Muravyeva, V. N. Reebakov, G. Chandra, and V. S. Shpinel, Izv. Akad. Nauk SSSR, Ser. Fiz. 24, 1484 (1960).

35. N. G. Zatseva, M. Ya. Kuznetsova, I. Yu. Levenberg, V. N. Pokrovski, and V. A. Khalin, Izv. Akad. Nauk SSSR, Ser. Fiz. 24, 1083 (1960).

36. N. G. Zatseva, M. Ya. Kunznetsova, I. Yu. Levenberg, and V. A. Khalin, Radiokhimya 2, 451 (1960).

37. J. Kantele and R. W. Fink, Nucl. Phys. 43, 187 (1963).

38. R. Vandenbosch and L. Haskin, Isomer Ratios for $Y^{87,87m}$ and the Spin Dependence of the Nuclear Level Density, Argonne National Laboratory (unpublished).

39. T. Darrah Thomas, The Cross Section for Compound Nucleus Formation in Heavy-Ion Induced Reactions, Lawrence Radiation Laboratory Report UCRL-8695, April 1956 (unpublished).

40. T. D. Thomas, Phys. Rev. 116, 703 (1959).

41. W. L. Hafner, Jr., J. R. Huizenga, and R. Vandenbosch, Computer Program for Calculation the Relative Yields of Isomers Produced in Nuclear Reactions, Argonne National Laboratory Report ANL-6662, Dec. 1962 (unpublished).

42. H. A. Bethe, Rev. Mod. Phys. 9, 84 (1937).

43. C. Bloch, Phys. Rev. 93, 1094 (1954).

44. The Harshaw Chemical Co. 113 John St., Elyria, Ohio.

45. Pacific Electro-Nuclear Corp., 9520 Jefferson Blvd., Culver City, California.

46. Radiation Instrument Development Laboratory, 4501 W. North Avenue, Melrose Park, Illinois.

47. F. L. Moseley Co., Pasadena, California.

48. R. L. Heath, Scintillation Spectrometry Gamma-Ray Spectrum Catalogue (Phillips Petroleum Co., Atomic Energy Division, Idaho Falls, Idaho), Report IDO-16408, July 1, 1957 (unpublished).

49. R. L. Chase, Nuclear Pulse Spectrometry (McGraw-Hill Book Company, Inc., New York, 1961).

50. P. R. Bell and K, Siegbahn, editors, Beta and Gamma-Ray Spectroscopy (Interscience Publishers, Inc., New York, 1955).

51. W. J. Price, Nuclear Radiation Detection (McGraw-Hill Book Company, Inc., New York, 1958).

52. C. D. Coryell and N. Sugarmann, editors Radiochemical Studies: The Fission Products, Book 3, (McGraw-Hill Book Company, Inc., New York, 1951).

53. W. W. Meinke, Chemical Procedure Used in Bombardment Work at Berkeley, U. S. Atomic Energy Commision Report AECD-2738, 1949 (unpublished).

54. Hidehiro Goto, Y. Kakita, and T. Furukawa, Nippon Kagaku Zasshi 79, 1513 (1958); UCRL Translation 541.

55. G. W. Leddicotte, The Radiochemistry of Tellurium (Subcommittee on Radiochemistry, National Academy of Sciences, National Research Council), Report NAS-NS 3038 (1961).

56. W. H. Sullivan, Trilinear Chart of the Nuclides (U. S. Atomic Energy Commission, 1957).

57. G. Friedlander and J. W. Kennedy, Nuclear and Radiochemistry (John Wiley and Sons, Inc., New York, 1949).

58. Edward L. Hubbard, Range-Energy Relation for Heavy Ions in Metals, Lawrence Radiation Laboratory Report UCRL-9053, Jan. 1960 (unpublished).

59. L. C. Northcliffe and R. L. Gluckstern, Penetration of Matter by Heavy Ions with Energies Above 1/2 MeV per AMU (National Academy of Sciences National Research Council, 1962) (unpublished).

60. R. Sternheimer, Phys. Rev. 115, 137 (1959).

61. T. Darrah Thomas, Spallation-Fission Competition From the Compound System U^{233} + He^{4} (thesis), Lawrence Radiation Laboratory Report UCRL-3791, July 1957 (unpublished).

62. E. L. Hubbard, W. R. Baker, K. W. Ehlers, H. S. Gordon, R. M. Main, N. J. Norris, R. Peters, L. Smith, C. M. Van Atta, and F. Voelker, Rev. Sci. Instr. 32, 621 (1961).

63. P. A. Seeger, Nucl. Phys. 25, 1 (1961).

64. B. G. Harvey, Introduction to Nuclear Physics and Chemistry (Prentice-Hall Inc., 1962).

65. Chromium Corp. of America, Waterbury 20, Connecticut.

66. Oak Ridge National Laboratory, Isotopes Division, Oak Ridge, Tennessee.

67. R. Kaufmann and R. Wolfgang, Phys. Rev. 121, 192 (1961).

68. S. K. Allison, M. Kamegai, and G. C. Morrison (Univ. of Chicago), Mechanisms of Nuclear Reactions Between Li Nuclei (Third Conference on Reactions Between Complex Nuclei, Held at Asilomar, Pacific Grove, California, April 1963), (unpublished).

69. R. Ollerhead, C. Chasman, and D. A. Bromley (Yale Univ.), Dissociation Reactions in Light Nuclei (Third Conference on Reactions Between Complex Nuclei, Held at Asilomar, Pacific Grove, California, April 1963) (unpublished).

70. R. M. Drisko, G. R. Satchler, and R. H. Bassell (Oak Ridge National Laboratory), Pickup of Heavy Clusters (Third Conference on Reactions Between Complex Nuclei, Held at Asilomar, Pacific Grove, California, April 1963), (unpublished).

71. M. Coste and L. Marquez, Compt. Rend. 254, 1768 (1962).

72. M. Coste, C. Lemeille, L. Marquez, and N. Saunier, J. Phys. Radium 22, 584 (1961).

73. L. Marquez and Pham-Dinh-Lien, J. Phys. Radium 22, 589 (1961).

74. Pham-Dinh-Lien and L. Marquez, Notas de Fisica 8, 187 (1961); Pham-Dinh-Lien and L. Marquez, Nucl. Phys. 33, 202 (1962).

75. Richard Kiefer (Lawrence Radiation Laboratory, Berkeley), private communication.

76. George Igo, Phys. Rev. Letters 1, 72 (1958).

77. D. L. Hill and J. A. Wheeler, Phys. Rev. 89, 1102 (1953).

78. Victor E. Viola, Jr., T. Darrah Thomas, and Glenn T. Seaborg, Phys. Rev. 129, 2710 (1963).

79. W. Hauser and H. Feshbach, Phys. Rev. 87, 366 (1952).

80. H. A. Bethe, Rev. Mod. Phys. 9, 84 (1937).

81. C. Bloch, Phys. Rev. 93, 1094 (1954).

82. L. S. Kisslinger and R. A. Sorensen, Kgl. Danske Videnskab. Selskab Mat.-Fys. Medd. 32, No. 9, (1960).

83. K. J. LeCouteur and D. W. Lang, Nucl. Phys. 13, 32 (1959).

84. R. L. Bramblett and T. W. Bonner, Nucl. Phys. 20, 395 (1960).

85. B. T. Feld, H. Feshbach, M. L. Goldberger, H. Goldstein, and V. F. Weisskopf, Final Report of the Fast Neutron Data Project, Nuclear Development Associates Report NYO-636, Jan. 1951.

86. E. J. Campbell, H. Feshbach, C. E. Porter, and V. F. Weisskopf, Some Optical Model Calculations, Mass. Inst. of Tech., Cambridge Lab. for Nuclear Science Report TID-5820, 1960.

87. B. B. Kinsey, in Encyclopedia of Physics, S. Flugge, Editor (Springer-Verlag, Berlin, 1957 Vol. 40).

88. V. M. Strutinsky, L. V. Groshev, and M. K. Akimova, Nucl. Phys. 16, 657 (1960).

89. J. F. Mollenauer, Phys. Rev. 127, 867 (1962).

90. J. H. Carver, G. E. Coote, and T. R. Sherwood, Nucl. Phys. 37, 449 (1962).

91. T. Erickson, Nucl. Phys. 11, 481 (1959).

92. T. Erickson, Advan. Phys. 9, 425 (1960).

93. J. R. Grover, Phys. Rev. 123, 267 (1961); Phys. Rev. 127, 2142 (1962).

94. D. W. Lang, Nucl. Phys. 42, 353 (1963).

95. T. Erickson, Nucl. Phys. 6, 62 (1958).

96. D. W. Lang and K. J. LeCouteur, Nucl. Phys. 14, 21 (1959).